University of Calgary

PRISM Repository **https://prism.ucalgary.ca**

The Vault Open Theses and Dissertations

2018-05-08

Effect of Grain Irregularity on Rock Petrophysical Parameters: A Numerical Pore-level Study

Rahmanian Shahri, Meysam

Rahmanian Shahri, M. (2018). Effect of Grain Irregularity on Rock Petrophysical Parameters: A Numerical Pore-level Study (Master's thesis, University of Calgary, Calgary, Canada). Retrieved from https://prism.ucalgary.ca. doi:10.11575/PRISM/31923

http://hdl.handle.net/1880/106642

Downloaded from PRISM Repository, University of Calgary

UNIVERSITY OF CALGARY

Effect of Grain Irregularity on Rock Petrophysical Parameters: A Numerical Pore-level Study

by

Meysam Rahmanian Shahri

A THESIS

SUBMITTED TO THE FACULTY OF GRADUATE STUDIES

IN PARTIAL FULFILMENT OF THE REQUIREMENTS FOR THE

DEGREE OF MASTER OF SCIENCE

GRADUATE PROGRAM IN CHEMICAL ENGINEERING

CALGARY, ALBERTA

MAY 2018

© Meysam Rahmanian Shahri 2018

ABSTRACT

A good evaluation of transport properties in reservoir rocks plays a major role in the design of recovery process and prediction of recovery performance. Permeability, thermal and electrical conductivity, are important physical properties affecting fluid flow and fluid distribution. Numerical techniques based on image analysis can be considered as reliable alternative approaches to either experimental methods or empirical correlations to estimate petrophysical properties.

There are various numerical approaches to directly simulate fluid flow through a virtual porous medium. For instance, Computational Fluid Dynamics (CFD) and Lattice-Boltzmann as dynamic methods, and pore morphological as quasi-static approaches are the most popular techniques to simulate flow through porous materials.

A virtual porous medium can be provided by binarizing either the real CT scan images of porous media or even the synthetic images generated by statistical approaches. In this regard, the virtual porous media have to properly mimic the physical features of real sands.

As providing real CT scan images with high-resolution of rock samples is expensive and time consuming, utilizing statistical approaches to generating synthetic porous media based on Particle Size Distribution (PSD) and porosity of real sands could be considered as an alternative to reconstruct virtual porous media.

To generate a virtual porous medium statistically, an innovative algorithm is proposed in this research generating irregular grains based on a given porosity and particle size distribution (PSD). The proposed procedure is inspired from the crystallization concept. In this method, the shape,

orientation and structure of the grains can be readily controlled by the user. This provides the opportunity to investigate the effect of some geometrical parameters such as grain irregularity on rock and flow properties.

In this study, several virtual porous media with different porosities, sphericities and PSD are constructed using the proposed approach. Based on the simulation results on these media the effect of grain irregularity on transport properties and onset of non-Darcy flow is investigated.

PREFACE

This thesis includes some materials (e.g. figures, tables, formulas and texts) from one journal paper which is in press, one published conference papers and one presentations as follows:

I) Publications:

1. Meysam Rahmanian, Apostolos Kantzas, “Stochastic generation of virtual porous media using a pseudo-crystallization approach. Journal of Natural Gas Science and Engineering.”, Journal of Natural Gas Science and Engineering, May 2018.

II) Presentations and Conferences:

1. Saeed Taheri, Peyman Mohammadmoradi, Meysam Rahmanian, Apostolos Kantzas, “Pore-Level Investigation of Heat Conduction during Thermal Recovery Methods”, World Heavy Oil Congress, Calgary, Canada, 2016.

2. Meysam Rahmanian Shahri, Saeed Taheri, Peyman Mohammadmoradi, Apostolos Kantzas, “Measurement of Tight Formation Transport Properties: A Sub-Pore Scale Approach”, Interpore, 9th International Conference on Porous Media and Annual Meeting, Rotterdam, Netherlands,2017

ACKNOWLEDGMENT

I would like to express my deepest appreciation and respect to my supervisors Dr. Apostolos Kantzas for his invaluable assistance, support and guidance. His supportive experience, encouragement and collaboration during the project promoted the work results and directed the research in a productive approach. His vast knowledge and experience have played an important role in success of this project. I am sincerely grateful for his help.

I would like to extend my most sincere appreciation to the members of my dissertation committee, Dr. Roberto Aguilera, Dr. Chris Clarkson for taking time to review my dissertation. I would also like to thank them for their valuable comments. They had a significant impact on the outcome of the research.

It has been a pleasure and privilege to work closely with Dr. Saeed Taheri. I thank him for taking keen interest in the project along with invaluable assistance and guidance and giving valuable comments and suggestions throughout several steps of this research.

I would like to express the deepest appreciation to Peyman Mohammadmoradi and Shahin Ghomeshi for their generous support during different stages of my project.

Special thanks go to my dear brother Mohammad Reza Rahmanian Shahri for his technical discussions and suggestions and my sister in law Mona, for her kindness and support during of my project.

I would like to extend my gratefulness to all my friends who created a warm and friendly environment during my study at the University of Calgary. Specially, I would acknowledge the support from Amir Ahmad Shirazimanesh.

I gratefully acknowledge the financial support of the FUR program from NSERC, AITF, and the sponsoring companies: Athabasca Oil Corporation, Devon Canada, Foundation CMG, Husky Energy, Brion Energy, Canadian Natural, Maersk Oil, Suncor Energy.

Furthermore, I would also like to acknowledge with much appreciation the academic and technical support of department of Chemical and Petroleum Engineering at the Schulich School of Engineering and its staff.

DEDICATION

This thesis is dedicated to my family. My father, Bahram, who have always encouraged and supported me during the years of my education and intellectual development. My mother, Mahin, who was a source of motivation and strength during moments of despair and discouragement. Her care and support have been shown in incredible ways during my life. My brother, Mohammad who have always helped me to make my best decisions in my life. My sister, Mina, for their endless love, support and encouragement. They have been always hoping in me and have never left my side. I would be forever indebted to such a lovely family.

TABLE OF CONTENTS

ABSTRACT I

PREFACE III

ACKNOWLEDGMENT IV

DEDICATION VI

TABLE OF CONTENTS VII

LIST OF TABLES X

TABLE OF FIGURES XII

NOMENCLATURE XX

1 INTRODUCTION 1

1.1 Background 1

1.2 Novelty for Case of Study 2

1.3 Simulation Tools 3

1.4 Organization of Dissertation 3

2 NUMERICAL CONSTRUCTION OF VIRTUAL POROUS MEDIA 4

2.1 Literature Review 4

2.2 Developed pattern generator 10

3 NUMERICAL CALCULATION OF PETROPHYSICAL PROPERTIES 19

3.1 Introduction 19

3.1.1 Pore Network Modeling 20

3.1.2 Direct Modeling 23

3.2 Methodology 25

3.3 Single Phase Fluid Flow Simulation 26

3.4 Results and Discussion 28

4 NON-DARCY FLUID FLOW 43

4.1 Literature Review 44

4.1.1 Onset of non-Darcy flow 45

4.1.2 Non-Darcy coefficient for single phase flow 48

4.1.3 Approaches to determine non-Darcy regime 55

4.2 Methodology 56

4.3 Physical Properties of Generated Virtual Porous Media 57

4.4 Governing Equations and Numerical Method 57

4.5 Numerical Results and Discussion 59

4.5.1 Comparison of experimental data set and simulation results 61

4.5.2 Effect of porosity on onset of non-Darcy flow and β factor 62

4.5.3 Effect of average grain sphericity on non-Darcy flow 70

4.5.4 Effect of connate water on non-Darcy flow 74

4.5.5 Multi-Phase fluid occupancies 76

5 CONCLUSIONS AND RECOMENATIONS 82

RECOMMENDATION 84

REFRENCES 85

APPENDIX A: COPYRIGHT PERMISSIONS 97

LIST OF TABLES

Table 3-1: Water properties used in Absolute permeability calculation..... 27

Table 3-2 : Brine physical properties used in formation factor calculation..... 28

Table 3-3: Characteristics and simulation results of virtual generated Fontainebleau sandstone 32

Table 3-4: Permeability in different directions for Fontainebleau sandstone..... 32

Table 3-5: Correlation constants for the permeability models..... 35

Table 3-6: The Residual sum of square (RSE) and R square for the proposed correlations to judge the accuracy of proposed correlations to estimate absolute permeability on two different experimental data set..... 38

Table 3-7: Correlation constants for the formation factor models..... 40

Table 4-1: Reported critical Re number as a criterion to identify the onset of non-Darcy flow .. 47

Table 4-2: The characteristics of generated porous media 57

Table 4-3: Calculated Forchheimer permeability, non-Darcy coefficient, Critical Reynolds number, and Tortuosity for all generated virtual porous media..... 60

Table 4-4: Comparison of calculated Non-Darcy coefficient (β(1/m)) obtained numerically with predicted value of some presented empirical correlations. 61

Table 4-5: Critical Velocity for different samples with different porosity..... 62

Table 4-6: Critical velocity for different samples with different average grain sphericity 71

Table 4-7: Critical Reynolds number and Darcy permeability for two samples with different average grains sphericity..... 73

Table 4-8: Critical Reynolds number , darcy permeability and non-Darcy coefficient for fully saturated case of sample 4 compared to unsaturated one (Immobile water occupied 8.7% of PV in sample 4) 78

Table 4-9: Estimation of available proposed empirical correlation to predict inertial coefficient 78

TABLE OF FIGURES

Figure 2-1: Random packing of sphere (a) Random packing of mono-sized sphere. (b) Random packing of sphere with different grain size. (Taheri et al., 2017) 5

Figure 2-2: Different steps of Particle Deposition Method (Taheri et al., 2015)..... 6

Figure 2-3: Different steps of swelling spheres algorithm (Taheri et al., 2017)..... 7

Figure 2-4: Different stage of rock formation. (a) deposition/packing of spheres representing sediment of clean, well sorted sand. (b) compaction forces sphere to interpenetrate each other. (c) a thin layer of cement covers each compacted sphere. 8

Figure 2-5: Random packing of non-spherical grain. a) Schwartz and Banavar (1989) numerically constructed packs of spheres, then, the spheres were deformed into ellipses b) Coelho (1996) used oblate ellipsoids packing to investigate the effect of grain geometry on transport properties. C) Pilloti (1997) deformed the surface of spherical grains to convert spherical grains to irregular grains..... 9

Figure 2-6: Simple representation of 2-D construction of a porous medium (pixel based). The red pixels are the center of each grain (nucleus). The locations of the nuclei are chosen randomly in the proposed algorithm. The black pixels are solids and white pixels are pores. 11

Figure 2-7: Converting cumulative frequency distribution to percent point function to dedicate a dimeter to a grain. 12

Figure 2-8: Sphericity variation vs. porosity with the same PSD .The proposed method always meets the target porosity and honors the given PSD. As the target porosity declines, grains tend to be more irregular but still obeying the same PSD. 13

Figure 2-9: 2D Schematic visual illustration of incrementally radial growth (crystallization) of a grain at 8 different directions; The user could control the sphericity of the grain by assigning different probability and promotional multiplier at various directions. The red section in (b-h) shows the incremental growth at that stage of crystallization. 14

Figure 2-10: Examples of generated irregular grain shapes with different sphericities (ψ). a) ψ=0.87, b) ψ =0.93, c) ψ =0.97, d) ψ =0.83, e) ψ =0.78, f) ψ =0.76, g) ψ =0.72, h) ψ = 0.73, j) ψ =0.7. 15

Figure 2-11: The Pseudo-Crystallization algorithm to generate a 3D porous medium containing irregular grains. 17

Figure 2-12: Effect of number of grains on the calculated absolute permeability in 20 reconstructed consolidated samples with the same particle size distribution (Fontainebleau PSD) and porosity (Φ =0.152). 18

Figure 3-1: Pore network models: (a) model reconstructed with a regular lattice (b) model extracted from the micro tomography images. (Varloteaux et al., 2013). 22

Figure 3-2: (a)Sub pore scale gridding, (b) is zoomed area indicated in (a) (Taheri et al., 2010) 26

Figure 3-3: Grain size distribution of Fontainebleau sandstone (Extracted from Delfosse, 2004). 28

Figure 3-4: Comparison of 2D CT scan real image sequences with 2D image sequences generated by the proposed methodology (The generated 2D images are (300*300) pixels with the

resolution of 7.5 μm). 2D real images of Fontainebleau were acquired at Brookhaven National Laboratory by Exxon- Mobil (The 2D real images are (288*288) with pixel scale of 7.5 μm)..... 29

Figure 3-5: (a) 3D real image of Fontainebleau, constructed by rendering of CT-scan images (acquired at Brookhaven National Laboratory by Exxon - Mobil (Digital Rock Physics Benchmarks, 2012)). The real image segmented binary data (288*288*300) with voxel scale of 7.5 μm. (b) 3D generated Fontainebleau sandstone. The generated porous medium is (300*300*300) with the resolution of 7.5 μm..... 29

Figure 3-6. (a) 3D Solid matrix of Synthetic Fontainebleau sandstone. (b) 3D Pore structure of the generated sandstone. (c) pressure profile between two opposite faces of a medium (steady state solution) (d) Velocity profile (stream line)..... 30

Figure 3-7: (a) Comparison of pore body size distribution for two 3D virtual Fontainebleau sandstone constructed by using real microscopic images and proposed 3D pattern generator. (b) Comparison of pore throat size distribution for both generated virtual Fontainebleau..... 31

Figure 3-8: (a) A typical PSD utilized to generate virtual porous media with different porosities. (b) Generated porous materials based on the PSD. (Φ =0.27, dimensions=200*200*200, voxel size = 5 μm and average grains sphericity =0.94). (c) Generated porous rock based on the PSD. (Φ =0.10, dimensions=200*200*200, voxel size = 5 μm and average grains sphericity =0.68). Both generated media have the same PSD and different porosity and sphericity..... 35

Figure 3-9: (a) Comparing different empirical correlations (Garcia et al., 2009; Carman,1937; Berg, 1975; Bourbie and Zinszner,1985; Revil and Cathles1999) with our proposed

correlationcoefficient (Eq 3-5). (b) Log scales of Figure 3-9.a to illustrate a better estimation of correlations at lower porosity range..... 36

Figure 3-10: Fitting empirical correlations on Fontainebleau dataset (D_{50} =250 μm). (a) Porosity range is between 3% - 28%. (b) porosity range is between 8% -32% porosity. It is shown that the proposed correlation coefficients in this research (Equation 3-5) has an acceptable conformance with the experimental data (Bourbie and Zinszner,1985)..... 37

Figure 3-11: Fitting empirical correlations on Ottawa dataset (D_{50}=860 μm). Experimental data belongs to various sandstones from Kameda, (2004). It is shown that the proposed correlation coefficients in this research (Equation 4-5) is in better conformance with the experimental data. As it is clear, the Bourbie correlation (Bourbie and Zinszner,1985) which was originally developed for Fontainebleau sandstone is not suitable to predict the permeability in Ottawa sandstone..... 38

Figure 3-12: The effect of sphericity on permeability estimation of sandstones while the porosity and PSD considered constant for each case of study. As the figure shows, the effect of sphericity on permeability for high range porosities is not significant. (the resolution of all generated porous media is 5 μm)..... 39

Figure 3-13: Formation factor versus porosity for the generated porous media with different particle size distributions and porosities. using the proposed algorithm 40

Figure 3-14: Comparison of the proposed constant for Archie's Equation in this study (Equation 3-7) with other empirical correlations relied on core experiment (Timur et al.,1972; Carothers,1968; Winsauer et al.,1952) to estimate formation factor versus porosity for different sandstones 41

Figure 3-15: Comparing the proposed correlation coefficients in this study with other empirical correlations relied on core experiment (Timur et al.,1972; Carothers,1968; Winsauer et al.,1952) to estimate formation factor versus porosity for various sandstones. Experimental data from Pape et al., 1987. (b) Comparison of all mentioned correlations at Log scale. 42

Figure 4-1: Non-Darcy coefficient as a function of permeability for hundreds of different types of rocks was collected and plotted. 54

Figure 4-2: The experimental data set classified into three categories, unconsolidated sands, consolidated sands with permeability greater than 0.1 md and consolidated sands with permeability less than 0.1 mD to present the most appropriate correlation for each category. 54

Figure 4-3: Comparison of the calculated non-Darcy coefficient for 10 virtual sandstone with collected experimental data set 61

Figure 4-4: The numerical approach presented by Rahmanian and Kantzas, 2018 applied to generate virtual porous media with different porosities (a) Sample 1 with 0.4 porosity. (b) The generated sandstone with porosity of 0.13. (c)The generated sandstone with porosity of 0.22. 62

Figure 4-5: Plots of flow streamlines within pores of three generated porous medium by applying pressure gradient at the opposite cross sections perpendicular to the flow direction. The streamlines are colored according to velocity magnitude. 63

Figure 4-6: Departure from linear relationship between pressure gradient with velocity for three virtual Fontainebleau sandstones with different porosities (Sample 1, Sample 3 and

Sample7) at high velocities. The red solid lines indicate the onset of the non-Darcy regime where the pressure gradient due to linear term becomes less than 99% of the total..... 64

Figure 4-7: The dimensionless permeability K* as a function of Re shows the transition from the Darcy to non-Darcy flow regimes for Samples 1, 3 and 7..... 65

Figure 4-8: Tortuosities and apparent permeabilities are plotted as functions of Re for the three virtual samples. 66

Figure 4-9: Calculated β factors for all three samples from the slopes of the graphs in the Forchheimer regime. 67

Figure 4-10: Calculated β factors for virtual samples with different PSD and porosities. 68

Figure 4-11: Tortuosities and apparent permeabilities are plotted as functions of Re for virtual samples with different porosity and PSD..... 69

Figure 4-12: Two porous media constructed with similar particle size distribution and porosity but different average grains irregularity (a) 3D virtual porous medium of Sample 2 with 0.22 porosity and 0.82 average grain sphericity. (b) 3D virtual porous medium of Sample 4 with 0.22 porosity and 0.75 average grain sphericity. Plots of flow streamlines within pores of two generated porous media (c) Flow streamline within pore structure of sample 2 (d) Flow streamline within pore structure of sample 4 by applying similar pressure gradient (8000 Pa) at the opposite cross sections perpendicular to the flow direction. The streamlines are colored according to the magnitude of velocity. 71

Figure 4-13: Departure from linear relationship between pressure gradient with velocity for two virtual Fontainebleau sandstones with similar porosities ($\Phi = 0.22$) but different average

grain sphericity (Sample 2 contain grains with average grains sphericity 0.82 and Sample 4 with average grains sphericity 0.75) is indicated by red solid line. 72

Figure 4-14: The dimensionless permeability K* as a function of Re shows the transition from the Darcy to non-Darcy flow regimes for sample 2 and sample 4. 73

Figure 4-15: Tortuosities and apparent permeabilities are plotted as functions of Re for two virtual samples. 74

Figure 4-16: Obtaining β factors for sample 2 and sample 4 from the slops of the graphs in the Forchheimer regime. 74

Figure 4-17: (a) Three-dimensional rendering of two-phase fluid occupancy at the end of drainage through Sample 4. (b) The connate water distribution profile at the end of drainage through Sample 4. (c) Pore structure after omitting connate water at the system. 79

Figure 4-18: Pressure gradient applied on two opposite faces perpendicular to fluid flow. The streamlines are colored according to the magnitude of velocity. 79

Figure 4-19: Departure from Darcy to non-Darcy regime for fully saturated ($\Phi = 0.22$) and unsaturated (containing immobile water at saturation of 8.7% PV) Fontainebleau sandstone is indicated with solid line. 80

Figure 4-20: The dimensionless permeability K* as a function of Re shows the transition from the Darcy to non-Darcy flow regimes (occurs at K*= 0.99) for fully saturated and unsaturated sandstone. 80

Figure 4-21: Tortuosities and apparent permeabilities are plotted as functions of Re for saturated and unsaturated sandstone 81

Figure 4-22: Obtaining of β factors for saturated and unsaturated of Sample 4 from the slops of the graphs in the Forchheimer flow regime. 81

NOMENCLATURE

Symbol	Unit	Description
A	Cm^2	Cross section perpendicular to flow
dp	m	Characteristics length
D_p	Micron	The Diameter of the related spherical particle
D_{50}	m	Mean grain diameter
E_e	V/m	Electric field
F	-	Formation factor
Fo	-	Forchheimer number
J	Amper $/m^2$	Current density
K *or* KD	D, mD or m^2	Darcy Permeability
KF	mD	Forchhemier permeability
Kg	mD	The gas effective permeability
K^*	-	Dimensionless permeability
L	mm	The straight-line length
$\langle \bar{\iota} \rangle$	mm	The Average tortuous length
p	Pa	Pressure
P	$Pa.m^3/kg$	Ratio of pressure to fluid density
$-\nabla p$	pa	Total pressure gradient
Q	Cm^3/s	Volumetric flow rate

Symbol	Unit	Description
R	*Ohm*	The electrical resistance of the material
Re^*	-	Critical Reynolds number
S_v	1/m	Specific surface area
S_{wr}	-	The residual water saturation
T	-	Tortuosity
u	m/s	Superficial velocity
U	m/s	Fluid velocity
$\langle \overline{U} \rangle$	m/s	The average velocity magnitude over the pore space
$\langle u_x \rangle$	m/s	The volumetric average velocity at the flow direction
V_e	Volt	The electric voltage
β	1/m	Non-Darcy coefficient
Φ	-	Porosity
μ	Pa. s	Viscosity
ρ	kg/m^3	Density
υ	m^2/s	The Kinematic viscosity of the fluid
σ	S/m	The electric conductivity of pore fluid (Brine)
Ψ	-	Average grain sphericity

1 INTRODUCTION

1.1 Background

3D virtual porous media can be either constructed by stacking CT scan images or from synthetic images generated by statistical approaches. These porous media can be used to extract the flow path network and simulate fluid flow through this network structure to obtain petrophysical properties such as permeability, electrical resistivity, and elastic moduli.

A revolution in digital rock characterization has been occurred since high-resolution CT- images provided the opportunity to capture all details and complexity of pore structure. (Lindquist and Venkatarangan, 1999; Ikeda *et al*. 2001; Dong and Blunt, 2009; Peng *et al*., 2012; Raeini *et al*.,2015). But real CT scan images with high-resolution of rock samples are not always available to generate 3D virtual porous media.

In contrast to high resolution x-ray tomography, utilizing statistical approaches to generate synthetic porous media based on PSD and porosity of real sands are less expensive and less time consuming. This is particularly true for unconsolidated media where PSD are abundantly available. Moreover, statistical approaches provide us the opportunity to deeply investigate the effects of one specific parameter (e.g. grain irregularity, particle size distribution, porosity, mean grain size) against others on transport properties (Bryant et al,1993; Garcia et al,2009; Day, 1965; Han et al., 1986). Therefore, statistical approaches give us a better understanding of the importance of each parameter on transport phenomena in a porous medium.

In this research, the main topic of interest is to propose a novel algorithm inspired from the crystallization process for numerical generation of 3D virtual porous media. The proposed algorithm allows control on grain geometry and orientation to investigate the influence of grains irregularity on petrophysical properties and onset on non-Darcy flow. Furthermore, the proposed algorithm is faster than other statistical models and also it provides the opportunity to control the shape, orientation and structure of the grains.

1.2 Novelty for Case of Study

- ✓ Compared to other presented algorithms to generate virtual 3D porous medium based on a given particle size distribution (PSD) and porosity, the proposed algorithm in this study is faster and more flexible. Besides, it is able to control the grain shapes and still honoring given particle size distribution and porosity.
- ✓ There is no limitation for construction of porous media at low porosity (i.e. it could be even less than 10%) while most of algorithms cannot cover low range porosity.
- ✓ There is no assumption for interpenetration among the grains, and grains could have a point, line or surface contact between each other. Grain interpenetration causes the constructed porous medium to not meet the real particle size distribution of rocks, but it can be used to generate corresponding “consolidated” virtual porous media.
- ✓ In the proposed algorithm, inspired from the crystallization process, the shape, orientation and structure of the grain can be readily controlled and provides this opportunity to investigate the effect of grain irregularity on transport properties.
- ✓ Using the simulation results on virtual porous media; two correlations; one for estimation of permeability vs. porosity and another for estimation of formation factor as a function

of porosity are presented. Compared to other available correlations, it was shown that the presented correlations provide better estimations against measured data sets.

1.3 Simulation Tools

The C# programming language is used to develop a user-friendly pattern generator which is able to generate virtual porous media based on predefined porosity and particle size distribution (PSD). The constructed medium is fed either to computational fluid dynamics (CFD) open-source package as finite volume based software or to COMSOL Multiphysics (finite element based software) to estimate the permeability and electrical resistivity values.

1.4 Organization of Dissertation

Chapter 2 briefly explains some well-known pattern generator methodologies for construction of porous media based on predefined porosity and particle size distribution. Moreover, in this chapter, an innovative approach will be proposed for numerical construction of virtual porous media.

In Chapter 3, different numerical approaches to estimate petrophysical properties of rocks for single phase flow are briefly reviewed. Moreover, simulation results on virtual constructed porous media ended up with two correlations; one for estimation of permeability vs. porosity and the other one for estimation of formation factor as a function of porosity.

In Chapter 4, the effects of grain irregularity, porosity and residual water on onset of non-Darcy flow through porous media are investigated. Furthermore, the simulation results are compared to experimental data sets.

In Chapter 5, general conclusions obtained on this research are collected and briefly discussed.

2 NUMERICAL CONSTRUCTION OF VIRTUAL POROUS MEDIA

2.1 Literature Review

Generation and modeling of random packings of spherical grains has a variety of applications in different fields including mathematics, chemical and petroleum engineering (Powell, 1980; Jin, 2003; Bashtani et al., 2016; Skripkin et al., 2016; Afshari et al., 2016 and Taheri et al., 2017).

Developing of different pattern generators to generate three-dimensional virtual porous media have been proposed by many researchers via packing of spherical grains. Packing methods of spheres are generally classified into regular and irregular arrangement methods.

In regular arrangement (lattice arrangement), equal spheres form a very symmetric pattern in contrast to irregular arrangement (Figure 2-1.a). Different lattice packing methods with various density arrangement are presented by several researchers (Carl Friedrich Gauss,1831; Brown and Hawksley,1945; László, 1953; Sloane,1977 and Visscher and Bolsterli,1973).

As many problems in the chemical and physical sciences can be related to packing problems where the grain size is distributed, researchers presented various irregular arrangement methods of spheres in a cube container (Figure 2-1.b) (Hudson,1949; Nolan and Kavanagh, 1995; O'Toole et al., 2011; de Laat et al., 2014).

Three commonly used computerized packing algorithms are the sequential sphere dropping algorithm, cooperative swelling spheres algorithm and geological rock formation. All trying to mimic different stages of rock formation including deposition/packing, compaction and cementation processes.

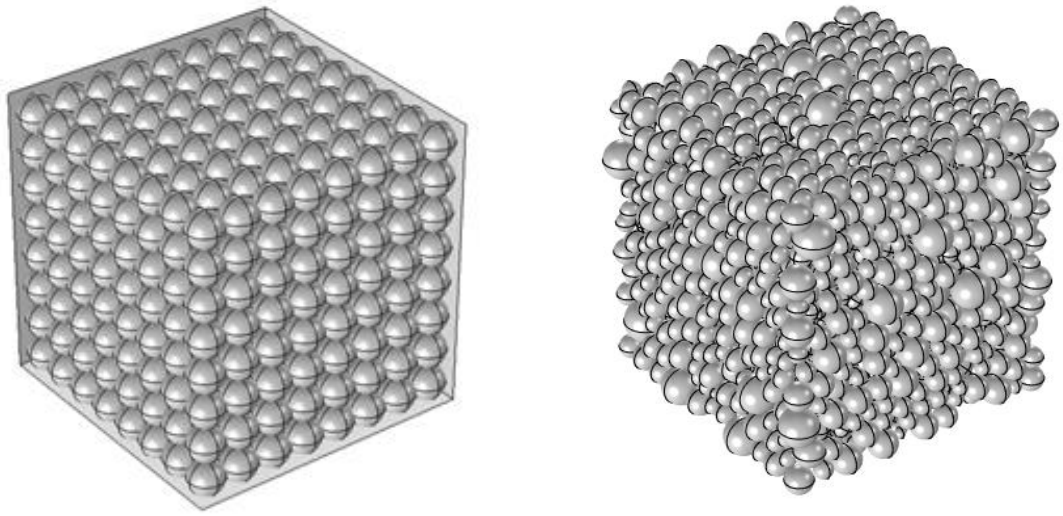

(a) (b)

Figure 2-1: Random packing of sphere (a) Random packing of mono-sized sphere. (b) Random packing of sphere with different grain size. (Taheri et al., 2017)

In the sequential sphere dropping method, a packing is built by pouring spherical particles one-by-one into a container under gravity in a control manner (Rodriguez, 1986). Figure 2-2 schematically illustrates different steps of the particle deposition method.

In the cooperative swelling spheres algorithm (Clarke and Wiley, 1987), a virtual random packing of spherical particles is constructed based on swelling of spheres in a container. The method generates a denser medium compared to the sequential addition algorithm. Different steps of the swelling spheres algorithm are shown at Figure 2-3.

In the geological rock formation algorithm, different stages of rock formation (deposition/packing, compaction, cementation and diagenesis) are simulated (Figure 2-4). The main difference of this approach compared to the aforementioned algorithms is that in this approach, spheres are allowed to interpenetrate vertically (Bryant et al.,1993). However, this process is time consuming and the grain shape and structure (irregularities) cannot be controlled during the construction.

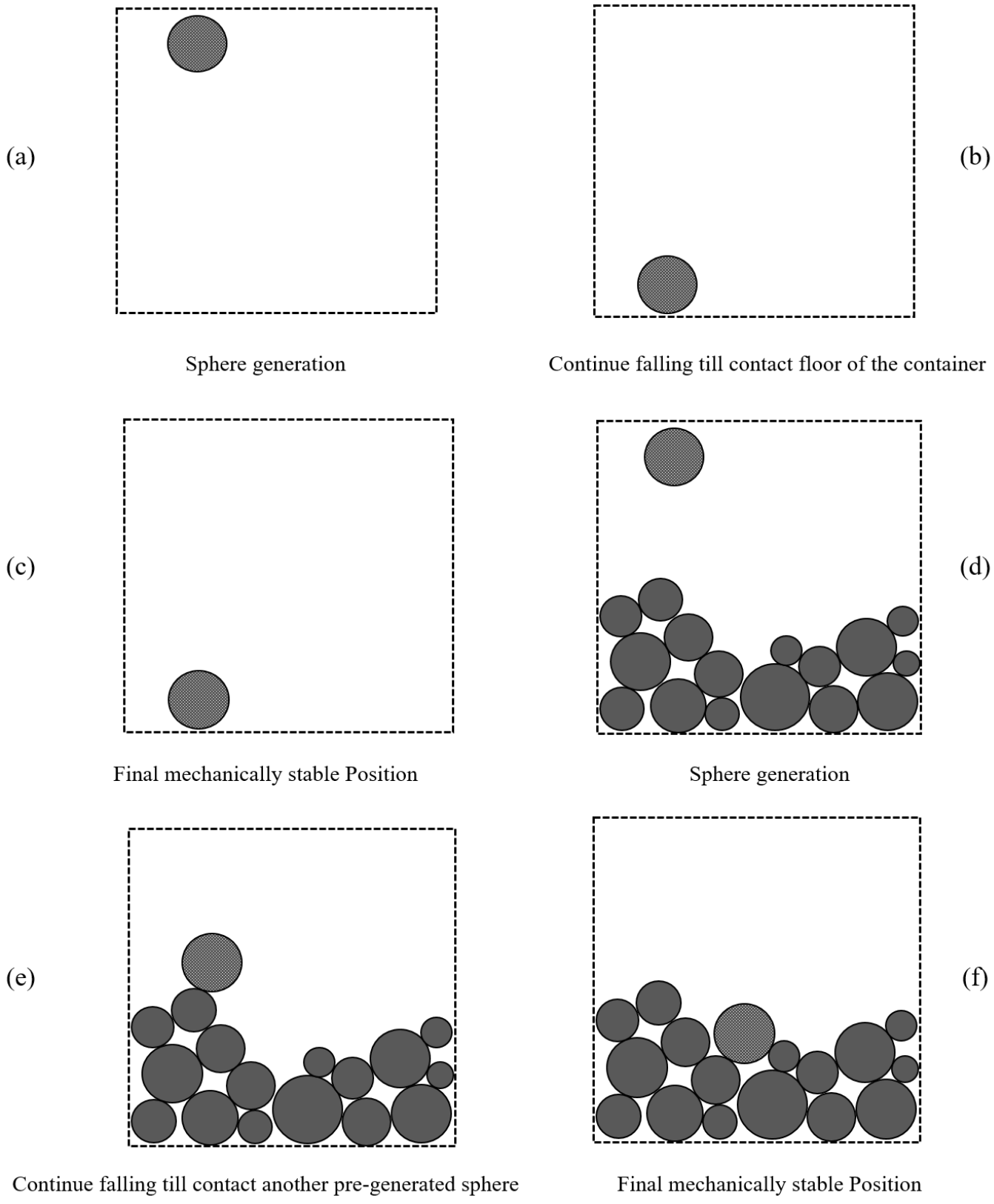

Figure 2-2: Different steps of Particle Deposition Method (Taheri et al., 2015)

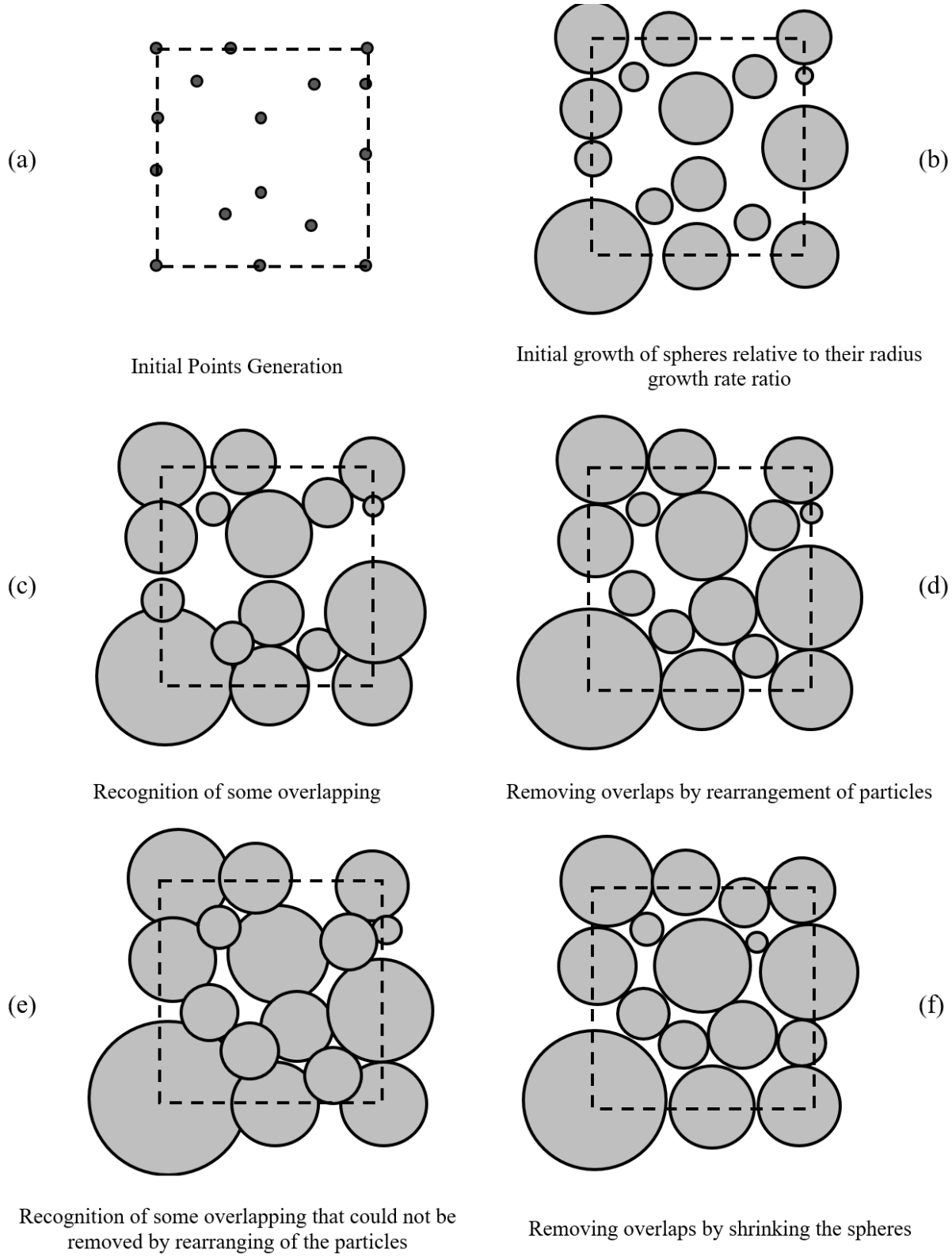

Figure 2-3: Different steps of swelling spheres algorithm (Taheri et al., 2017).

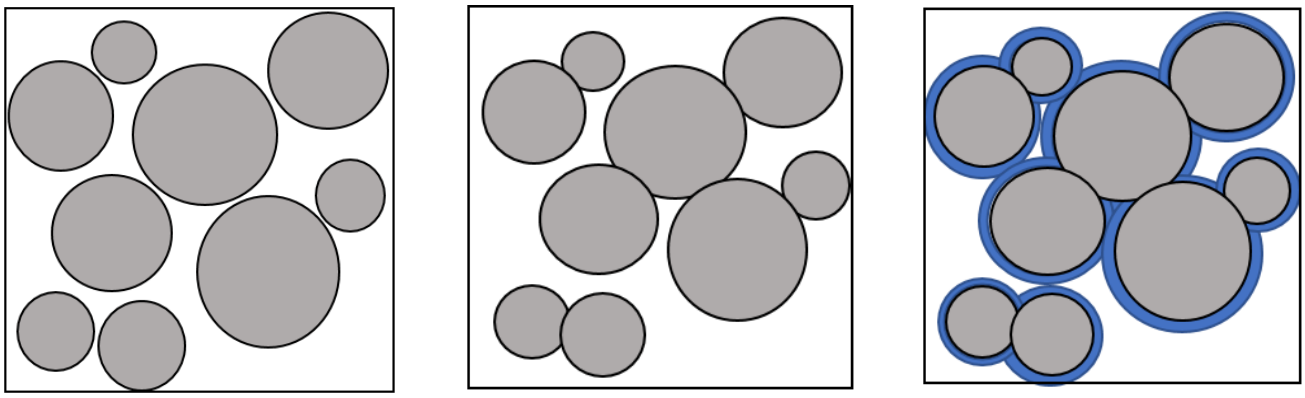

(a) (b) (c)

Figure 2-4: Different stage of rock formation. (a) deposition/packing of spheres representing sediment of clean, well sorted sand. (b) compaction forces sphere to interpenetrate each other. (c) a thin layer of cement covers each compacted sphere.

Many numerical algorithms have been developed to generate virtual random packings of non-spherical particles (Schwartz and Banavar, 1989; Coelho, 1997; Pilloti, 1997; Garcia et al.,2009) to examine the influence of grains geometry on transport properties. Schwartz and Banavar, 1989. (Figure 2-5.a) numerically constructed packs of spheres. In their algorithm, the spheres were deformed into ellipses while the center of each sphere was kept fixed. In their study, it was concluded that permeability anisotropy is strongly affected by the particle shape. Coelho et al. (1997) (Figure 2-5.b) considered mono-sized spherical and elliptical grains to simulate grains irregularity in rocks. They concluded that transport properties in the high porosity range (40% - 80%) is independent of the shape of the particles used in their numerical construction model. In another research, Pilotti et al. (1998) (Figure 2-5.c) deformed the surface of sphere particles to model the irregularity in a sandstone. In later studies, researchers investigated the effect of grain irregularity on petrophysical properties of porous material such as hydraulic permeability and electrical conductivity. Garcia et al. (2009) constructed and compared several packs including different grain shapes found in natural sands by simulation of settling under gravity using the discrete element method (DEM). They found out that packs of irregular particles are less

permeable than regular sphere packs with the same porosity. Also, their results indicated that the details of irregularity have only a small impact on the permeability of the systems. Furthermore, hydraulic conductivity is more affected by porosity and mean grain size. There are few limitations and drawbacks when applying the published approaches of random spherical packing methods to generate a porous medium. For instance, considering a spherical shape for grains is far from reality, leading to overestimation of physical properties of porous materials. Moreover, if interpenetration does not occur for spherical grains in a virtual sand pack, these methods will not be able to generate a porous medium with porosity less than 35-38% based on the given particle size distribution. Nonetheless, even for spherical packing methods with grain interpenetration (e.g. the model presented by Bryant et al., 1993), there are few disadvantages. For example, the author expressed that the measured vertical permeability for generated 3D virtual sandstone is more than the horizontal permeability, which is in contrast with reality. The reason for this contradiction is that the compaction applies at vertical direction leading to short vertical flow paths.

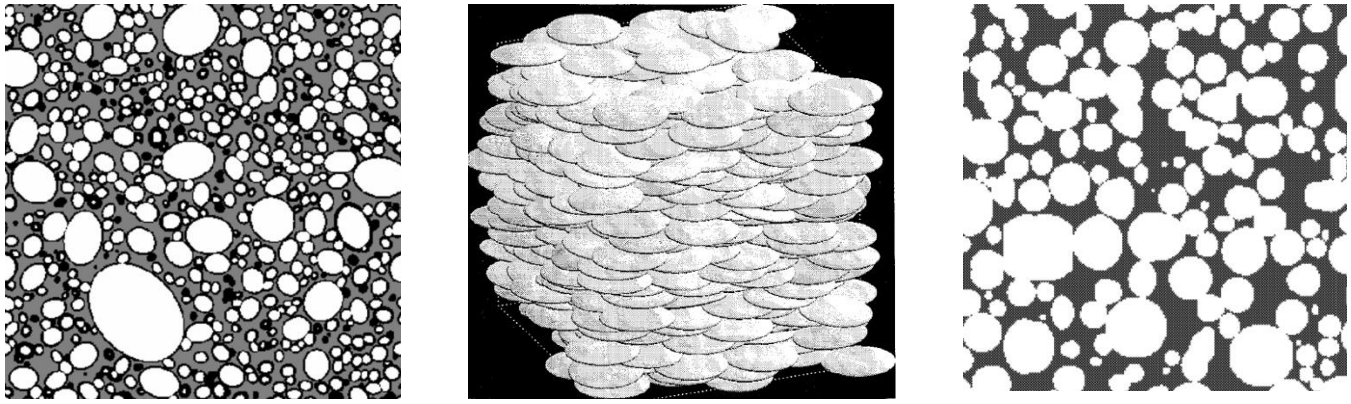

(a) (b) (c)

Figure 2-5: Random packing of non-spherical grain. a) Schwartz and Banavar (1989) numerically constructed packs of spheres, then, the spheres were deformed into ellipses b) Coelho (1996) used oblate ellipsoids packing to investigate the effect of grain geometry on transport properties. C) Pilloti (1997) deformed the surface of spherical grains to convert spherical grains to irregular grains.

2.2 Developed pattern generator

The main idea for the proposed approach in this project came from a crystallization concept. The crystallization process consists of two major stages, nuclei formation (nucleation) and crystal growth (crystallization). In the nucleation step, all grains need a nucleus location (center) to commence crystallization. For each grain with a given size, the location of the nucleus is determined by a random search through the entire free void space. The searching algorithm would find the appropriate location that could properly accommodate the grain. When the location is found, then the grain starts growing in different directions. The probability of growing in different directions could be controlled via defining promotion factors. If all directions have the same probability (controlled by user) and enough space to grow, the final grain shape would be spherical. Otherwise the grains will have various shapes. In the proposed model, each grain pixel (voxel) mimics a molecule or atom gathering into a cluster as expected to occur in a real crystallization process. The grain (crystal) grows in different directions by biased user defined increments. The size of each grain is randomly chosen from the given particle size distribution. The crystallization process continues until the porosity of the whole medium reaches the target porosity. Consequently, the constructed virtual 3D porous medium would have the same PSD and the same porosity as the provided input parameters. Furthermore, the shape and geometry of the grains would be adjusted if required to be more realistic. Figure 2-6 illustrates the grain formation (pseudo-crystallization process) in a simple 2-D schematic.

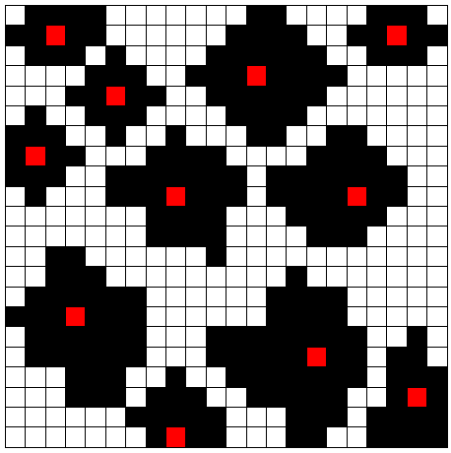

Figure 2-6: Simple representation of 2-D construction of a porous medium (pixel based). The red pixels are the center of each grain (nucleus). The locations of the nuclei are chosen randomly in the proposed algorithm. The black pixels are solids and white pixels are pores.

In the presented procedure, porosity, particle size distribution, cube size based on number of voxel (3D pixel) and synthetic pack length (in mm) should be provided. Accordingly, the resolution of a single voxel is determined. Alyafei et al., 2015 studied the effect of image resolution on estimation of physical properties on pore network modeling and direct simulation. They found that image resolution can have a significant effect on estimation of petrophysical properties. The minimum image resolution should be equal or less than the minimum sample throat size in order to capture the smallest flow paths. The particle size distribution in Figure 2-7.a is the cumulative frequency of the particles with specific size which is usually reported based on weight fractions. However, in the presented methodology, it is required to convert the weight based PSD into a number based one. Then the PSD is inversed to get the equivalent percent point function (PPF) Figure 2-7.b. This PPF is applied to randomly assign a specific diameter to the grains in the porous medium. A randomly generated probability number (between 0 and 100.0) is fed to the PPF and the corresponding grain diameter is obtained.

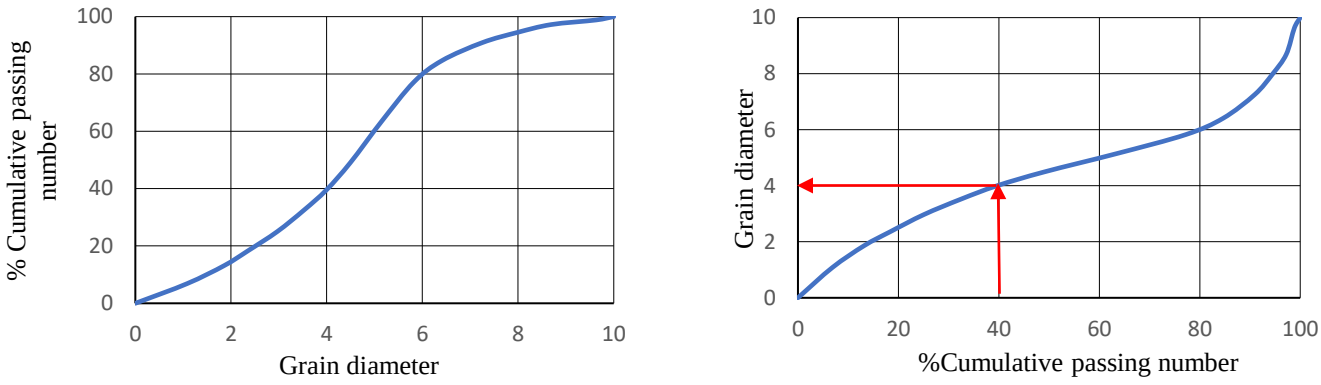

(a) Cumulative frequency distribution

(b) Percent point function

Figure 2-7: Converting cumulative frequency distribution to percent point function to dedicate a dimeter to a grain.

The irregular grain volume would have the same volume as the spherical grain with the assigned diameter. However, they would have different surface areas. The concept of sphericity is considered here to measure the degree of irregularity. Sphericity is the ratio of the surface area of a perfect sphere to the surface area of a non-spherical particle with the same volume (Wadell, 1935). In the presented algorithm, average grain sphericity can be controlled by adjusting the parameters called directional growth promotion multipliers. (i.e. if all directional growth promotion multipliers approach unity, the algorithm will create perfect spherical grains). After adding each new grain to the medium, the porosity is checked against the target porosity. If they meet, the Pseudo-Crystallization process will stop.

One Advantage of the proposed method is that it always meets the target porosity and honors the given PSD. As the target porosity declines, grains tend to be more irregular but still obeying the same PSD (Figure 2-8) (i.e. average grain sphericity decreases to satisfy the grain size distribution which is set by the user). In some previous pattern generation methods grains tend to have smaller mean grain size by porosity decrement, which affects the grain size distribution and thus violate to honor the provided PSD (Bryant et al.,1993).

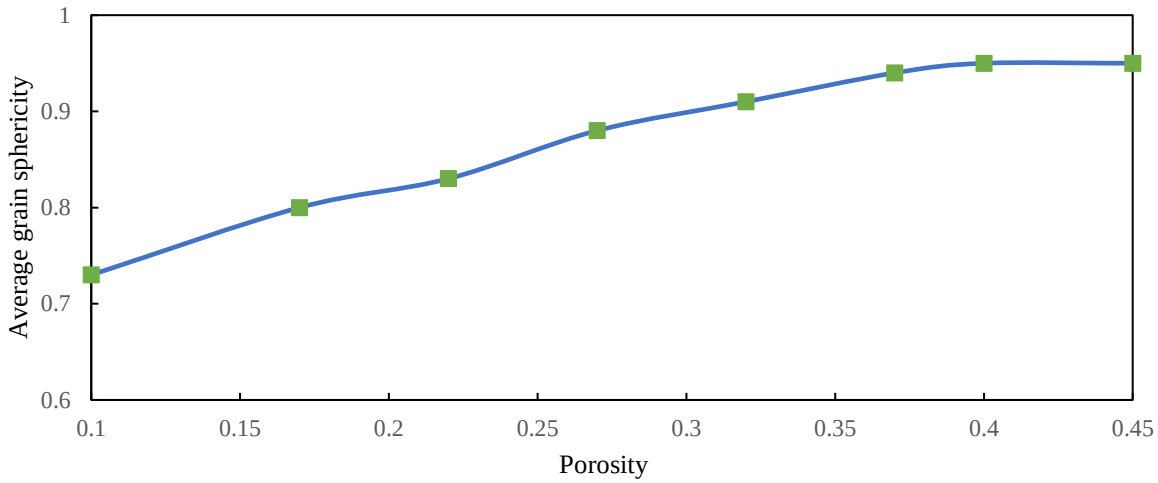

Figure 2-8: Sphericity variation vs. porosity with the same PSD .The proposed method always meets the target porosity and honors the given PSD. As the target porosity declines, grains tend to be more irregular but still obeying the same PSD.

For a better illustration of the algorithm, a 2D grain slice growth is schematically shown in Figure 2-9. Direction 1 is randomly chosen as the first direction for the grain to grow (Figure 2-9. b). The directional growth continues until it reaches the pre-specified increment. The program calculates the distance between the center of the grain and every pixel which is included in the chosen slice direction. Similarly, other directions (which may have different probabilities and growth increments) are randomly chosen. Each time a direction is chosen, its probability will be either boosted or dampened based on its directional growth promotion multiplier. The growing in different directions (Pseudo-Crystallization) will continue until the volume of the irregular grain becomes equal to the volume of a perfect sphere with the allocated radius. All these steps will be repeated for all grains inside the porous medium until the target porosity is achieved. Each grain can keep growing until touches another grain in any direction and then the grain will miss the opportunity to grow in that direction anymore. However, there is yet opportunity for other directions to be selected for growth.

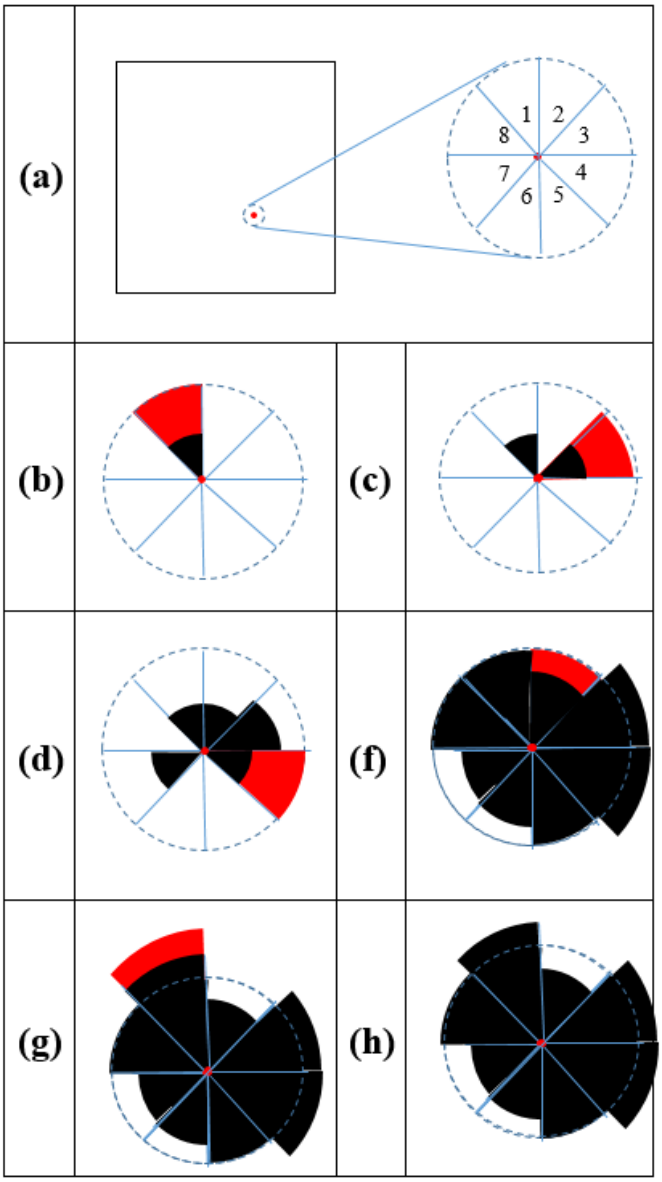

Figure 2-9: 2D Schematic visual illustration of incrementally radial growth (crystallization) of a grain at 8 different directions; The user could control the sphericity of the grain by assigning different probability and promotional multiplier at various directions. The red section in (b-h) shows the incremental growth at that stage of crystallization.

Few examples of generated irregular grains with different sphericities are shown in Figure 2-10.

The proposed algorithm to generate porous media is summarized in Figure 2-11.

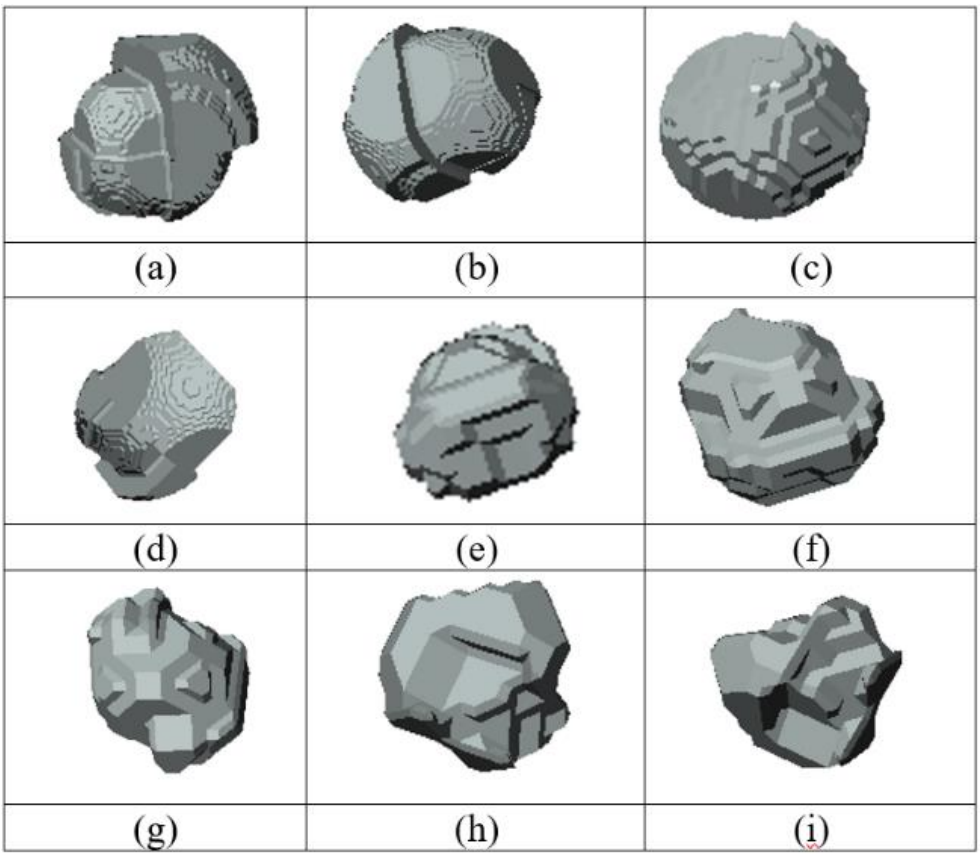

Figure 2-10: Examples of generated irregular grain shapes with different sphericities (ψ). a) ψ=0.87, b) ψ =0.93, c) ψ =0.97, d) ψ =0.83, e) ψ =0.78, f) ψ =0.76, g) ψ =0.72, h) ψ = 0.73, j) ψ =0.7.

It is worth mentioning that the total number of grains inside the virtual porous medium should be sufficiently large; otherwise it will not be a reliable representative of the real sand pack or sandstone. The effect of grain population on transport phenomena estimation depends on how the grains are distributed. Thus, the number of grains included becomes a variable for sensitivity analysis. A sensitivity analysis for 20 generated consolidated samples with the same particle size distribution (Fontainebleau PSD) and porosity (Φ =0.152) including various number of grains is conducted. The permeability values of all 20 samples were calculated and the results are sorted according to the number of grains. Simulated results demonstrated that measured physical properties such as permeability would not be reliable, unless the number of grains in the porous medium exceeds a threshold value (Figure 2-12). In other words, the higher number of grains in

the medium, the less inconsistency between calculated permeability of the samples. It is observed that permeability values of the generated samples with more than 1500 grains converge to a dependable value. In this study, the converging permeability was about 1104 mD.

Taheri et al. (2017) performed a sensitivity analysis to determine the appropriate number of spherical grains inside a synthetic porous medium containing spherical grain. According to their analysis, it is implied that the permeability variability is negligible for sand packs containing at least 2000-2500 grains. In the presented study, the total number of voxels inside the virtual porous medium (cube container) can be calculated even before executing the construction algorithm if user follows a specific number of grains based on the predefined cube size and given PSD. The total number of voxel inside the virtual porous medium (cube) can be calculated based on the size of each direction (Nx * Ny * Nz). Porosity is also predefined as an input data by user. Based on the provided particle size distribution, a specific radius is dedicated for every single grain by using the PPF function. Therefore, the total number of voxels which is going to be considered as grain can be calculated by summation of the volume of every single grain. After adding each grain, the porosity gets updated until the target porosity is me. The number of grains inside the porous medium can be estimated accordingly. This is a validation check before execution of the real construction algorithm which will alert the user if the size of the media (cube container) is not large enough to represent a dependable sample. Consequently, it will save time before going through the main execution of semi-crystallization process and flow simulation.

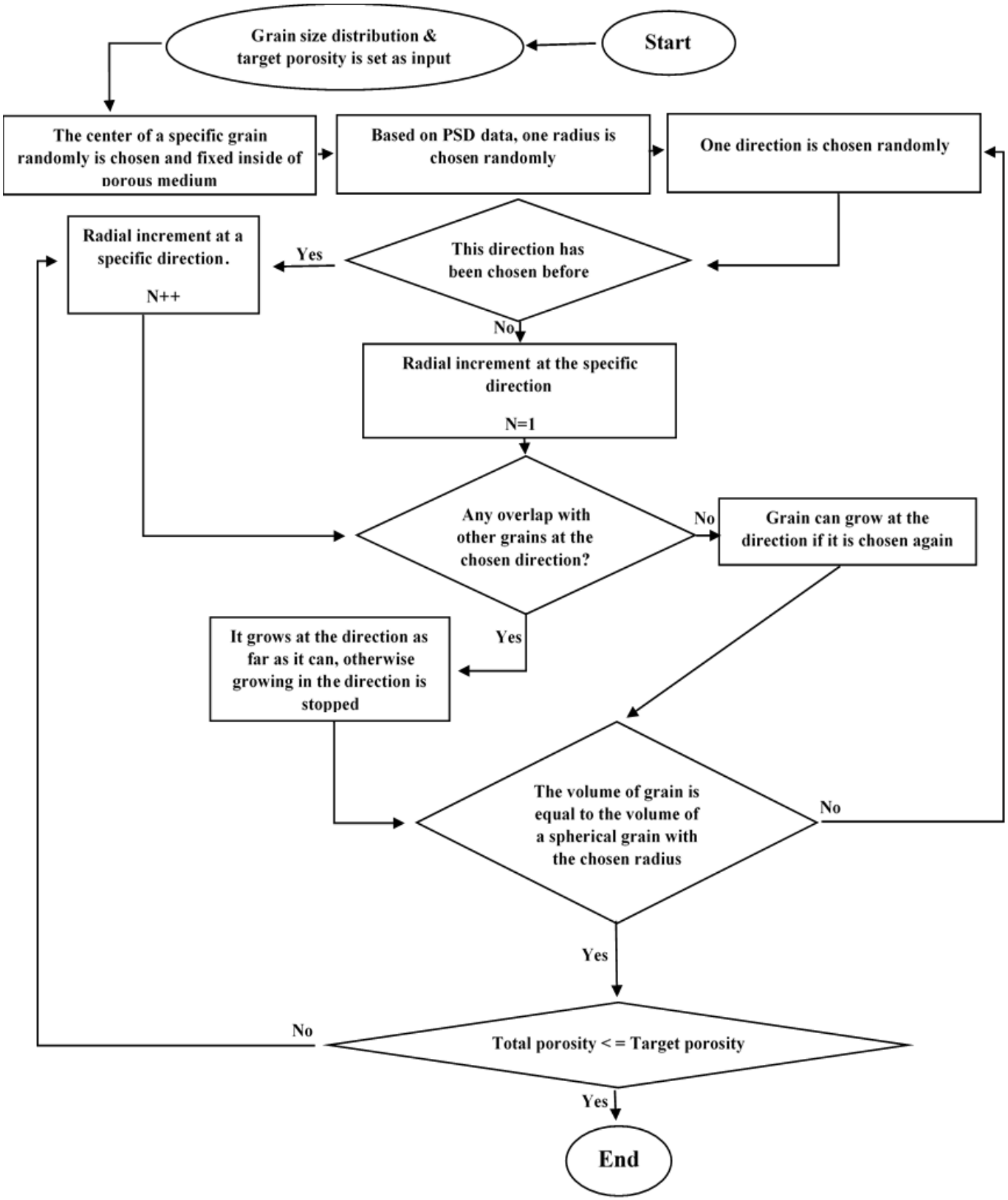

Figure 2-11: The Pseudo-Crystallization algorithm to generate a 3D porous medium containing irregular grains.

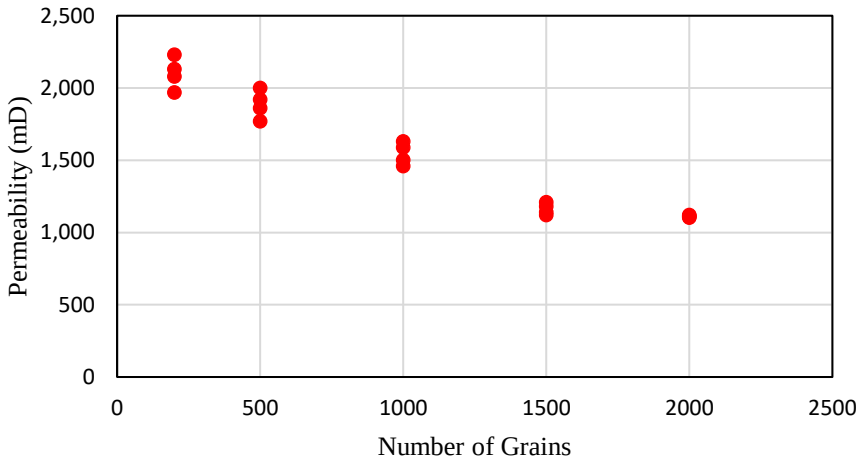

Figure 2-12: Effect of number of grains on the calculated absolute permeability in 20 reconstructed consolidated samples with the same particle size distribution (Fontainebleau PSD) and porosity (Φ =0.152).

3 NUMERICAL CALCULATION OF PETROPHYSICAL PROPERTIES

3.1 Introduction

The origin of observable macroscopic behavior of fluid is what occurring on a microscopic level. Thus, simulation of a process on the macroscopic scale will not be reliable and accurate if there is not an appropriate understanding of the details occurring at a microscopic level in the porous media.

The transport properties of a porous medium can be dependably determined if we can solve the physical equations exactly on a real pore space; provided that all microscopic and macroscopic details description of pore geometry is known.

As conducting physical experiment at micro-scale is not feasible, numerical models allow us to investigate the range of behavior that cannot be studied experimentally. For instance, numerical simulation provides us the opportunity to study the effect of some geometrical parameters (e.g. grain irregularity) on petrophysical properties which are not easy to be examined experimentally (Garcia et al., (2009)).

Among all numerical techniques, pore scale modeling received lots of interest to use for studying the impact of pore-level phenomena on fluid flow behavior and macroscopic flow properties (Blunt et al., 2002; Ovaysi and Piri, 2010; Santiago et al., 2016; Ghomeshi et al., 2018). Pore scale modeling offers a direct approach to estimate petrophysical properties in porous media. Applying pore scale modeling to study physics of transport phenomena is less expensive and time-consuming compare to experimental tasks.

Pore-level modeling is generally divided into two main categories:

- Pore network modeling
- Direct pore-level modeling

3.1.1 Pore Network Modeling

Pore network modeling is a common numerical method to simulate fluid flow in porous medium.

Presenting a reliable pore structure for a porous material have been one of most challenging topics in pore networking modeling. The primary pore structure model was considered as a cluster of separated capillary tubes. Fatt (1956) found that pore bodies in void structure are connected to each other and cross-flow exists among them. He proposed a pore network model to consider this cross flow. His model can almost follow aspects of flow in a porous medium.

Considering a simplified geometry for pore-bodies and pore-throats reduces the complexity of void space which make it much easier to be solved by using (semi-) analytical solutions. Network modeling are being used to simulate fluid flow in porous media to measure transport properties such as absolute permeability, formation factor, relative permeability and capillary pressure.

In the past decades, many different types of pore network generators were presented to mimic real void space in rocks (Valvatne and Blunt, 2004; Varloteaux et al., 2013 and Békri and Vizika, 2006). As an example, the network with a regular lattice structure where each pore-body is assumed to be connected by six identical diameter pore-throats determined based on a given probability density function (Figure 3-1.a). In this model, the constant aspect ratio is assumed between pore-body and pore-throat diameters. Békri and Vizika, 2006 applied this model to estimate petrophysical properties to homogenous carbonate.

Researchers have recently developed an alternative to regular lattice structure approach which is able to mimic the real pore structure more appropriately. In this approach, synthetic pore structure of a rock is generated according to real medium geometry.

To capture the exact 3D pore space of the rock, a virtual 3D image is extracted by using X-ray micro-tomography. Then, pores and rocks are distinguished in 3D image by threshold binarization. At this point, the virtual pore structure is extracted and according to the conceptual approach of the pore network model, the pore-bodies need to be distinct from pore-throats in virtual 3D pore structure based on pore space partitioning (Figure 3-1.b). This model assumes the pore structure as a collection of pores connected by throats (cylindrical channel with a circular, triangular or square cross section) through which transport properties can be computed (Blunt et al, 2002; Laroche and Vizika, 2005; Valvatne and Blunt, 2004; Faisal and Kantzas, 2016).

Quasi-static flow displacements are conducting to pore structure in order to simulate multiphase flow inside the pore structure. Capillary pressure or relative permeability curves can be extracted as output results. The capillary pressure curve is obtained by applying rising pressure on the injected fluid while the pressure of the fluid in pore structure is kept constant. It is assumed that viscous pressure gradients are negligible and the pressure of each phase is constant everywhere within the network. The absolute permeability of the pore structure is obtained from Darcy's law by considering single phase flow inside the porous medium. The two phase relative permeability curves are calculated at each step of the two-phase quasi-static displacements when capillary equilibrium is reached. Laroche and Vizika, (2005) assessed the accuracy of network modeling to calculate transport properties.

Some researchers (Youssef et al., 2007; Caubit et al., 2009) reported that prediction of pore network modeling to estimate the petrophysical properties of the porous medium is not accurate

because the extracted pore structure in pore network modeling is not able to capture complex and detailed pore geometries. Moreover, idealizing the geometry of pore body and pore-throat lead to missing of some topological features which can affect the predictions of petrophysical properties.

Youssef et al. (2007) demonstrated that the predictability of pore network modeling depends on how accurate the extracted pore structure is compared to real void space in rock. He found that extracting virtual pore structure from high resolution micro-CT images which can capture all details and topological properties of the pore space leading to more appropriate results.

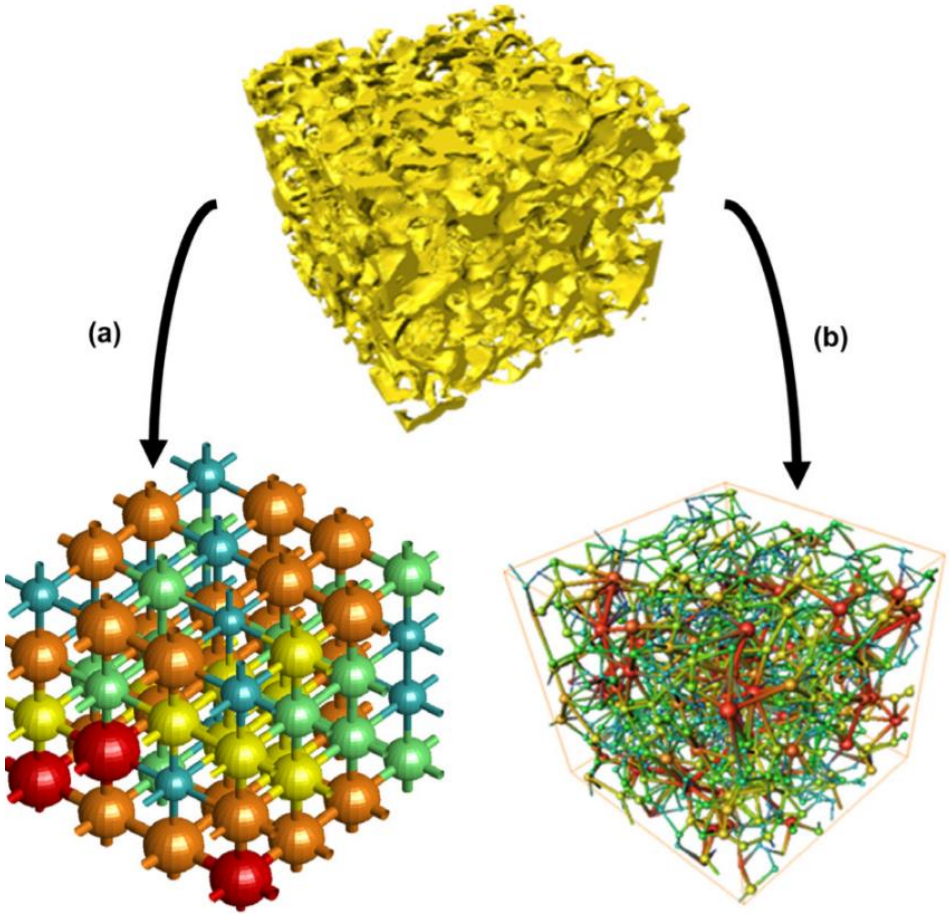

Figure 3-1: Pore network models: (a) model reconstructed with a regular lattice (b) model extracted from the micro tomography images. (Varloteaux et al., 2013).

3.1.2 Direct Modeling

Progress in image analysis and x-ray tomography provide the opportunity to extract complex and detailed void spaces to simulate transport phenomena directly on pore space images. Using these technologies capable us to eliminate the simplified assumptions considered in pore network modeling (Lindquist and Venkatarangan 1999; Wildenschild et al., 2005; Wildenschild and Sheppard, 2013; Ghomeshi et al., 2015).

Direct numerical modeling can be generally classified into two categories: conventional computational fluid dynamics (CFD) methods, which solve the governing equations at the continuum scale; and unconventional numerical methods, which utilize microscopic kinetic equations to recover the macroscopic flow equation in the long-time and large-scale limit.

The Lattice Boltzmann Method is based on a simplified gas-kinetic model. This approach is designed to bridge the gap between the micro-scale and the macro-scale by focusing on the behavior of a collection of particles as a unit instead of on the individual behavior of single particles. This scale is known as the mesoscopic scale (Almalowi, 2012).

The finite difference approach is another method of direct numerical modeling used extensively to model flow at the pore scale (Adler, 1988; Schwartz et al., 1989; Manwart, et. al., 2002). This method makes it possible to incorporate a wide variety of boundary conditions, such as constant pressure or a no-slip boundary condition.

Direct simulations can be applied directly on pore structure to computed flow and transport properties on three-dimensional pore space.

Arns et al. (2001) applied direct simulation on microtomographic images of Fontainebleau sandstone to estimate transport properties of the sandstone. The simulation results were in excellent agreement with experimental measurements over a wide range of porosity.

Auzerais et al. (1996) used high resolution micro-CT image to simulate fluid flow in virtual 3D porous medium. They did a direct comparison between theoretical calculations and laboratory measurements and found it promising.

Spanne et al. (1994) applied direct simulation on void space which was derived from the tomographic image of the volume. Simulation result such as permeability and conductivity were computed and found in good agreement with experimental data.

Raeini et al. (2014) demonstrated the substantial effect of Pore-scale forces on the macroscopic behavior of multiphase flow through porous media. They conducted a finite volume method to simulate two-phase flow directly on micro-CT images of porous media.

Mostaghimi et al. (2012) used a finite-difference method based simulator to simulate fluid flow directly onto pore-space images extracted from a microcomputed-tomography (microCT) scan of rock cores. They estimated permeability, and compared the result with lattice-Boltzmann-method (LBM) numerical results and available experimental data.

Ramstad et al. (2012) applied two-phase lattice Boltzmann (LB) to simulate steady state and unsteady state experiments for measuring relative permeability on X-ray microtomography pore space images of Bentheimer and Berea sandstone. They concluded that the LB method is an appropriate approach to compute multiphase flow properties from pore space images.

3.2 Methodology

As it mentioned in previous chapter, pore-level modeling is generally divided into two main categories:

- Pore network modeling
- Direct pore-level modeling

Direct pore-level modeling has attracted lots of interest since image analysis and x-ray tomography progressed and provided the opportunity to solve the governing equations of flow directly on complex void spaces with no simplification.

The single-phase fluid flow in a porous medium can be precisely simulated by numerically solving the Navier-Stokes equation (Equation 3-1) as the momentum balance equation and the Continuity equation as a mass balance equation (Equation 3-2).

$$\rho\left(\frac{\partial\vec{V}}{\partial t}+\vec{V}.\nabla\vec{V}\right)=-\nabla\vec{P}+\mu\nabla^2\vec{V} \qquad 3\text{-}1$$

$$\frac{\partial\rho}{\partial t}+\nabla.\left(\rho\vec{V}\right)=0 \qquad 3\text{-}2$$

Where, $V=$ fluid velocity field, $t=$ time, $p=$ pressure, $\rho=$ density, and $\mu=$ Dynamic viscosity.

Although utilizing high resolution micro-CT images to generate virtual 3D porous medium is an appropriate approach to extract pore structure and simulate fluid flow through porous medium, it is an expensive approach compare to generating virtual porous medium statistically.

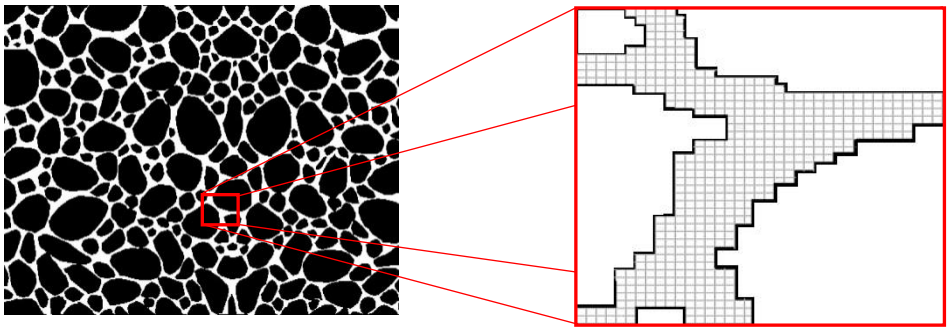

(a) (b)

Figure 3-2: (a)Sub pore scale gridding, (b) is zoomed area indicated in (a) (Taheri et al., 2010)

3.3 Single Phase Fluid Flow Simulation

After generating virtual 3D porous material based on given particle size distribution and porosity, pores and rocks are distinguished in 3D image by threshold binarization and then pore-networks representing the void spaces of the media needs to be extracted. Fluid flow is then simulated by applying a finite volume method (FVM). As a prerequisite step to speed up computations, we need to remove isolated islands from the pore volume. Since there is no flow in the trimmed void spaces, neglecting them should not have any impact on the flow properties (e.g. permeability) estimation. At the next step, to compute absolute permeability of the virtual media, boundary conditions are defined as a pressure gradient across the medium. The OpenFOAM software is used to run the simulation. The solver setting is adapted for steady state flow of single-phase incompressible fluid (SimpleFoam Solver). Consequently, the average velocity at each cross section can be calculated based on the simulation results. In our simulations, the assigned fluid properties are assumed to be the same as those of water. Knowing surface porosity at each cross section, absolute permeability can be calculated by using Darcy's law. In addition, COMSOL Multiphysics (finite element based software) is used to calculate the formation factors of the virtual porous media.

The governing equations for single-phase incompressible flow are the continuity, Equation 3-1, and the momentum conservation equations, Equation 3-2.

In our simulation, water is assumed as the pore fluid to calculate permeability. Physical properties are listed in Table 3-1.

Table 3-1: Water properties used in Absolute permeability calculation

Name	Unit	Symbol	value
Density	kg /m^3	ρ	1000
Viscosity	Pa / s	μ	0.001
Pressure difference	Pa	ΔP	5000

The no-slip boundary condition ($u = 0$) is adjusted at the solid boundaries (walls). The constant normal fluid pressure (5000 Pa) is set at the inlet while the outlet pressure is zero ($p = 0$).

The semi-implicit method for pressure-linked equations (SIMPLE) algorithm is utilized to deal with the pressure-velocity coupling.

In order to measure resistivity factor of the sample material, stationary electrical current is simulated using the following governing equation.

$$\nabla . J = \nabla . \sigma E_e = \nabla . (\sigma \nabla V_e) = 0 \qquad 3\text{-}3$$

Where J, E_e, V_e, and σ are current density, electric field, electric voltage and the electric conductivity of the pore fluid (Brine), respectively. Electric voltages at the boundaries are set to 5.0 V for the inlet and 0 V for the outlet, respectively. Brine physical properties used in formation factor calculation are listed in Table 3-2.

Using calculated average normal current density and Ohm's law, rock resistivity is calculated.

Table 3-2 : Brine physical properties used in formation factor calculation

Material	Voltage [Δv]	Density [kg/m^3]	Electrical Conductivity [S/m]	Dielectric constant
Brine	5	1000	5	81

3.4 Results and Discussion

The Pseudo-Crystallization approach was applied to generate virtual 3-D porous media providing grain size distribution and porosity from Fontainebleau sandstone samples. Fontainebleau is a natural, fine, well sorted sand with angular grains. The lab measured porosity and permeability for the Fontainebleau sandstone are 0.152 and 1100 mD respectively, reported by Keehem (2003). Also, the reported formation factor is 32. Figure 3-3 shows the grain size distribution of the sandstone sample.

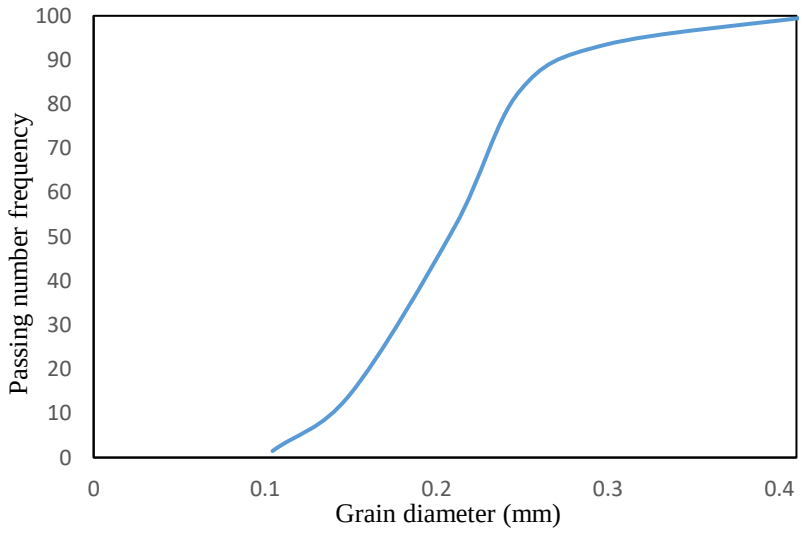

Figure 3-3: Grain size distribution of Fontainebleau sandstone (Extracted from Delfosse, 2004).

Figure 3-4 exhibits visual comparison of several 2D cross sections of the generated porous medium vs. real raw image sequences. Figure 3-5 displays the same comparison for the 3D images. Some of the simulation outcomes are presented in Figure 3-6.

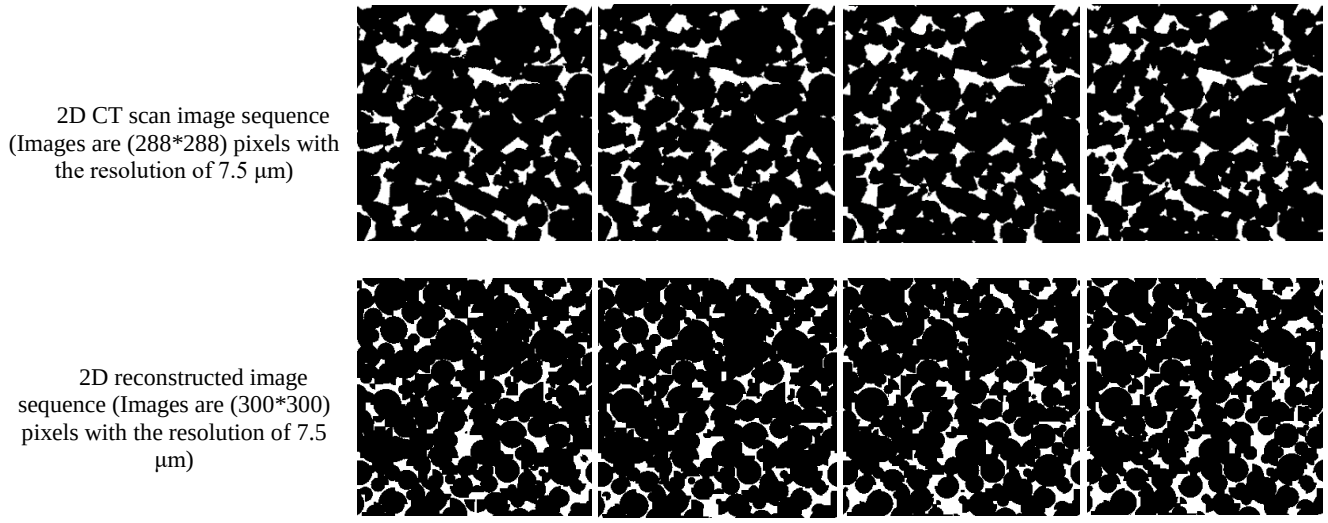

Figure 3-4: Comparison of 2D CT scan real image sequences with 2D image sequences generated by the proposed methodology (The generated 2D images are (300*300) pixels with the resolution of 7.5 µm). 2D real images of Fontainebleau were acquired at Brookhaven National Laboratory by Exxon- Mobil (The 2D real images are (288*288) with pixel scale of 7.5 µm).

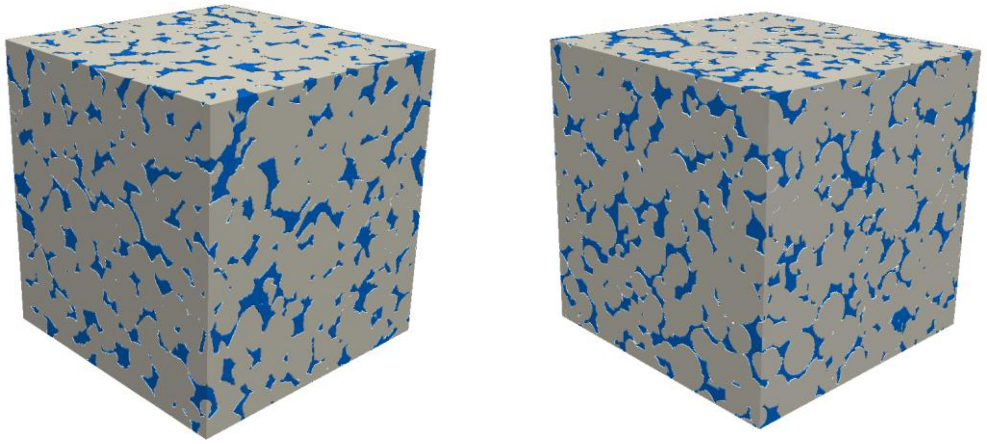

(a) 3D real image of Fontainebleau (b) 3D generated Fontainebleau sandstone by applying presented approach

Figure 3-5: (a) 3D real image of Fontainebleau, constructed by rendering of CT-scan images (acquired at Brookhaven National Laboratory by Exxon - Mobil (Digital Rock Physics Benchmarks, 2012)). The real image segmented binary data (288*288*300) with voxel scale of 7.5 µm. (b) 3D generated Fontainebleau sandstone. The generated porous medium is (300*300*300) with the resolution of 7.5 µm.

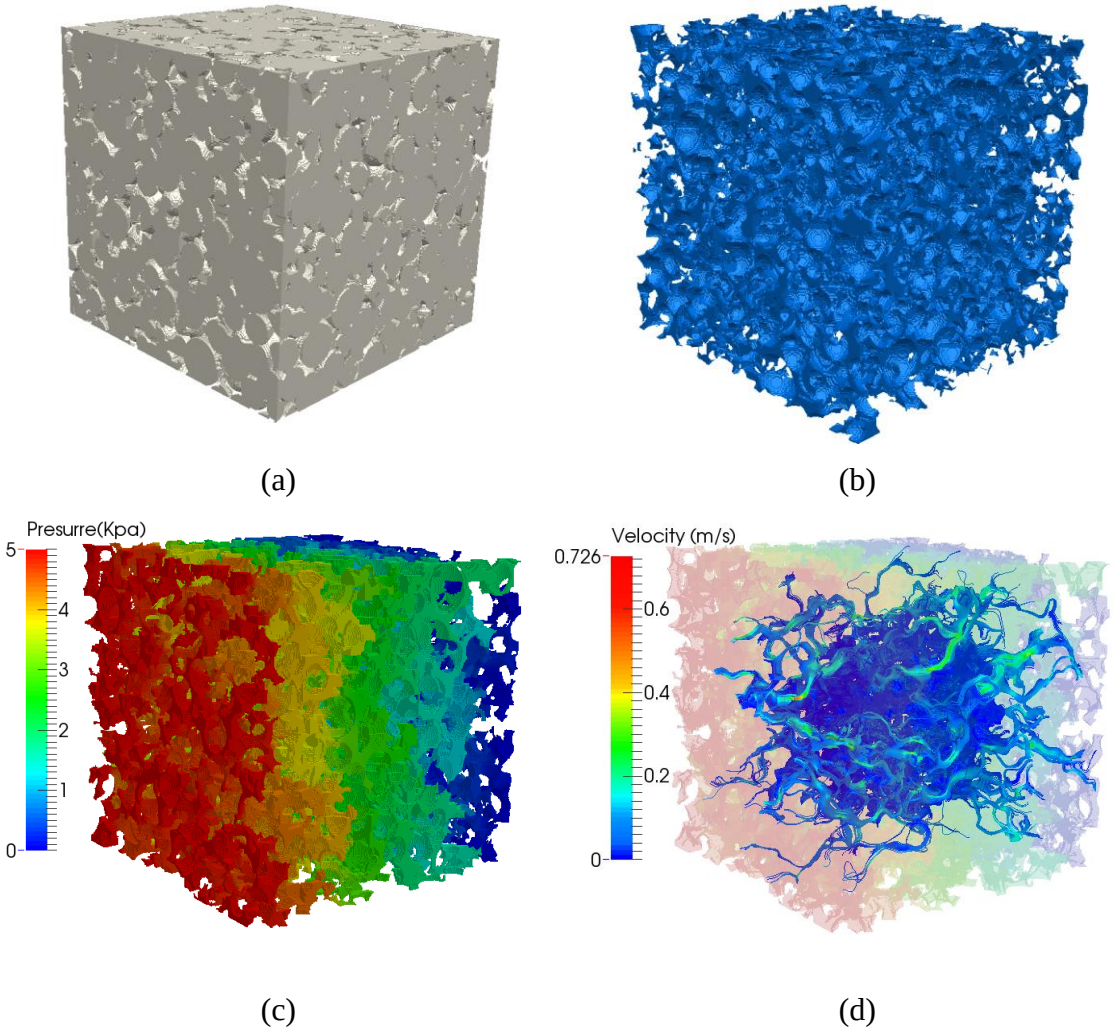

Figure 3-6. (a) 3D Solid matrix of Synthetic Fontainebleau sandstone. (b) 3D Pore structure of the generated sandstone. (c) pressure profile between two opposite faces of a medium (steady state solution) (d) Velocity profile (stream line).

As it was mentioned, rendering of real CT-images and generating virtual porous medium numerically are two approaches to digitally reconstruct porous materials. Rendering of real CT-images is expensive and time-consuming task comparing to numerical approaches to generate virtual porous media. Both approaches utilized to reconstruct 3D virtual media as a representative for Fontainebleau sandstone. Extracted pore and throat size distributions from generated virtual porous medium are comparable with the data extracted from the real images (Figure 3-7.a and Figure 3-7.b).

Table 3-3 shows the characteristics and simulation results of synthetic Fontainebleau sandstone. The results of these simulations are very close to the measured properties of the real sandstone samples. This could be considered as a validation of the proposed approach of numerical construction of the porous media. The generated synthetic Fontainebleau sandstone is almost homogeneous and the calculated permeabilities in different directions are reported in Table 3-4.

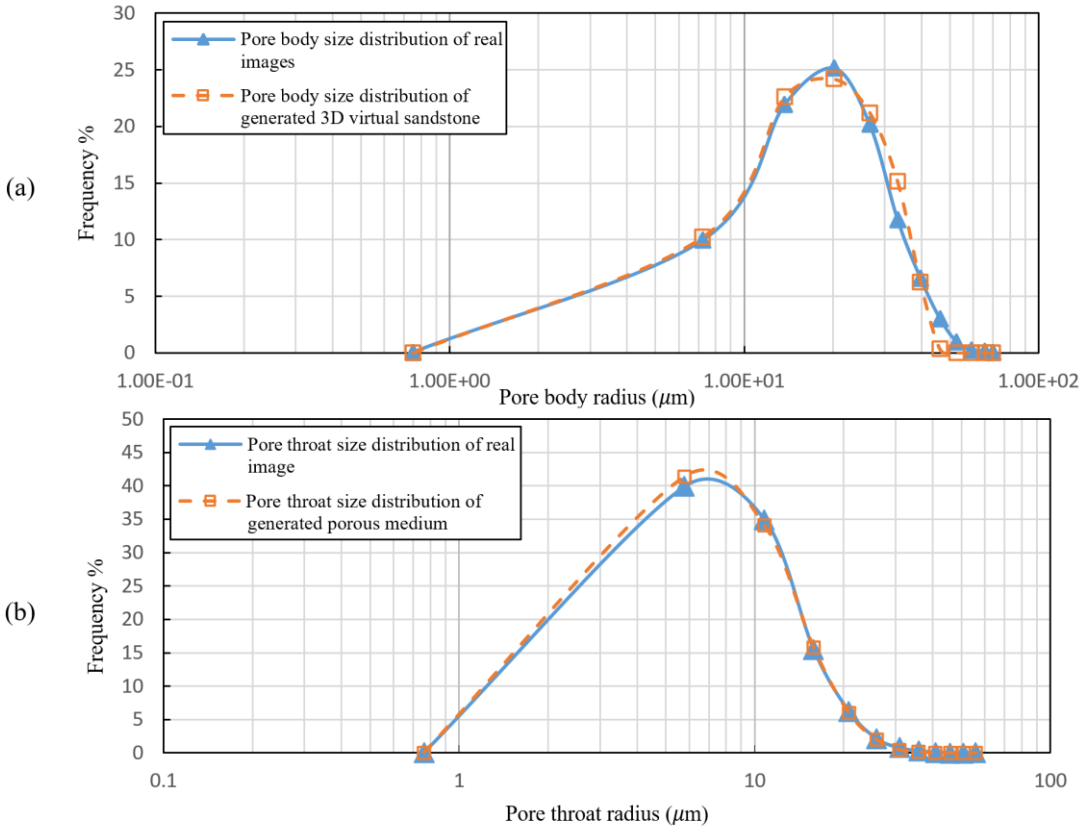

Figure 3-7: (a) Comparison of pore body size distribution for two 3D virtual Fontainebleau sandstone constructed by using real microscopic images and proposed 3D pattern generator. (b) Comparison of pore throat size distribution for both generated virtual Fontainebleau

Table 3-3: Characteristics and simulation results of virtual generated Fontainebleau sandstone

Characteristics of generated Fontainebleau sandstone		
Dimension (pixel)	300*300*300	
Synthetic Cube length (mm)	2.25	
Average Grain sphericity	0.80	
Resolution (μm)	7.5	
Mean Grain size (μm)	210	
Coordination number	4.1	
Simulation results through generated Fontainebleau sandstone		
Properties	Calculated	Measured Experimentally
Porosity	0.151	0.152
permeability (mD)	1104	1100
Formation factor	30.1	32

Table 3-4: Permeability in different directions for Fontainebleau sandstone

Direction	**Permeability (mD)**
X-Direction	1126
Y-direction	1035
Z-direction	1153
Harmonic average permeability	1088
Arithmetic average permeability	1104

Single phase permeability (*K*) can be expressed as a dimensionless parameter by dividing the absolute permeability value by square of harmonic mean grain diameter (Dullien, 2012; Sahimi, 2011 and Torquato, 2013):

$$\frac{K}{D_{50}^2} = F(\varphi).g_0(X_0, X_1, X_2, \dots) \qquad 3\text{-}4$$

where term F (Φ) denotes the dependency of the permeability on the porosity and g_0 is a geometric parameter, which depends on shape of grains, tortuosity, connectivity and how pores and throats are distributed (Ioannidis et al., 1996; Stewart et al.,2006; Bear, 2013). In this study, synthetic data

set is created to investigate the functionality of the dimensionless parameter ($\frac{K}{D_{50}^2}$) with porosity. Several porous media are constructed using the proposed methodology; considering a wide range of target porosity (0.1 - 0.4) and variety of PSD and grain sphericity values (Figure 3-8). Afterwards, simulations were run on these generated samples to compute their absolute permeabilities. Subsequently, based on these synthetic dataset, the dimensionless function of permeability versus porosity proposed by Bourbié et al.,1987. (Equation 3-5) was utilized and coefficient values (a and b) were calculated.

$$\frac{K}{D_{50}^2} = a.\Phi^b \qquad 3\text{-}5$$

where K is absolute permeability (m^2), Φ is volume porosity and D_{50} is mean grain diameter (m) and "a" and "b" are the correlation coefficients.

Calculated constants values (a and b in Equation 3-5) in this study and previous works (Garcia et al., 2009; Carman, 1937; Berg, 1975; Bourbie and Zinszner, 1985; Revil and Cathles, 1999) are listed in Table 3-5. Figure 3-9 shows a comparison of permeability estimation for the proposed correlation coefficients of Equation 3-5 in this study with other correlations which are applied on our synthetic dataset. A more impartial comparison between the proposed correlation coefficients and the others could be done on real measured data. Therefore, two well-known regular sandstone datasets, Fontainebleau with the reported mean grain size of 250 microns (Bourbie and Zinszner,1985) and Ottawa sandstone with the mean grain size 860 microns (Omidvar et al., 2014) are chosen for this examination. Both data sets (permeability versus porosity) cover wide range of porosity and permeability (Bourbie and Zinszner, 1985; Feia et al., 2015). The results indicate that in contrast to other correlations, the proposed correlation coefficients in this study is more reliable

and could be applied for a wider range of porosity (porosity more than 0.09) for both mentioned datasets (Figure 3-10 and Figure 3-11). To quantitatively compare the accuracy of the correlations, a log-log regression model was utilized. The Residual Sum of Square (RSE) is calculated using the following equation:

$$RSE = \sum_{n=1}^{N} (Y_i - \widehat{Y}_i)^2 \qquad 3\text{-}6$$

Where Yi is our observed data and $\widehat{Y}_i$ is our expected data and R2 for the accuracy of the proposed correlations were compared for Fontainebleau and Ottawa datasets (Table 3-6).

Among all correlations to estimate absolute permeability, the proposed correlation coefficients in this study and Bourbie and Zinszner correlation provide the best fits over Fontainebleau sandstone dataset. However, the Bourbie and Zinszner correlation fails to reproduce the experimental data for Ottawa sandstone. Even compared to Carman-Kozeny (CK) correlation which is widely accepted in the industry, our correlation provides a better estimation in our studied dataset. The negative R^2 in Table 3-6 proposed correlation is not an appropriate correlation to estimate absolute permeability in the studied range of porosity for the available dataset.

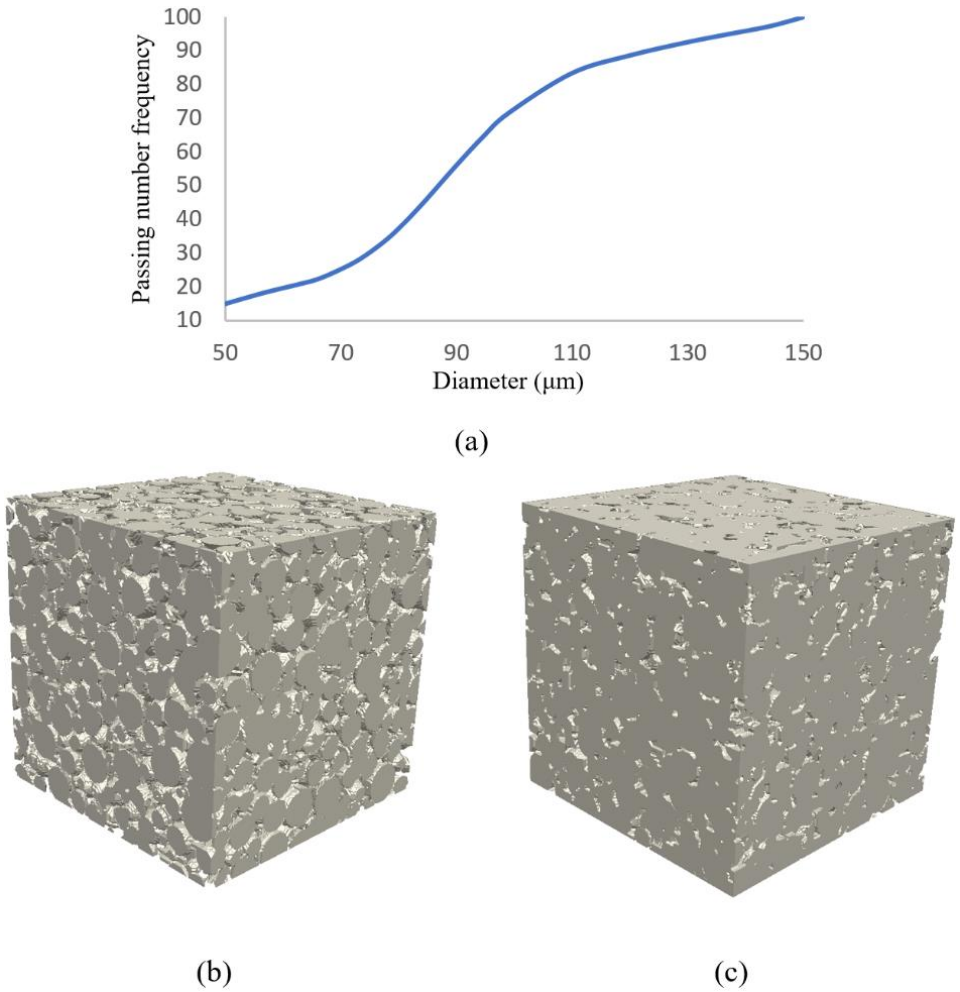

Figure 3-8: (a) A typical PSD utilized to generate virtual porous media with different porosities. (b) Generated porous materials based on the PSD. (Φ =0.27, dimensions=200*200*200, voxel size = 5 µm and average grains sphericity =0.94). (c) Generated porous rock based on the PSD. (Φ =0.10, dimensions=200*200*200, voxel size = 5 µm and average grains sphericity =0.68). Both generated media have the same PSD and different porosity and sphericity.

Table 3-5: Correlation constants for the permeability models

Correlations	**a**	**b**
Berg (Berg,1975)	0.84	5.1
Garcia (Garcia et al., 2009)	0.11	5.6
Revil (Revil and Cathles,1999)	0.0416	4.5
Bourbie (Bourbie and Zinszner,1985)	0.303	3.05
This work	0.0211	3.773

(a)

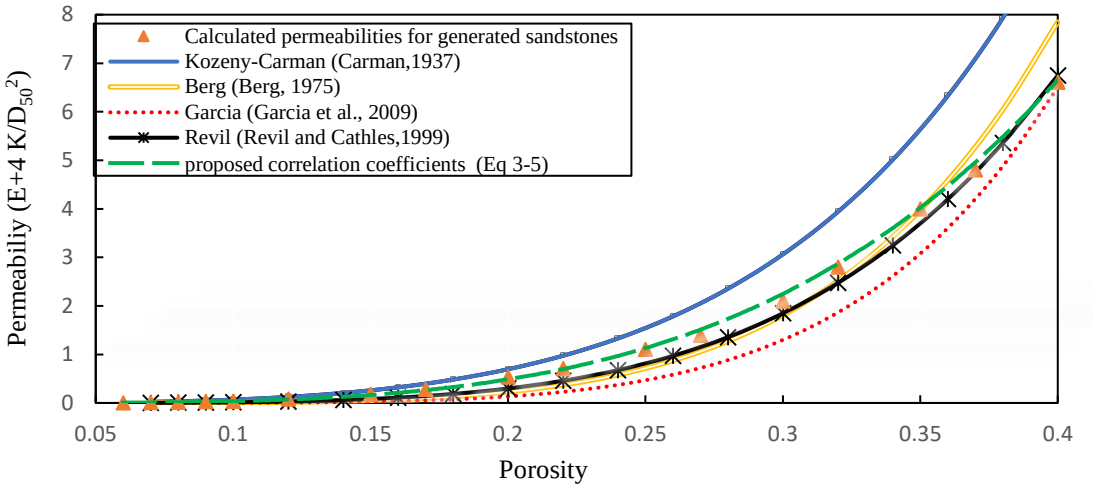

(b)

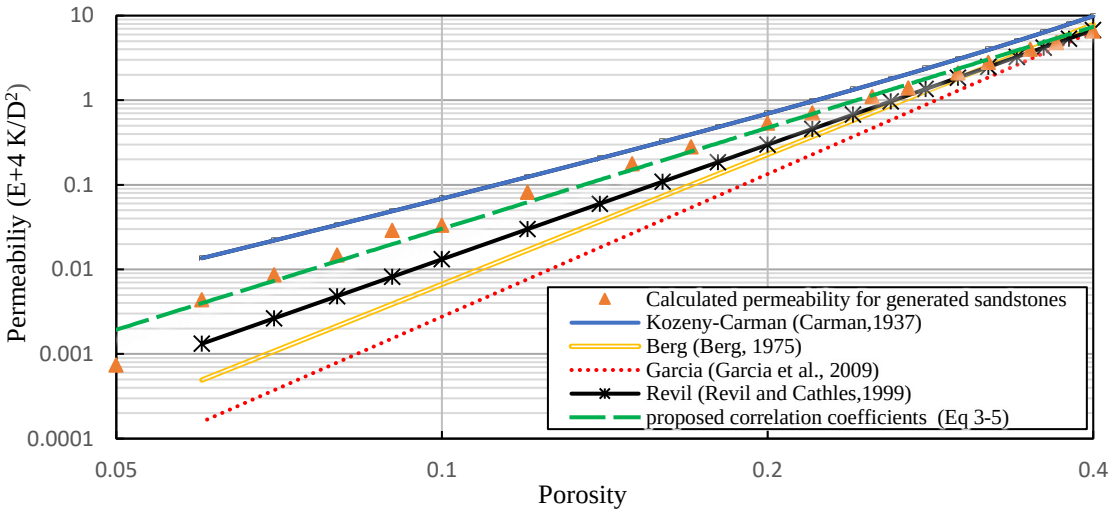

Figure 3-9: (a) Comparing different empirical correlations (Garcia et al., 2009; Carman,1937; Berg, 1975; Bourbie and Zinszner,1985; Revil and Cathles1999) with our proposed correlationcoefficient (Eq 3-5). (b) Log scales of Figure 3-9.a to illustrate a better estimation of correlations at lower porosity range.

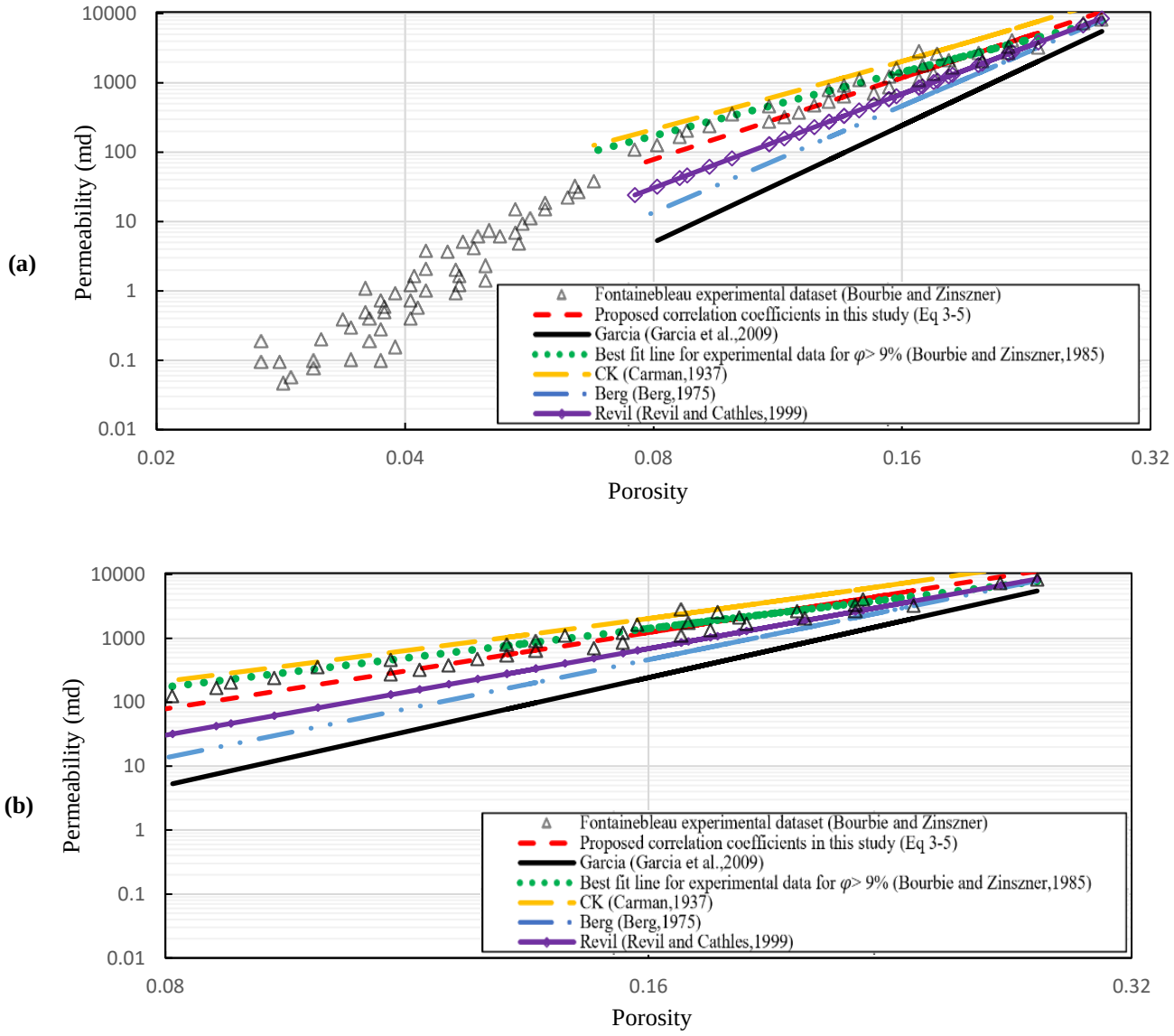

Figure 3-10: Fitting empirical correlations on Fontainebleau dataset (D_{50} =250 µm). (a) Porosity range is between 3% - 28%. (b) porosity range is between 8% -32% porosity. It is shown that the proposed correlation coefficients in this research (Equation 3-5) has an acceptable conformance with the experimental data (Bourbie and Zinszner,1985).

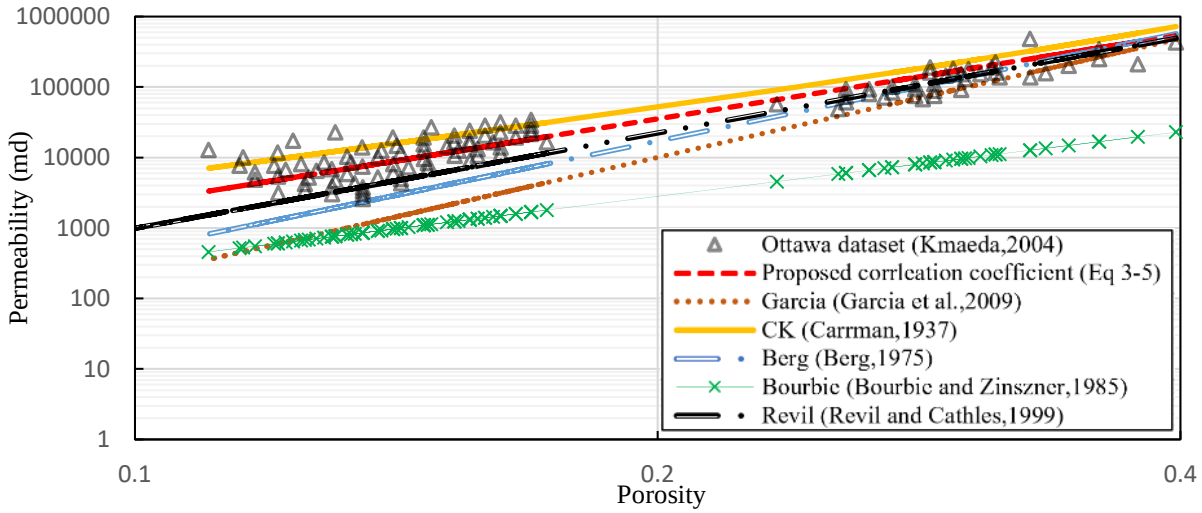

Figure 3-11: Fitting empirical correlations on Ottawa dataset (D_{50}=860 µm). Experimental data belongs to various sandstones from Kameda, (2004). It is shown that the proposed correlation coefficients in this research (Equation 4-5) is in better conformance with the experimental data. As it is clear, the Bourbie correlation (Bourbie and Zinszner,1985) which was originally developed for Fontainebleau sandstone is not suitable to predict the permeability in Ottawa sandstone.

Table 3-6: The Residual sum of square (RSE) and R square for the proposed correlations to judge the accuracy of proposed correlations to estimate absolute permeability on two different experimental data set

Dataset	Fontainebleau dataset		Ottawa dataset	
Correlation	Residual sum of square	R2	Residual sum of square	R2
This study	3.76	90.1	32.47	0.89
Carman	10.49	0.73	70.2	0.76
Berg (Berg,1975)	55.54	0.45	193.78	0.37
Garcia (Garcia et al., 2009)	129.57	2.39	446.12	-0.45
Revil (Revil and Cathles,1999)	22.72	0.41	87.10	0.71
Bourbie (Bourbie and Zinszner,1985)	2.755	0.93	786.58	-1.55

As previously discussed, the irregularity of grains in our approach is adjustable by user. We used this capability to explore the possible effects of sphericity on physical properties of the media. Accordingly, several media were constructed with a similar resolution (5 micron) at different porosity values. At each porosity value different level of average grain irregularity was considered.

In this research, the effect of sphericity on physical properties is investigated for a wide range of porosity (15% - 40%). It is concluded that the effect of sphericity (e.g. permeability) for high porosity value (32%-40%) is not noticeable (Figure 3-12). Garcia et al. (2009) investigated the effect of sphericity on permeability for sandstones in the range of 32%-40%. Similarly, they indicated that porosity and mean grain size distribution are the most important parameters which affect physical properties of porous media. In our study, it is indicated that although the impact of sphericity on permeability estimation is not tangible for high porosity value, is more remarkable in low porosity values.

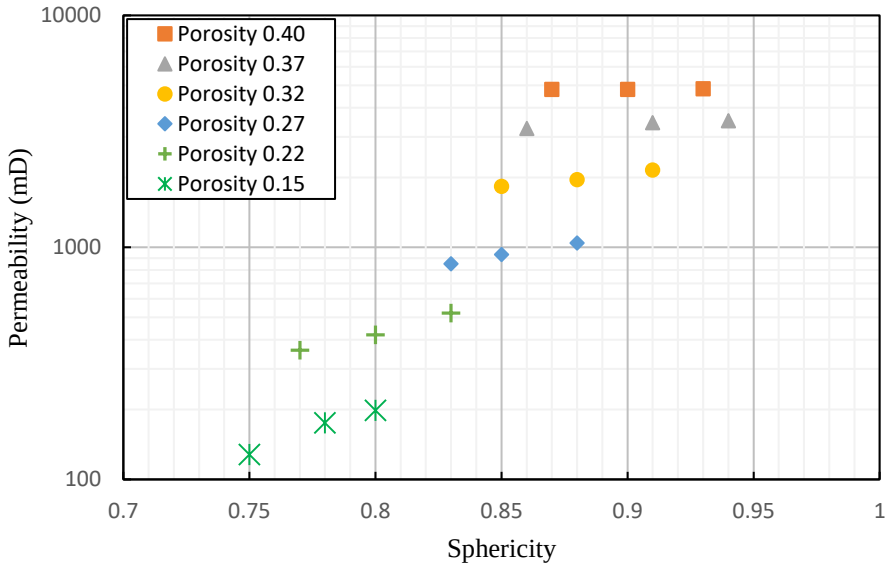

Figure 3-12: The effect of sphericity on permeability estimation of sandstones while the porosity and PSD considered constant for each case of study. As the figure shows, the effect of sphericity on permeability for high range porosities is not significant. (the resolution of all generated porous media is 5 µm).

Based on the Archie's law (Archie,1942), correlating formation factor as a function of porosity (Equation 3-7), several researchers experimentally obtain two constances (m) and (c) in order to estimate formation factor as a function of porosity. The constant values which were achieved either experimentally or numerically (In this study) for different sandstones are listed in

Table 3-7 (Timur et al.,1972; Carothers,1968; Winsauer et al.,1952).

$$F = \frac{c}{\Phi^m} \qquad 3\text{-}7$$

The formation factors of numerically generated sandstones were plotted versus their porosities. Then, two constances (m) and (c) were extracted based on the Archie's law (Figure 3-13).

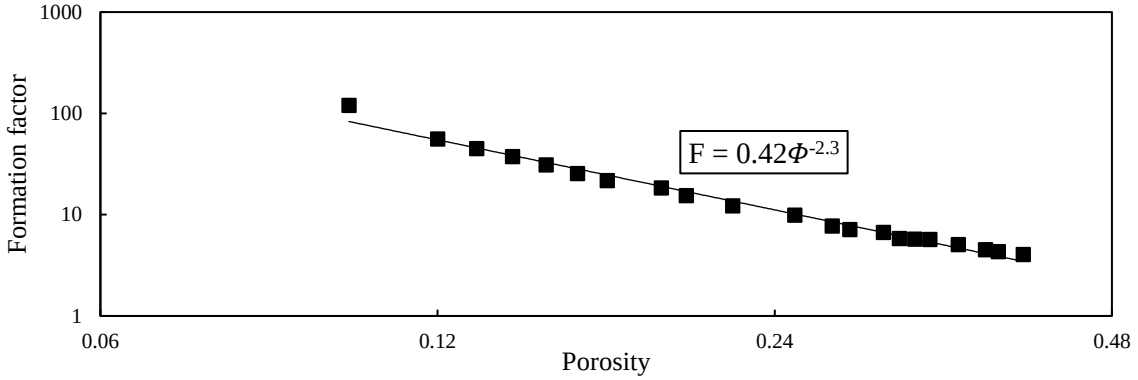

Figure 3-13: Formation factor versus porosity for the generated porous media with different particle size distributions and porosities. using the proposed algorithm

Table 3-7: Correlation constants for the formation factor models

Correlations	c	m
Winsauer (Winsauer et al.,1952)	0.62	2.1
Carothers (Carothers,1968)	1.45	1.54
Timur (Timur et al.,1972)	1.13	1.73
This work	0.42	2.3

The proposed correlation coefficients for estimation of formation factor as a function of porosity (Equation 3-7) were applied for two different experimental datasets of various sandstone reported by Winsauer et al.,1952 and Pape et al.,1987. The proposed correlation coefficients in this study which is acceptable for these two datasets is compared with other empirical correlations (Figure 3-14 and Figure 3-15).

(a)

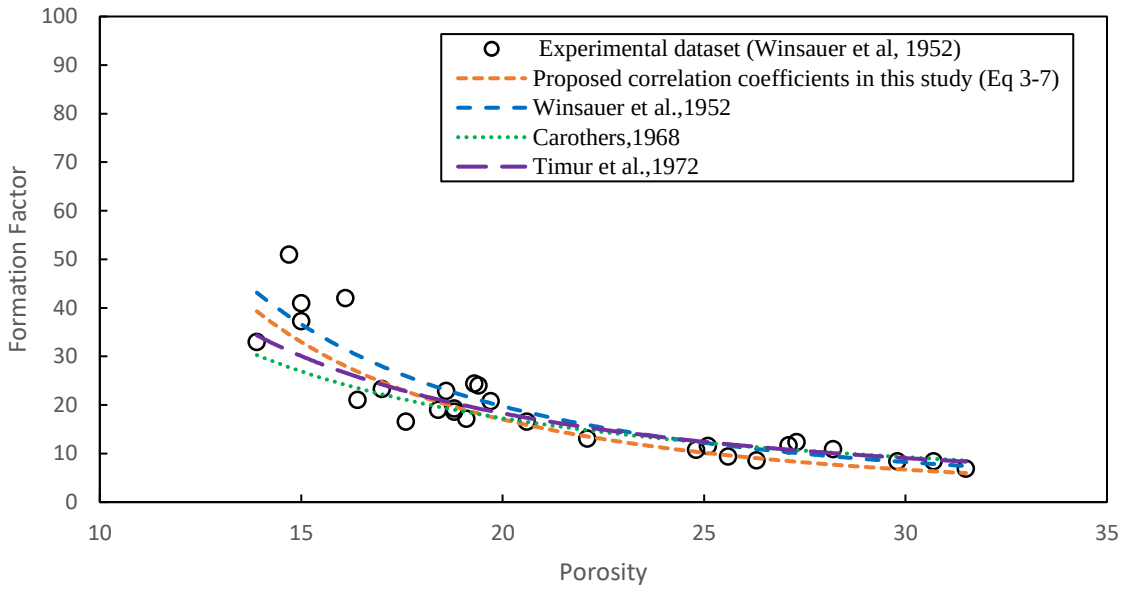

(b)

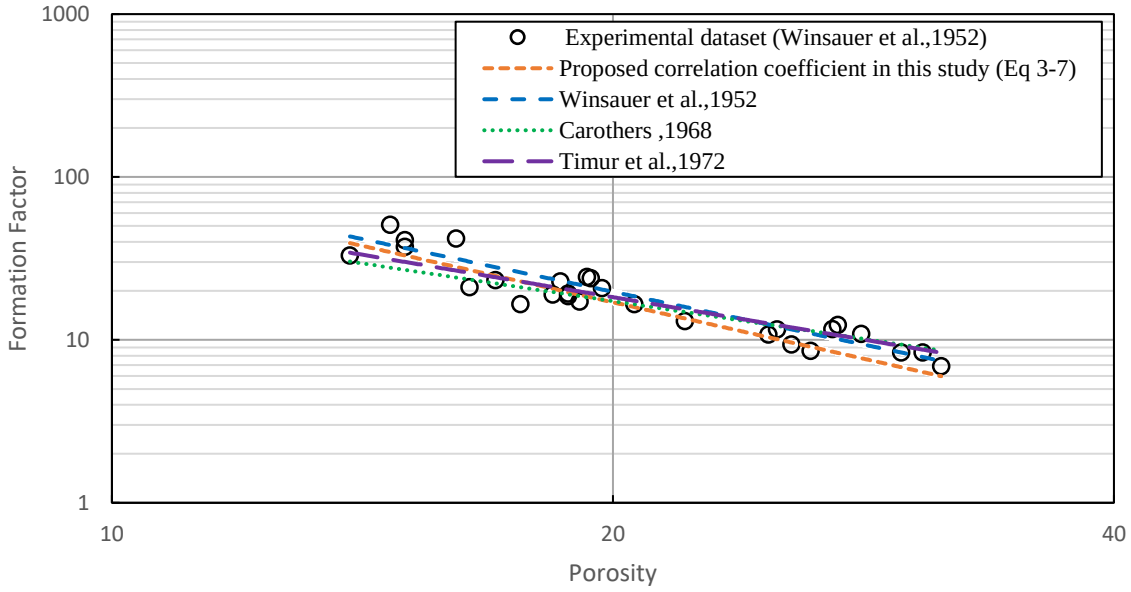

Figure 3-14: (a) Comparison of the proposed constant for Archie's Equation in this study (Equation 3-7) with other empirical correlations relied on core experiment (Timur et al.,1972; Carothers,1968; Winsauer et al.,1952) to estimate formation factor versus porosity for different sandstones. (b) presents figure (a) at log scale.

(a)

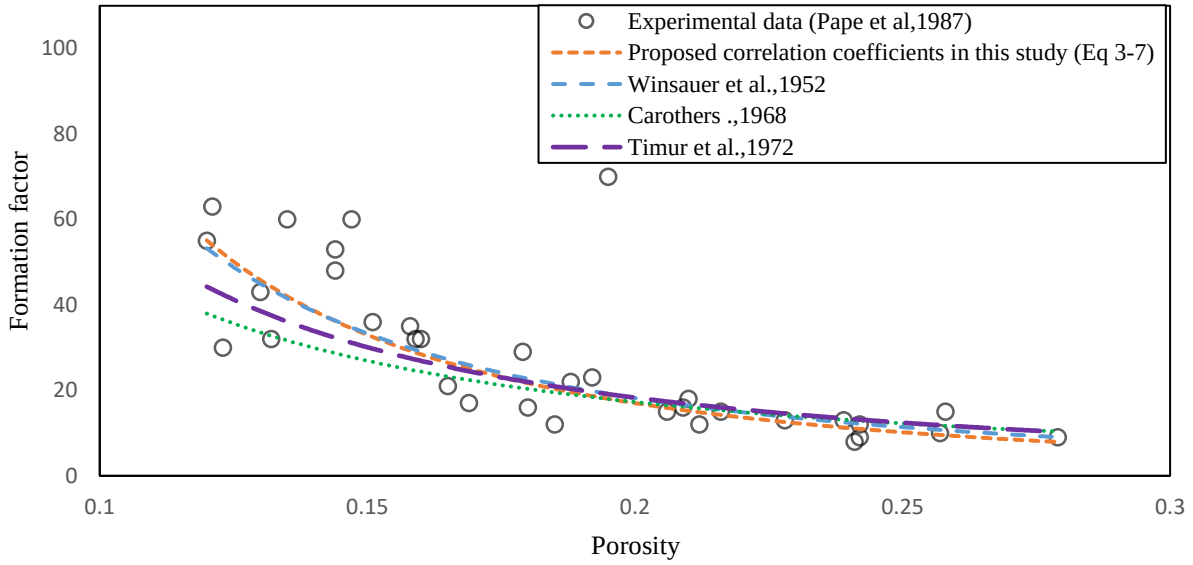

(b)

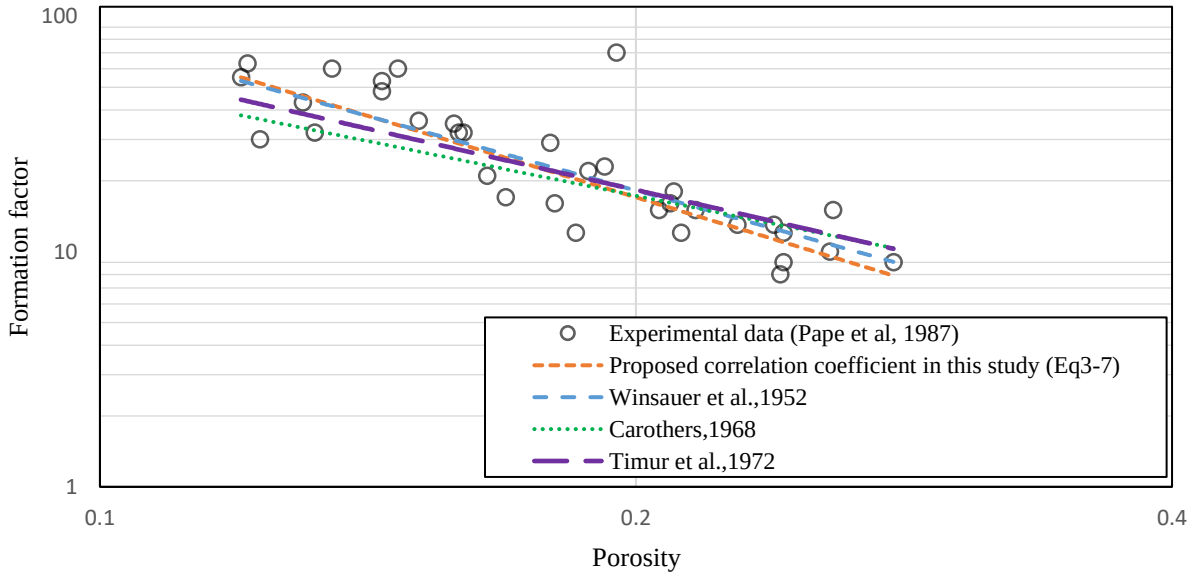

Figure 3-15: (a) Comparing the proposed correlation coefficients in this study with other empirical correlations relied on core experiment (Timur et al.,1972; Carothers,1968; Winsauer et al.,1952) to estimate formation factor versus porosity for various sandstones. Experimental data from Pape et al., 1987. (b) Comparison of all mentioned correlations at Log scale. (b) presents figure (a) at log scale.

4 NON-DARCY FLUID FLOW

Non-Darcy flow in porous media is a critical issue which can significantly affect the prediction of reservoir production performance. Onset of non-Darcy flow can be either examined experimentally, via applying empirical correlations or via numerical modelling. The experimental approach is the most reliable way to determine the non-Darcy coefficient and identify the onset of non-Darcy flow. The other common approach to predict the inertial coefficient (non-Darcy coefficient), β is by utilizing empirical correlations. Although these correlations are easy to use, they are not so reliable to generally be applied for identification of non-Darcy regime in the absence of experimental data. Alternatively, numerical simulations are an appropriate substitution for these empirical correlations. Moreover, numerical simulations give us the opportunity to investigate the effects of physical parameters such as porosity and pore heterogeneity on the onset of non-Darcy flow in porous media which could not efficiently be studied experimentally. An innovative statistical approach was utilized to generated ten numerically constructed sandstone samples. The effects of porosity, immobile water saturation and average grain sphericity on pore structure heterogeneity were investigated via simulations through generated 3-D images. It is found that, porosity is a key parameter can significantly affect the non-Darcy coefficient and the onset of non-Darcy flow. It is concluded that effect of average grain sphericity in porous medium for fluid flow in higher pore velocity ranges is more tangible. As geological formations are usually partially saturated with water, it was shown that the presence of immobile water can drastically affect the beginning of the non-Darcy flow as well as the non-Darcy coefficient value. Numerical simulation results show when immobile water saturation is around 8.7%, the β factor increases by 180% compared to a fully oil saturated sample.

4.1 Literature Review

Over the past few decades, modelling of flows within porous media has been the subject of various fields of study such as civil engineering, hydrogeology and petroleum engineering (Martins, 1990; Hansen,1992; Khalifa et al.,2000)

The flow pattern in porous media is typically governed by Darcy's law as long as the fluid velocity is low enough to neglect the inertial effects. Darcy's law describes a linear relationship between pressure gradient and velocity as follows:

$$-\nabla \mathrm{p} = \frac{\mu}{K_D} u \qquad 4\text{-}1$$

Where p is pressure, μ is viscosity u is superficial velocity, K_D is permeability.

Forchheimer (1901) observed situations in which a non-linearity exists between pressure gradient and velocity so that Darcy's law was no longer sufficient for explaining fluid flow through porous media. Therefore, a quadratic term as a modification term was added to the Darcy equation. The new modified equation is known as the Forchheimer equation:

$$-\nabla \mathrm{p} = \frac{\mu}{K_F} u + \beta \rho |\, \mathrm{u} \,|^{2} \qquad 4\text{-}2$$

In equation (4-2), β is named the non-Darcy, inertial or turbulent coefficient. The quadratic term is small and negligible at low velocities so Darcy's Law is sufficient to describe flow. In the Forchheimer equation, the left-hand-side term, $-\nabla p$, is the total pressure gradient. The first term in the right-hand side, $(\frac{\boldsymbol{\mu}}{\boldsymbol{K}}\mathrm{u})$, can be considered as the pressure gradient to overcome viscous resistance. Similarly, the second term, $\beta\rho|\,\mathrm{u}\,|^{2}$, is the pressure gradient needed to overcome solid–liquid interactions.

The assessment of non-Darcy flow has always been a critical issue in petroleum engineering, as it provides an appropriate evaluation of production performance. Non-Darcy flow is typically observed near wells and in hydraulic fractures where fluids can flow at high velocity due to drastic pressure gradient (Kalaydjian et al.,1996).

Although earliest works attributed the nonlinearity between pressure gradient and velocity to turbulent flow in a porous medium (Chilton and Colburn,1931; Cornell and Katz,1953), subsequent researches demonstrated that the nonlinearity is due to inertial effects and not turbulence flow at least for incompressible fluid (Bear,1972; Scheidegger,1958; Ruth and Ma,1992).

4.1.1 Onset of non-Darcy flow

The Reynolds number and the Forchheimer number are two criteria which have been widely used to identify the beginning of non-Darcy flow.

Generally, the Reynolds number is described by Equation 4-3 which was proposed by Chilton and Colburn (1931) presenting the mean grain size as a characteristic length. But there are also different proposed equations to define the Reynolds number through porous materials. Ergun,1952 modified the Chilton and Colburn's definition (Equation 4-4). Durlofsky and Brady (1987) proposed Equation 4-5 as the critical Reynolds number where $\sqrt{K_D}$ was considered as a characteristic length. Comiti et al. (2000) suggested the pore Reynolds number (Equation 4-6) for flow in a porous medium as a criterion to identify the beginning of Non-Darcy flow. Patil and Liburdy (2013) used Equation 4-7 as the definition of pore Reynolds number for randomly packed porous beds.

$$Re = \frac{\rho u d_p}{\mu} \quad 4\text{-}3$$

$$Re = \frac{\rho U d_p}{\mu} \frac{1}{1-\Phi} \quad 4\text{-}4$$

$$Re = \frac{\rho u \sqrt{K_D}}{\mu} \quad 4\text{-}5$$

$$Re_p = \frac{4\,\rho u T}{\mu\,(1-\Phi)\,S_v} \quad 4\text{-}6$$

$$Re_p = \frac{2}{3}\frac{\rho u d_p}{\mu\,(1-\Phi)} \quad 4\text{-}7$$

Where, d_p is the characteristic length of the porous medium. However, there is not a clear agreement in the characteristic length definition within porous media. For instance, Chilton and Colburn ,1931 applied a mean diameter grain size as the characteristic length. Ma and Ruth ,1993 used pore throat diameters as the characteristic length for Equation 4-3, while Comiti and Renaud,1989 proposed Equation 4-8 as the characteristic length:

$$d_p = \frac{4\Phi}{(1-\Phi).S_v} \quad 4\text{-}8$$

Where, S_v is the dynamic specific surface area defined as the ratio of the total pore surface area to the volume of solid.

Macdonald et al. (1979) suggested Equation 4-9 as the characteristic length for spherical packings.

$$d_p = \frac{6}{S_v} \quad 4\text{-}9$$

Mostaghimi et al. (1979) proposed Equation 4-10 as a pore diameter for real sands where S_v is the specific surface area of the pore which is defined as the ratio of pore surface area to the total (pore-grain) volume.

$$d_p = \frac{\pi}{S_v} \quad 4\text{-}10$$

It is worth mentioning that there is a large inconsistency in reporting of critical Reynolds numbers as a parameter to identify the onset of non-Darcy flow reported by different researchers. Some of the reported data are shown in Table 4-1.

Table 4-1: Reported critical Re number as a criterion to identify the onset of non-Darcy flow

Published	**Porous medium**	**Reported critical Re number**
Chilton and Colburn, 1931	Packed particles	40-80
Fancher and Lewis, 1933	Unconsolidated sandstones	10-1000
	Loosely Consolidated sandstones	0.4-3
Scheidegger, 1958	Packed particle	0.1-75
Bear, 1972	Packed particle	3-10
Hassanizadeh and Gray, 1958	Packed particle	1-15

Although, using critical Reynolds numbers can be considered as a criterion for identification of non-Darcy flow for unconsolidated and loosely consolidated media, determining the characteristic length is not always feasible. Thus, Ruth and Ma (1992) proposed a modified version of Reynolds number called the Forchheimer number (Equation 4-11). The Forchheimer number has not only the advantage of clear definition but also wide applicability for various rock types.

$$F_o = \frac{K_D \beta \rho u}{\mu} \qquad 4\text{-}11$$

Where K_D (m^2) is absolute permeability and β (1/m) is non-Darcy coefficient.

The Forchheimer number can be defined as the ratio of the pressure drop caused by the liquid-solid interaction ($\beta \rho u^2$) to that by the viscous resistance ($\frac{\mu u}{k}$) (Saboorian and Pourafshary, 2015). The Forchheimer number defines a better physical concept as a criterion to identify the beginning of non-Darcy flow and also, it is more applicable for different porous media compared to applying the concept of critical Reynolds number. However, it is not an appropriate criterion for the onset of non-Darcy flow because of the inconsistency of the reported values (Ma and Ruth,1993; Zeng and Grigg, 2006).

Although there is not yet a comprehensive agreement among researchers to estimate the onset of non-Darcy flow in porous materials, Comiti et al. (2000) defined two criteria for fluid transition of creeping to inertial regime in porous media. The first criterion defines the onset of non-Darcy flow where pressure drop due to the linear term becomes less than 95% of the total. The second criterion is where the linear pressure drop becomes less than 99%. The second criterion was used in this study because Comiti et al. (2000) claimed that it is the more appropriate and stringent definition to determine onset of non-Darcy flow. Muljadi et al. (2016) also applied the second criterion as a transition limit from Darcy to non-Darcy flow regime to numerically calculate inertial coefficient for three various types of rocks.

4.1.2 Non-Darcy coefficient for single phase flow

Numerous researchers tried to find a general correlation to predict non-Darcy coefficient (β) for porous media. Based on experimental results, various empirical correlations were presented relating non-Darcy coefficient (β) to different medium properties (e.g. porosity, permeability, tortuosity). However, the reservoir rock heterogeneities make using these correlations an uncertain approach to estimate the β factor.

Ergun (1952) studied fluid flow through bead packed beds. He found that the solid properties and the morphology of the pore space can affect the relationship between pressure drop and flow rate during fluid flow through sand packs. The non-Darcy coefficient can be identified by

$$\beta = a \times b^{-0.5} \times 10^{+4} \times K^{-0.5} \times \Phi^{-1.5} \qquad 4\text{-}12$$

Where a=1.75, b=150 and β in cm^{-1} and K in Darcy.

MacDonald et al. (1979) generalized and modified the Ergun equation which was derived based on considering spherical particle shape for grains. They found that b=180 and a vary based on the roughness of the particle in the range of 1.8- 4.

$$\beta = a \times b^{-0.5} \times 10^{+4} \times K^{-0.5} \times \Phi^{-1.5} \qquad 4\text{-}13$$

Where a = 180 and b = 1.8 – 4 and β in cm^{-1} and K in Darcy.

Janicek and Katz (1955) solved the unsteady state differential equation for flow of gas through reservoirs by assuming a constant diffusivity. They claimed that the presented procedure may be used for predicting of single phase non-Darcy coefficient.

$$\beta = 1.82 \times 10^{8} \times \Phi^{-0.75} K^{-1.25} \qquad 4\text{-}14$$

Where β in cm^{-1} and K in mD.

Geertsma (1974) introduced an empirical correlation based on a relationship between inertia coefficient, permeability, and porosity, carried out an experimental measurement on dry cores from the same reservoir.

$$\beta = 0.005 \times \Phi^{-5.5} K^{-0.5} \qquad 4\text{-}15$$

Where β is in cm^{-1} and K is in cm^{2}.

Pascal et al. (1980) explored the variation of the non-Darcy coefficient with permeability as derived from the well test data.

$$\beta = 4.8 \times 10^{12} \times K^{-1.176} \qquad 4\text{-}16$$

Where β is in ft^{-1} and K is in mD.

Jones ,1987 carried out experimental measurement on 355 sandstones and 29 limestones taken from different reservoirs to propose a comprehensive correlation for estimation of the inertial

coefficient on sandstones. All the plugs were consolidated. He proposed a β correlation in a single-phase system based on the measured permeability.

$$\beta = 6.15 \times 10^{10} \times K^{-1.55} \quad \text{4-17}$$

Where β is in ft^{-1} and K is in mD.

Frederick and Graves (1994) developed a correlation to estimate non-Darcy coefficient by using experimental data set obtained on 24 cores over variable confining stress. The cores permeability range was from 0.00197 to 1230 mD.

$$\beta = 1.98 \times 10^{11} \times K^{-1.64} \quad \text{4-18}$$

Where β is in ft^{-1} and K is absolute permeability in mD.

Liu et al. (1995) proposed an empirical correlation using experimental data correlated with the petrophysical properties such as permeability, porosity, and tortuosity to estimate the non-Darcy flow coefficient.

$$\beta = 8.911 \times 10^{8} \times \Phi^{-1} \times K^{-1} \times T \quad \text{4-19}$$

Where β in ft^{-1} and K in mD.

Thauvin and Mohanty, 1998 found a general correlation between the non-Darcy coefficient and other flow properties including permeability, porosity and tortuosity. They also investigated the effect of morphological characteristics of rocks on non-Darcy coefficient and proposed 3 different correlations based on various types of properties involved to estimate the non-Darcy coefficient.

$$\beta = 1.55 \times 10^{4} \times \Phi^{-0.29} \times T^{3.35} \times K^{-0.98} \quad \text{4-20}$$

$$\beta = 2.5 \times 10^{5} \times K^{-1} \quad \text{4-21}$$

$$\beta = 3.1 \times 10^{4} \times T^{3} \times K^{-1} \quad \text{4-22}$$

Where β in cm^{-1} and K in D.

Coles and Hartman (1998) presented a correlation to estimate the inertial coefficient based on experimental measurements on dry cores. They also explored the effect of immobile liquid on non-Darcy coefficient as well.

$$\beta = 1.07 \times 10^{12} \times \Phi^{0.449} K^{-1.88} \qquad 4\text{-}23$$

Where β in ft^{-1} and K in mD.

Cooper et al. (1999) studied non-Darcy gas flow in anisotropic and layered dry cores, both experimentally and through macroscopic and microscopic models. Non-Darcy flow coefficients, permeabilities, and electrical tortuosities are measured in various samples including layered, nonlayered and anisotropic cores. They also investigated how connate water in rocks can affect non-Darcy coefficient.

$$\beta = 10^{-3.25} \times T^{1.943} \times K^{-1.023} \qquad 4\text{-}24$$

Where β in cm^{-1} and K in mD.

Some researchers either performed experiments or obtained from well test data to compare their results with proposed correlations to investigate the accuracy of various presented correlations.

Johnson and Taliaferro (1938) tried to present a general empirical correlation to estimate fluid flow behavior at high range of velocities by performing experiments on consolidated and unconsolidated rocks (e.g. sandstones and limestones).

Cornell and Katz (1953) obtained experimental data by flowing gas through 24 samples of sandstones, limestones, and dolomites to correlate and predict the flow of gases in the Forchheimer regime. They used permeability, porosity, and electrical resistivity factor of the solid and the properties of the fluid to predict the inertial coefficient in porous media.

Gewers and Nichol (1969) performed a laboratory study of the non-Darcy coefficient in carbonates. It is concluded that the inertial factor correlated with permeability, like other rock types. It was found that the non-Darcy coefficient for the carbonate rocks can be an order of magnitude higher than other rock types (e.g. sandstones) at a given permeability (Figure 4-1).

Firoozabadi and Katz (1979) collected available data from past researchers investigating non-Darcy flow in porous media to compare and improve the best correlation to estimate the inertial coefficient based on permeability, porosity, and character of the rock. They found that the Greesma correlation (Equation 4-15) was the best fit for the available data set.

Avila and Evans,1986 carried out experiments on sandstones (e.g. Berea, Cleveland and Bandera) to investigate the effect of temperature and overburden pressure on non-Darcy coefficient in single phase and multi-phase flow. The results indicated that the non-Darcy flow coefficient increases where temperature and overburden pressure increase. However, the non-Darcy flow coefficient is more sensitive to temperature rather than the overburden pressure. Results indicated that the permeability for sandstones are inversely proportional to overburden pressures and temperature.

Noman and Archer (1987) performed experiments on 40 core samples to measure porosity, permeability, inertial coefficient and capillary pressure to investigate the effect of pore heterogeneity on non-Darcy gas flow. The results demonstrated that the inertial effect is not only a function of porosity and permeability, but is also controlled by other factors such as aspect ratio, surface roughness, heterogeneities, and coordination number, etc.

Evans (1988) investigated the Non-Darcy flow coefficient on single-phase flow, single phase flow in the presence of an immobile liquid saturation, and multiphase flow on Ottawa sandstones. The results of this study demonstrated that a small mobile liquid saturation may increase the non-

Darcy flow coefficient by nearly an order of magnitude over that of the dry case and by up to three times that for a sand containing an immobile liquid saturation.

Narayanaswamy et al. (1998) investigated non-Darcy flow in tight heterogeneous formations from well test data obtained from 12 wells in a carbonate gas condensate reservoir. Analyzed data demonstrated that non-Darcy flow coefficients for heterogeneous formation is significantly larger compared to homogeneous formation. They used numerical simulation to confirm that formation heterogeneity can significantly affect non-Darcy flow coefficients. Moreover, it is indicated that non-Darcy flow coefficient obtained from well tests are noticeably larger than those obtained experimentally or estimated from experimental correlations. Permeability heterogeneity was expressed as a likely reason for the differences (Figure 4-1).

Experimentally measured non-Darcy coefficients by reviewed researchers were collected to investigate the variance of the inertial coefficient (β) for different rocks as a function of absolute permeability (Figure 4-1).

Firoozabadi and Katz (1979) showed that there is different correlation line to estimate the non-Darcy coefficient as a function of absolute permeability for consolidated and unconsolidated data. The same results can be observed in Figure 4-1and Figure 4-2. Based on the collected experimental data, it could be observed that the functionality of non-Darcy coefficient to absolute permeability for very tight consolidated rocks with permeability less than 0.1 mD is quite different from consolidated sands with permeability greater than 0.1 mD.

In Figure 4-2, the experimental data set classified into three categories, unconsolidated sands, consolidated sands (permeability greater than 0.1 md) and very tight consolidated sands (permeability less than 0.1 mD).

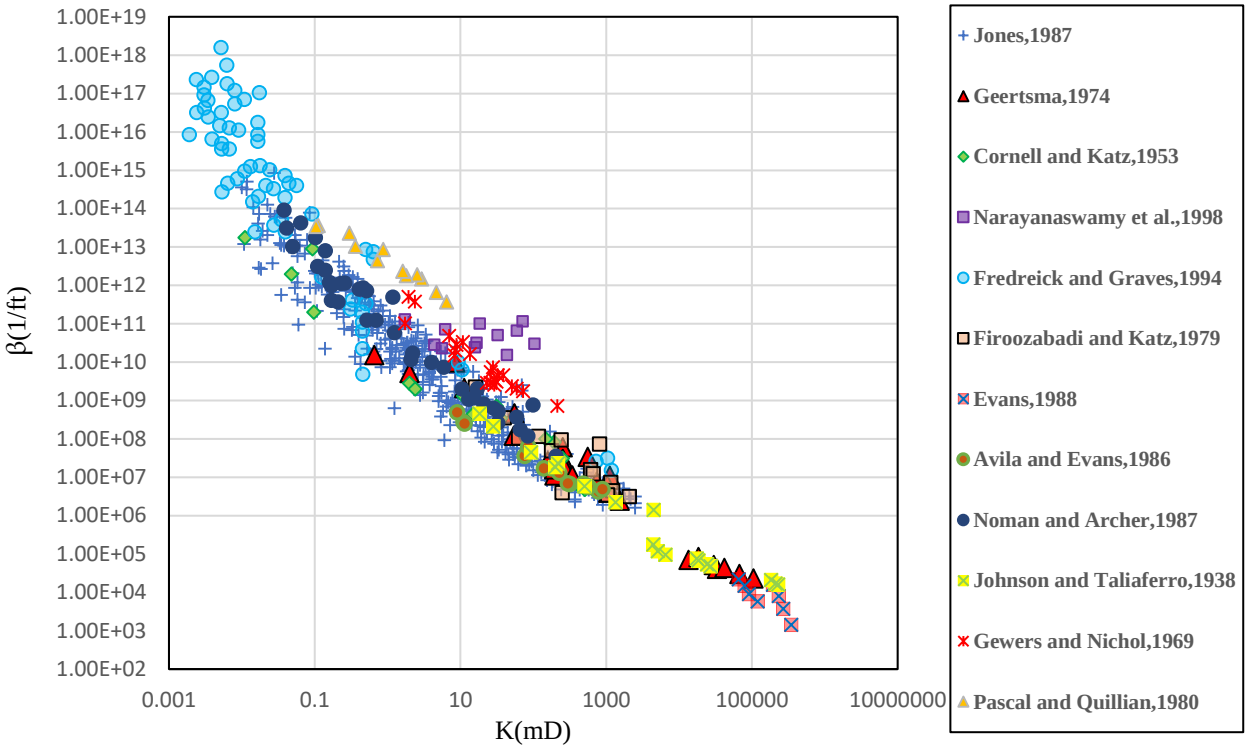

Figure 4-1: Non-Darcy coefficient as a function of permeability for hundreds of different types of rocks was collected and plotted.

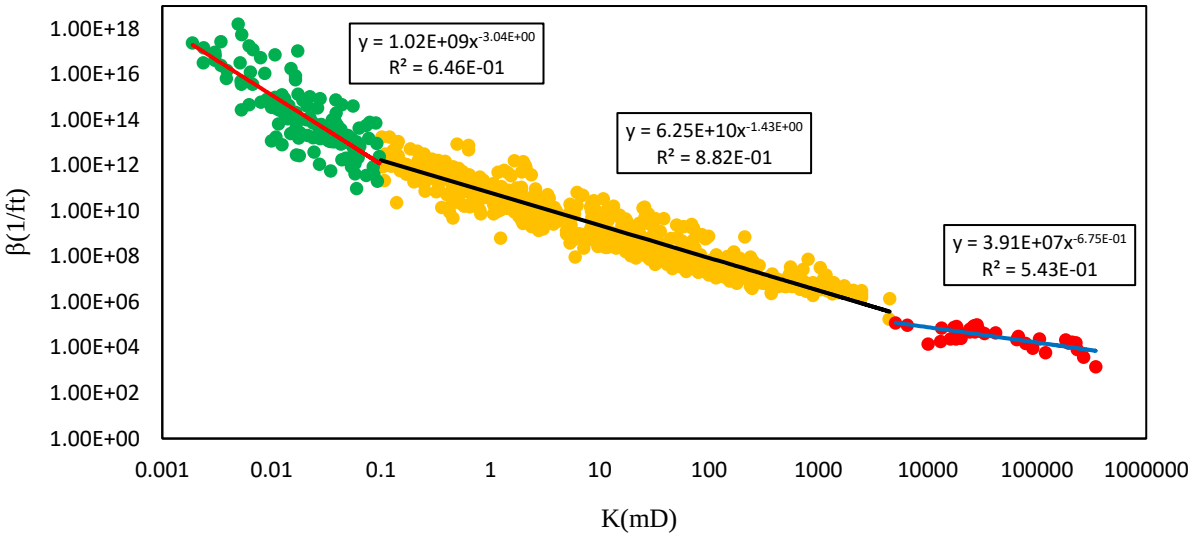

Figure 4-2: The experimental data set classified into three categories, unconsolidated sands, consolidated sands with permeability greater than 0.1 md and consolidated sands with permeability less than 0.1 mD to present the most appropriate correlation for each category.

4.1.3 Approaches to determine non-Darcy regime

A multi-rate pressure test is a reliable experimental method to determine the inertial coefficient (β), and the onset of non-Darcy flow in porous media. However, it is a time-consuming test and detailed production data are not always available. On the other hand, numerical approaches are less expensive and time consuming compared to experimental methods and more reliable rather than empirical correlations.

Several numerical studies on sphere packs have been reported. Andrade et al. (1999) used finite difference techniques to investigate the onset on non-Darcy flow in two-dimensional disordered porous media. Fourar et al. (2004) applied a finite-element method for 2-D and 3-D periodic sphere packs to evaluate the onset of non-Darcy flow. Newman and Yin (2013) applied the Lattice Boltzmann method to predict the onset of non-Darcy flow and inertial coefficient, β, for synthetic 2-D media. They found that the larger the aspect ratio, the earlier transition from Darcy to non-Darcy occurs in a porous medium. Aharonov and Rothman (1993) used a Lattice-Boltzmann method to simulate non-Newtonian flow through synthetic 2-D porous media.

Thauvin and Mohanty (1998) developed a pore- level network model to explore high velocity flow in porous media and onset of non-Darcy flow. They observed that the correlation between the inertial coefficient and other flow properties (permeability, porosity and tortuosity) depends on the morphological parameters. Wang et al. (1999) studied the effect of pore-scale anisotropy on non-Darcy flow behavior in porous media by using pore network modeling. They generated three various structural models of anisotropy to study non-Darcy flow regime. They computed non-Darcy coefficients, as well as the tortuosity of the media.

Muljadi et al. (2016) numerically explored the impact of pore-scale heterogeneity on non-Darcy flow behavior by employing a finite-volume method to simulate fluid flows directly on real 3-D

images of three various types of rocks with different complexity and heterogeneity (artificial sand pack, sandstone and carbonates). The non-Darcy coefficient β and the Darcy permeability for all samples were obtained and compared to empirical correlations to verify their approach. They demonstrated that numerical approaches can be used as an appropriate method to estimate non-Darcy coefficient and departure of Darcy regime.

The simulation results provide a new comprehension of the parameters affecting the transition of flow from Darcy to non-Darcy regimes. In the next sections, the physical properties of the samples used in this thesis are presented. The results of our numerical simulations are given, discussed and compared to various empirical correlations.

This study provides a comprehensive study of porosity, grain irregularity, and immobile water saturation effects on non-Darcy flow.

4.2 Methodology

The algorithm presented and verified in previous chapters is applied to generate virtual sandstones with different porosities and average grain sphericities using different particle size distributions.

Different media with different porosities and average grain sphericities based on different particle size distributions (PSD) are generated. Then, simulations were directly conducted on pore structures extracted from generated samples to compare our calculated results with available experimental data.

4.3 Physical Properties of Generated Virtual Porous Media

Different particle size distributions were used to generate 3D virtual sandstones. The constructed virtual sandstones are cubes characterized with resolution of 7.5 µm and dimension of 300 ×300 ×300 voxels. Ten artificial samples with various porosity, average grain sphericity and range of permeability between 0.3-13 Darcy were generated (Table 4-2). The characteristic length of each medium is calculated using Equation 4-10 (Mostaghimi et al., 2012).

Table 4-2: The characteristics of generated porous media

The characteristics of generated porous media				
		Dimension(pixel)	300*300*300	
		Resolution (μm)	7.5	
Sample	**Porosity**	**Average grains sphericity**	**Absolute Permeability(mD)**	**Characteristic length** $(\frac{\pi}{S_v})$
Sample 1	0.27	0.90	5528	178.04 µm
Sample 2	0.22	0.82	3159.8	193.41 µm
Sample 3	0.13	0.64	706.46	258.65 µm
Sample 4	0.22	0.75	3021.2	203.0 µm
Sample5	0.35	0.93	9030.4	160.63 µm
Sample6	0.18	0.73	2216.5	230.7 µm
Sample7	0.40	0.84	23021.5	150.05 µm
Sample8	0.10	0.62	302.29	315.2 µm
Sample9	0.25	0.78	4514.2	180.34 µm
Sample10	0.20	0.71	2577.3	217.03 µm

4.4 Governing Equations and Numerical Method

The OpenFOAM software is used to simulate fluid flow through generated porous media. IcoFoam Solver, which is a Transient solver, is adapted for incompressible, laminar flow of Newtonian fluids. In our simulations, water was assigned as a fluid flow through porous medium with viscosity $\mu = 0.001 Pas$ and density $\rho = 1000.0\ kg/m^3$.

Darcy's law is no longer valid in high flowrate, as permeability is not constant anymore and reduces by increasing the fluid velocity. Therefore, an apparent permeability (K_{app}) is defined and correlated as a function of velocity (Equation 4-25).

$$\frac{1}{K_{app}} = \frac{1}{K_F} + \beta\frac{\rho u}{\mu} \qquad 4\text{-}25$$

The dimensionless apparent permeability K^* is defined as the ratio of apparent permeability to absolute permeability (Equation 4-26, Newman and Yin (2013)). K^* is used to predict the onset of non-Darcy flow. In this study, Criterion for the onset of non-Darcy flow is defined as the moment which the total pressure drop deviates from the linear pressure drop (Darcy's law) by 1%. Using this criterion and substituting Equation 4-26 into Equation 4-1, the onset of non-Darcy flow will be the point where K^*= 0.99.

$$K^* = \frac{K_{app}}{K_D} \qquad 4\text{-}26$$

Where β factor is the inertial coefficient. It can be estimated by plotting the inverse of apparent permeability $\frac{1}{K_{app}}$ against $\frac{\rho u}{\mu}$ and obtaining the slope of line in the Forchheimer regime. The intercept of the line gives the inverse of Forchheimer permeability which is close to the Darcy permeability.

In this study, tortuosity for all synthetic porous media can numerically be measured. Tortuosity is generally defined as:

$$T = \frac{\langle \bar{\iota} \rangle}{L} \geq 1 \qquad 4\text{-}27$$

Where $\bar{\iota}$ is the average length of fluid particle paths (average tortuous length paths) and L is the straight-line distance through the medium in the direction of fluid flow.,

As computation of tortuosity in porous medium is not feasible, Koponen et al. (1996) proposed a method to estimate tortuosity from the fluid velocity in a porous medium without using flow path measurement (Equation 4-28).

$$T = \frac{\langle \bar{U} \rangle}{\langle u_x \rangle} \qquad 4\text{-}28$$

Where $\langle \bar{U} \rangle$, is the average velocity magnitude over the pore space and $\langle u_x \rangle$ is the volumetric average velocity at the flow direction.

4.5 Numerical Results and Discussion

Ten virtual porous media with different porosities, particle size distributions and average grain sphericities were constructed and used to investigate non-Darcy flow behavior and physical properties which can affect the departure of Darcy to non-Darcy flow. Simulation of flows in these synthetic rocks was implemented by varying the pressure gradients through the pore spaces. The departure of Darcy to non-Darcy flow was observed for all generated porous media by monitoring the corresponding flow rate increase until deviation from linearity started.

The Forchheimer permeability and inertial coefficient for all synthetic porous media were numerically calculated from Equation 4-25 and presented in column 4th and 5th of Table 4-3, respectively.

Researchers have always struggled to propose a criterion to determine the onset of non-Darcy flow. As there are different proposed definitions of Reynolds number to determine the onset of non-Darcy flow, we used two popular formulations of Reynolds number using as a criterion to study the onset of non-Darcy flow; the first is the standard definition of Reynolds number (Equation 4-3) based on the characteristic length (d_p) proposed by Mostaghimi et al. (2012). The second formulation is the modified Reynolds number (Forchheimer number) (Equation 4-11) presented by Ruth and Ma (1992). The second definition of Reynolds number is the more reliable criterion to determine the onset of non-Darcy flow for various rock types (Li and Engler,2001). The calculated value for both mentioned critical Reynolds number (Re_c) are illustrated in 6th and

7th column of Table 4-3. As it can be observed the second Reynolds number (Equation 4-11) is more physically consistent criterion for non-Darcy flow.

Some researchers considered tortuosity as a significant parameter which can affect the onset of non-Darcy flow. We used Equation 30 presented by Koponen et al. (1996) to numerically measure tortuosity of synthetic porous media. The estimated tortuosity of the generated virtual porous media is included in the last column of Table 4-3.

Table 4-3: Calculated Forchheimer permeability, non-Darcy coefficient, Critical Reynolds number, and Tortuosity for all generated virtual porous media

Sample	Porosity	KD(mD)	KF (mD)	β (1/m)	Re_c (Eq 4-3)	Re_c (Eq 4-11)	Tortuosity
Sample 1	0.27	5528	5536.88	4.84E+05	1.71	0.0253	1.458
Sample 2	0.22	3159.8	3156.54	1.27E+06	0.796	0.0163	1.528
Sample 3	0.13	706.46	703.646	2.91E+07	0.135	0.0106	1.627
Sample 4	0.22	3021.2	3015.625	1.34E+06	0.665	0.0131	1.53
Sample5	0.35	9030.4	9046.87	2.23E+05	1.92	0.0210	1.413
Sample6	0.18	2216.5	2169.7	1.87E+06	0.62	0.0098	1.556
Sample7	0.40	23021.5	23028.4	5.63E+04	11.09	0.0784	1.363
Sample8	0.10	302.29	302.46	8.99E+07	0.0835	0.0070	1.66
Sample9	0.25	4514.2	4523.437	8.24E+05	0.912	0.0194	1.45
Sample10	0.20	2577.3	2571.7	2.03E+06	0.708	0.0173	1.548

In Table 4-4, some of the proposed empirical correlations utilized to predict non-Darcy coefficient (β(1/m)) are compared to the numerical result for all synthetic porous media. The results illustrate that the correlations proposed with Coles and Hartman,1998 and Jones 1987, are more appropriate to estimate β factors for the synthetic sandstones.

Table 4-4: Comparison of calculated Non-Darcy coefficient (β(1/m)) obtained numerically with predicted value of some presented empirical correlations.

Sample	In this study	Janicek, 1955	Geertsma, 1974	Jones, 1987	Liu,1995	Thauvin, 1998	Coles, 1998	Cooper,1999
1	4.84E+05	1.02E+06	2.87E+06	3.19E+05	2.86E+06	1.50E+06	1.79E+05	3.15E+06
2	1.27E+06	2.46E+06	1.19E+07	7.59E+05	6.43E+06	3.22E+06	4.90E+05	6.27E+06
3	2.91E+07	2.31E+07	4.47E+08	7.74E+06	5.18E+07	2.01E+07	6.18E+06	3.20E+07
4	1.34E+06	2.53E+06	1.20E+07	8.14E+05	6.73E+06	3.39E+06	5.10E+05	6.43E+06
5	2.23E+05	4.54E+05	5.39E+05	1.49E+05	1.31E+06	7.75E+05	8.02E+04	1.79E+06
6	1.87E+06	4.33E+06	4.22E+07	1.32E+06	1.14E+07	5.14E+06	8.34E+05	9.11E+06
7	5.63E+04	1.28E+05	1.62E+05	3.50E+04	4.33E+05	2.64E+05	1.47E+04	6.43E+05
8	8.99E+07	8.12E+07	2.89E+09	2.89E+07	1.67E+08	6.04E+07	2.71E+07	8.52E+07
9	8.24E+05	1.39E+06	4.85E+06	4.37E+05	3.76E+06	1.84E+06	2.54E+05	3.84E+06
10	2.03E+06	3.31E+06	2.19E+07	1.04E+06	8.78E+06	4.22E+06	6.58E+05	7.73E+06

4.5.1 Comparison of experimental data set and simulation results

The numerically calculated non-Darcy coefficients for ten artificial sandstones with different porosities, particle size distributions and average grains sphericities are plotted in the same graph as the experimental data from the literature. As it can be seen Figure 4-3 the generated data fall within the same trend as the experiments. This is very encouraging.

The results are consistent with the hypothesis that numerical approaches can be utilized as an appropriate and alternative method to evaluate the non-Darcy coefficient.

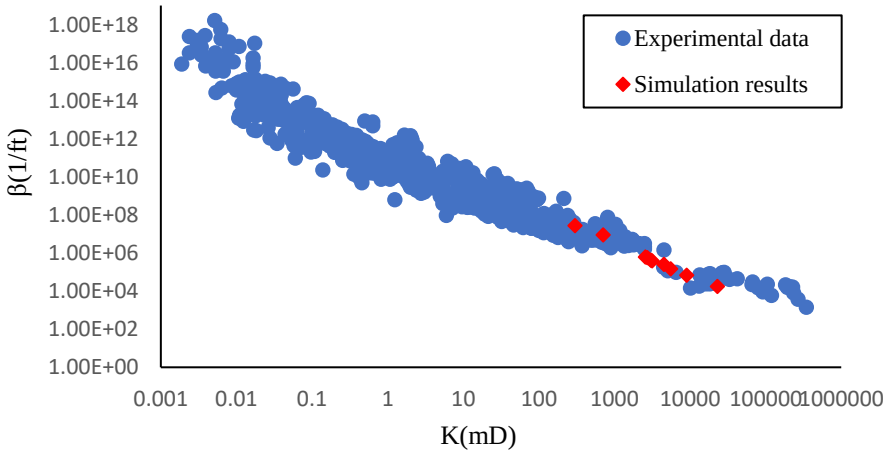

Figure 4-3: Comparison of the calculated non-Darcy coefficient for 10 virtual sandstone with collected experimental data set

4.5.2 Effect of porosity on onset of non-Darcy flow and β factor

Researchers always considered porosity as a key parameter in their empirical correlations to estimate inertial coefficient because different sample porosities can lead to variable pore-scale heterogeneity affecting the non-Darcy coefficient estimation.

Three samples with variable porosities (0.13, 0.27 and 0.4) but similar particle size distribution was chosen to obviously illustrate the effect of porosity on non-Darcy flow (Figure 4-4). The same approach as before was followed in simulating single phase flow.

Figure 4-5 shows the flow streamlines for three generated porous media at similar applied pressure gradients. Moreover, it indicates the critical velocity (minimum velocity for transition from Darcy to non-Darcy flow) where transition from Darcy to non-Darcy flow occurs ($K^* = 0.99$). Table 4-5 shows that critical velocity decreases by reducing the medium porosity (Figure 4-6).

Table 4-5: Critical Velocity for different samples with different porosity

Sample #	Porosity, fraction	Critical Velocity, m/s
7	0.40	0.074
1	0.27	0.00959
3	0.13	0.000323

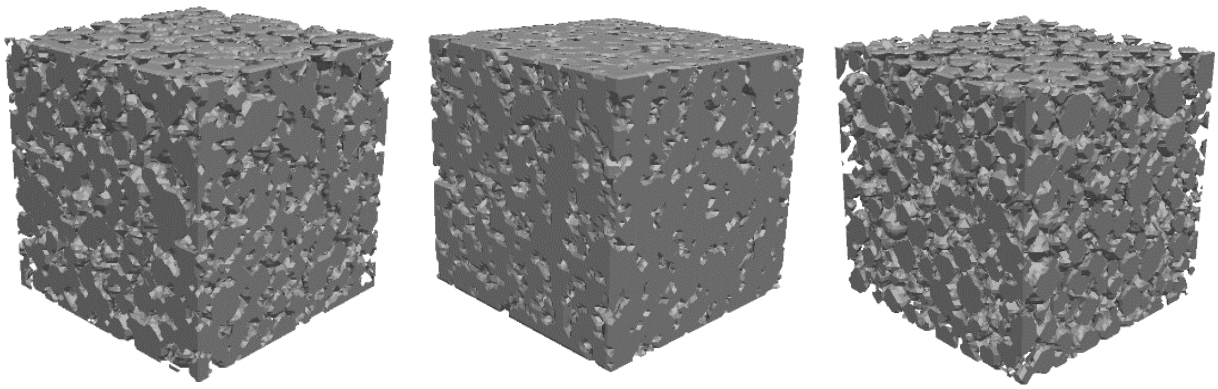

(a) Sample1 (b) Sample3 (c) Sample7

Figure 4-4: The numerical approach presented by Rahmanian and Kantzas, 2018 applied to generate virtual porous media with different porosities (a) Sample 1 with 0.4 porosity. (b) The generated sandstone with porosity of 0.13. (c)The generated sandstone with porosity of 0.22.

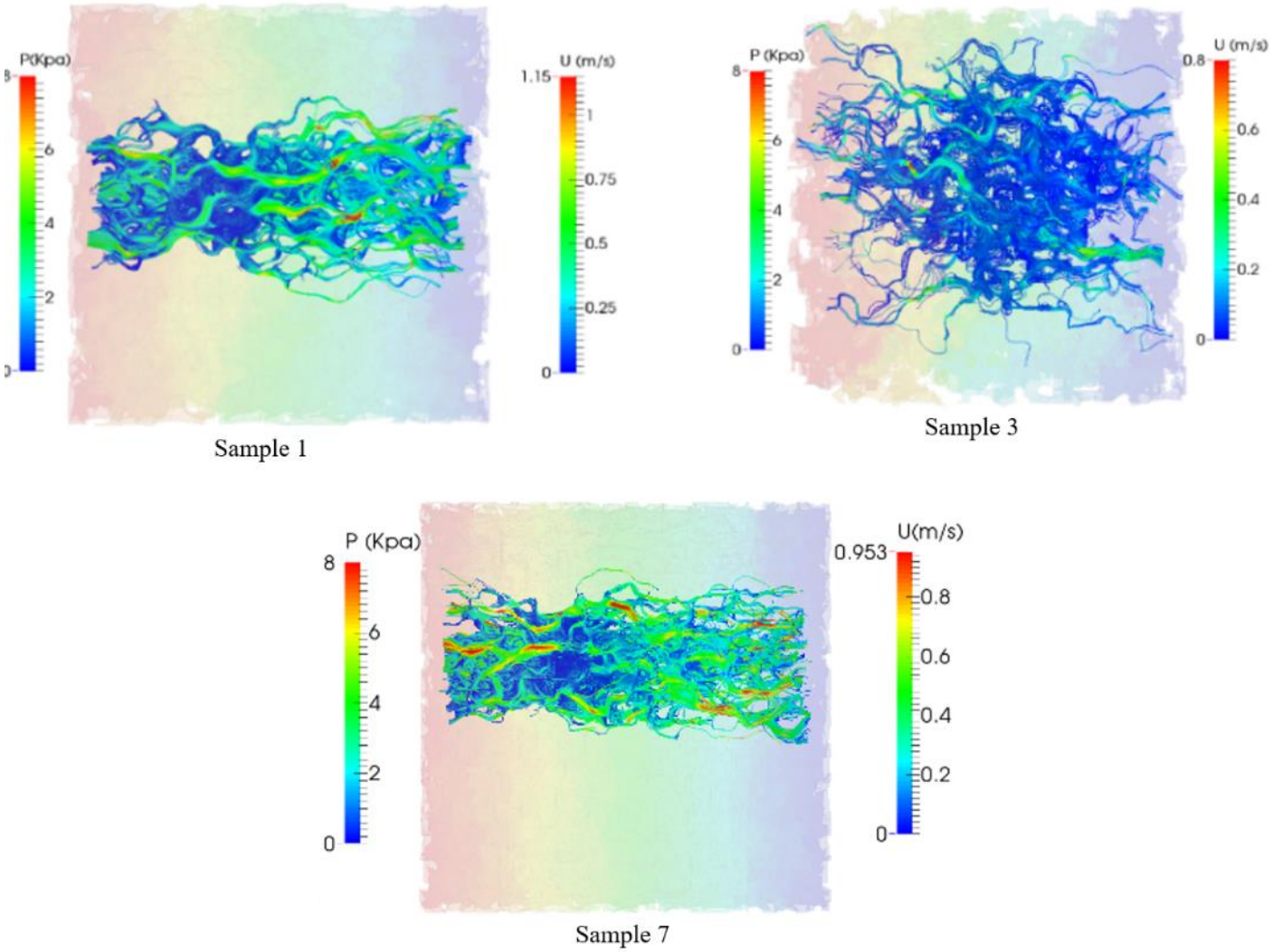

Figure 4-5: Plots of flow streamlines within pores of three generated porous medium by applying pressure gradient at the opposite cross sections perpendicular to the flow direction. The streamlines are colored according to velocity magnitude.

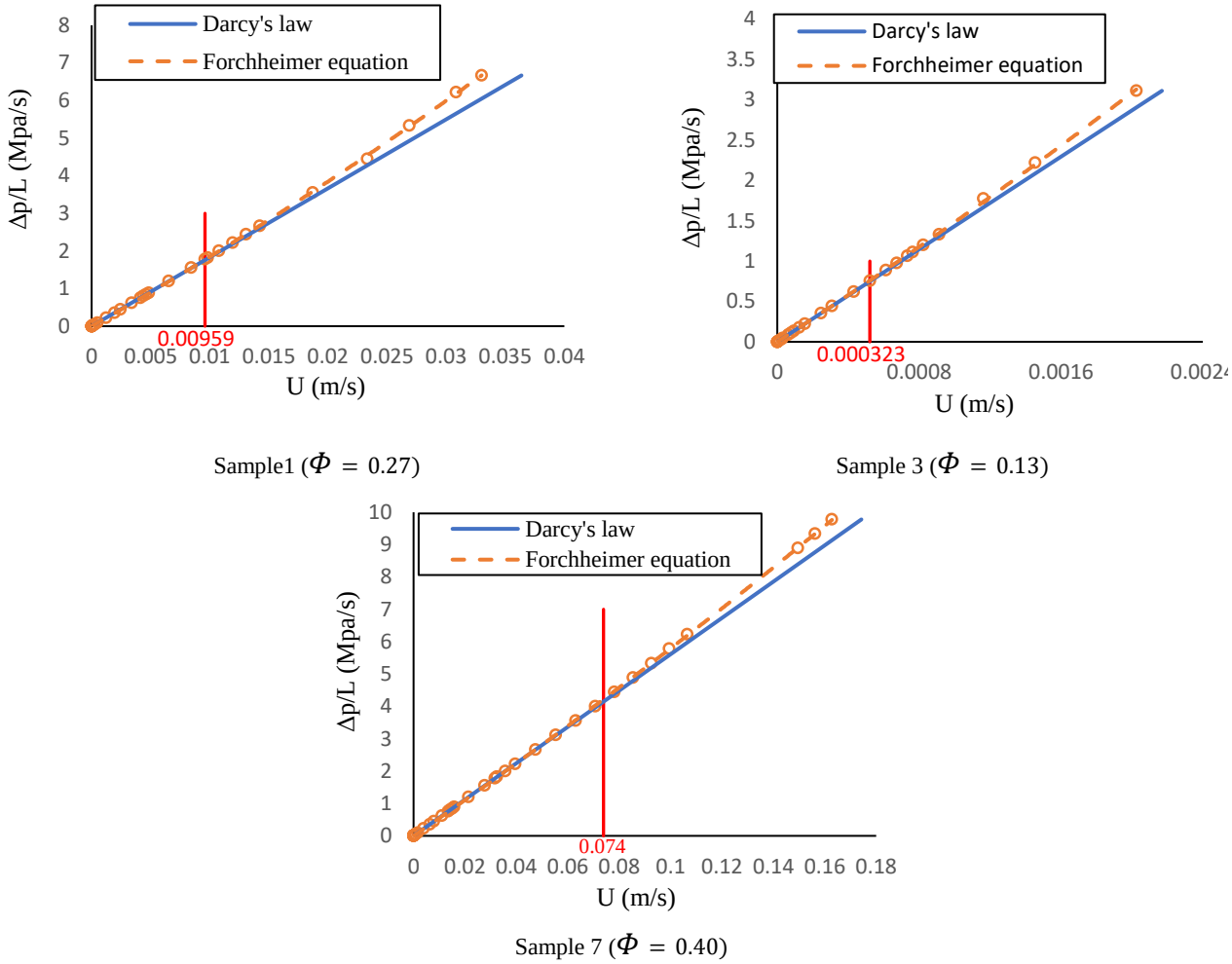

Figure 4-6: Departure from linear relationship between pressure gradient with velocity for three virtual Fontainebleau sandstones with different porosities (Sample 1, Sample 3 and Sample7) at high velocities. The red solid lines indicate the onset of the non-Darcy regime where the pressure gradient due to linear term becomes less than 99% of the total.

In Figure 4-7, the dimensionless permeabilities K^* for all samples are given as functions of the Reynolds number ($Re = \frac{\rho U d}{\mu}$) to indicate the transition from Darcy to non- Darcy flow where $\frac{\pi}{S_v}$ is considered as a characteristic length in this study. According to Figure 4-7, it is demonstrated that departure from Darcy flow to non-Darcy flow occurs in lower range of velocity where porosity decreases.

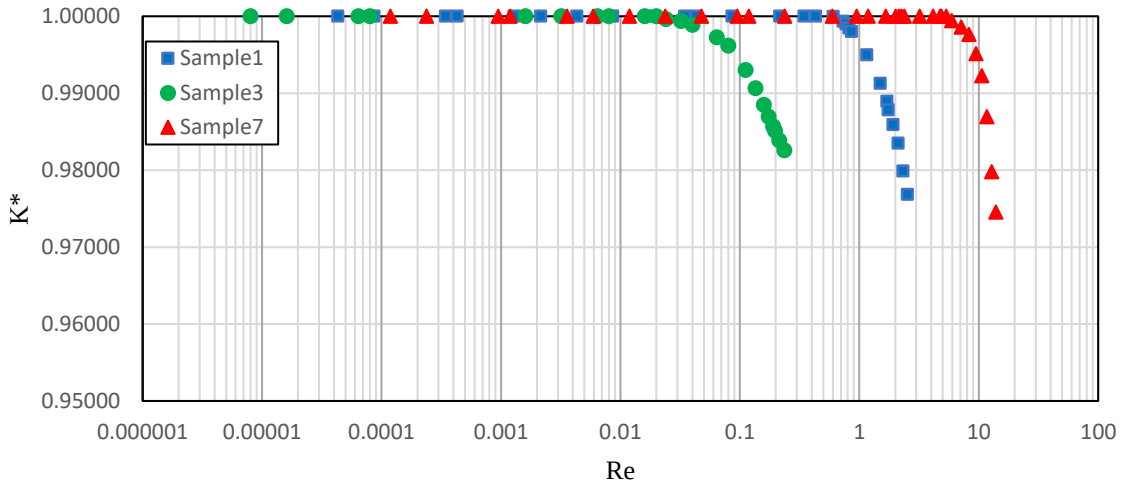

Figure 4-7: The dimensionless permeability K* as a function of Re shows the transition from the Darcy to non-Darcy flow regimes for Samples 1, 3 and 7

As measurement of tortuosity in porous media is not feasible if possible, Equation 4-28 proposed by Koponen et al. (1996) utilized to estimate tortuosity from the fluid velocity in a porous medium without using flow path measurement.

By applying this method, the tortuosity of a porous medium is estimated in different velocities. (Figure 4-8) shows the functionality of tortuosity and apparent permeability versus velocity for the three synthetic samples.

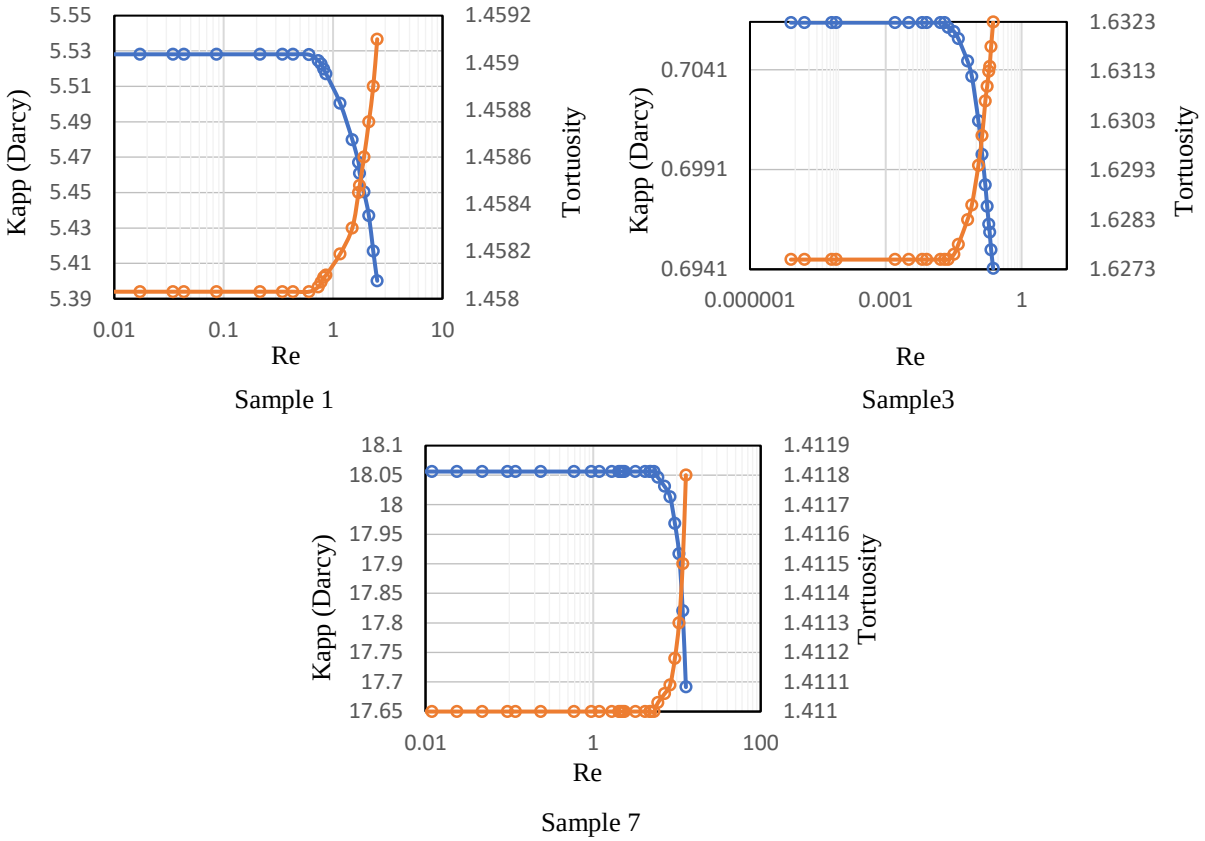

Figure 4-8: Tortuosities and apparent permeabilities are plotted as functions of Re for the three virtual samples.

According to Equation 4-25, non-Darcy coefficient β can be estimated by plotting $\frac{1}{K_{app}}$ against $\frac{\rho U}{\mu}$ and obtaining the slope of line in the Forchheimer regime (Figure 4-9).

In Figure 4-9, the β factors for three samples with different porosities are obtained (Sample 1(Φ =0.27)), β=4.84E+5 m^{-1}; Sample 3 (Φ =0.13), β=2.91E+7 m^{-1} and Sample 7 (Φ =0.40), β=5.63E+4 m^{-1}. The calculations demonstrate that samples with lower porosity have larger non-Darcy coefficient which means the inertial term is more significant in lower porosity. Figure 4-10 and Figure 4-11 illustrates calculated non-Darcy coefficient β and functionality of tortuosity and apparent permeability versus velocity for other synthetic samples respectively.

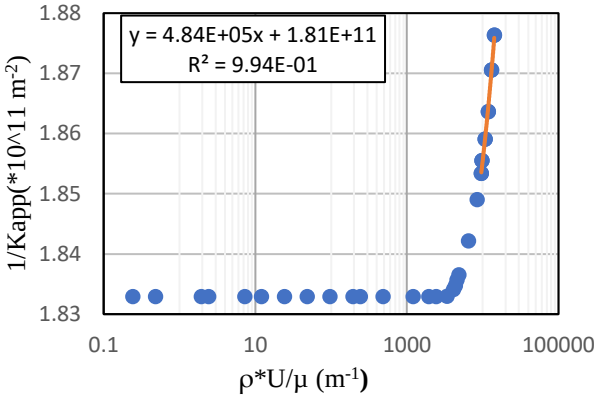

Sample 1

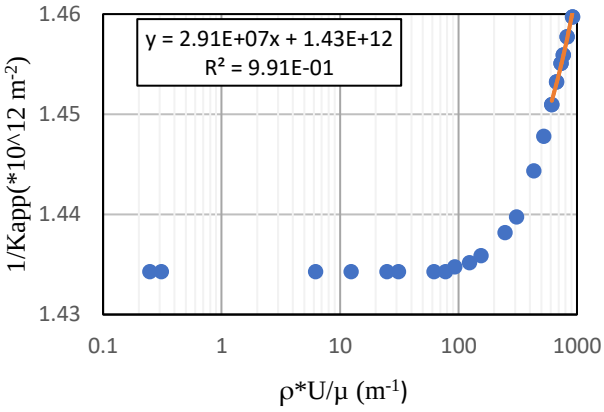

Sample 3

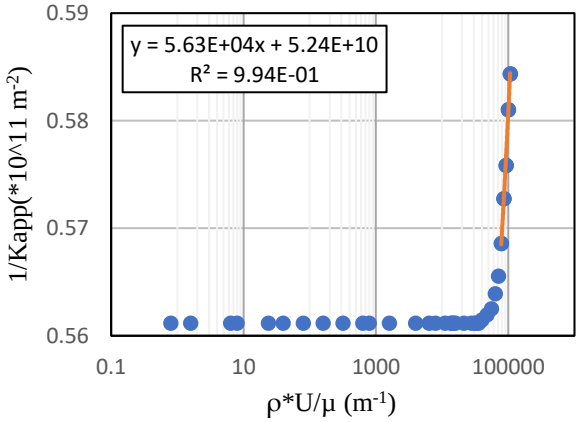

Sample 7

Figure 4-9: Calculated β factors for all three samples from the slopes of the graphs in the Forchheimer regime.

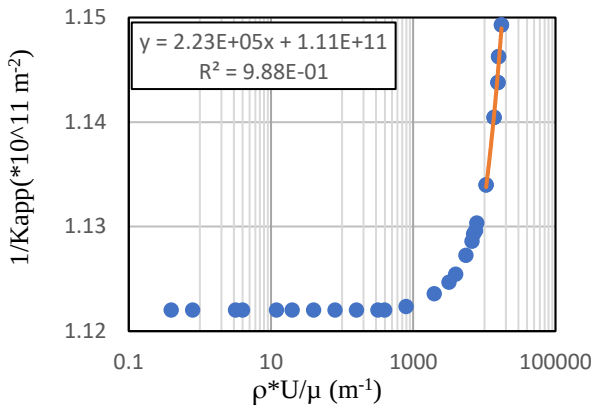

Sample5 (ø = 0.35)

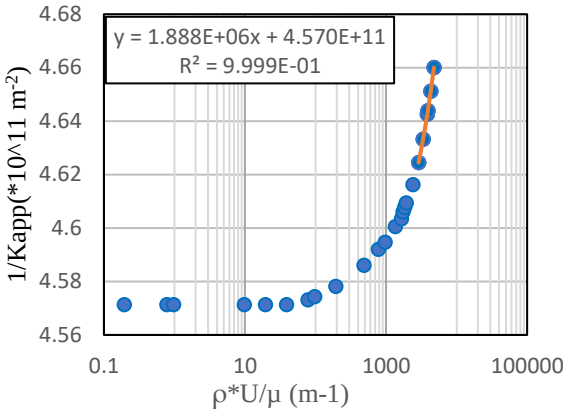

Sample 6 (ø = 0.18)

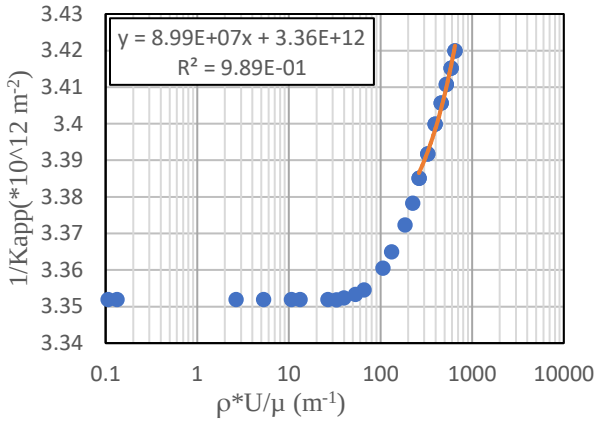

Sample8 (ø = 0.10)

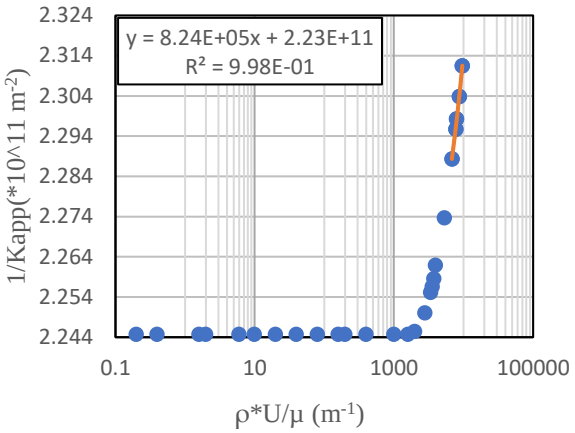

Sample9 (ø = 0.25)

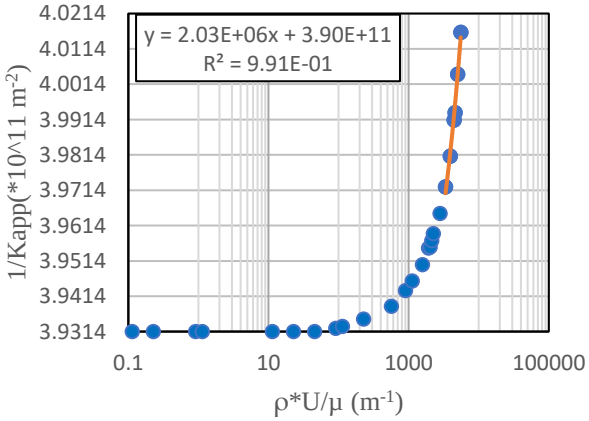

Sample 10 (ø = 0.2)

Figure 4-10: Calculated β factors for virtual samples with different PSD and porosities.

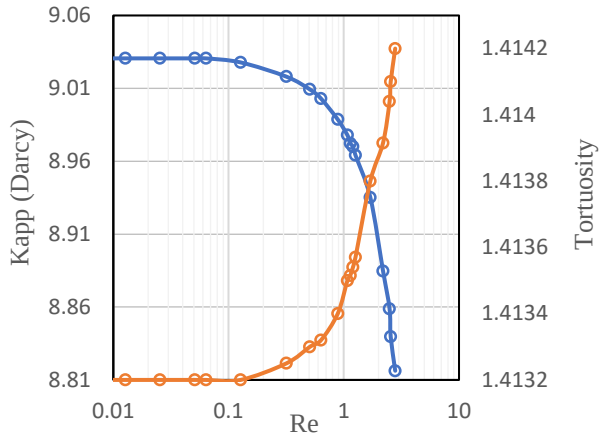

Sample5 ($\emptyset = 0.35$)

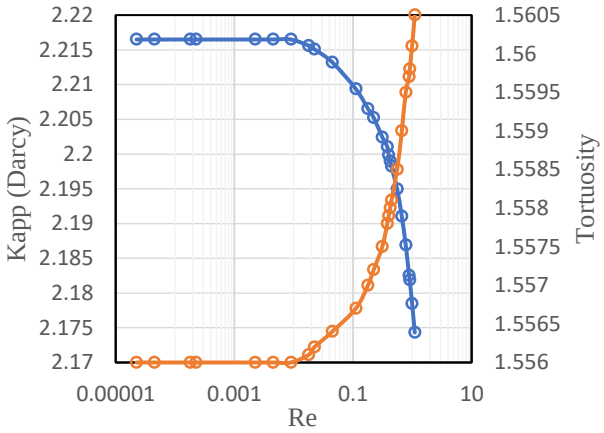

Sample 6($\emptyset = 0.18$)

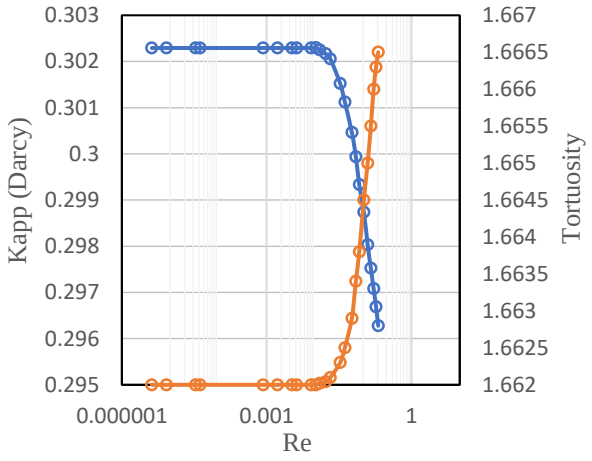

Sample 8($\emptyset = 0.10$)

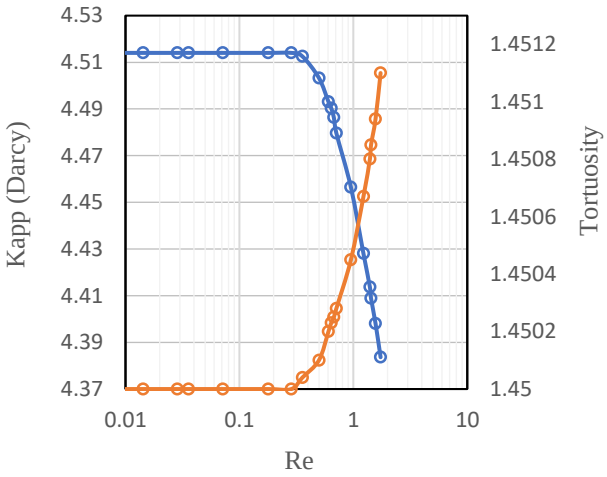

Sample 9($\emptyset = 0.25$)

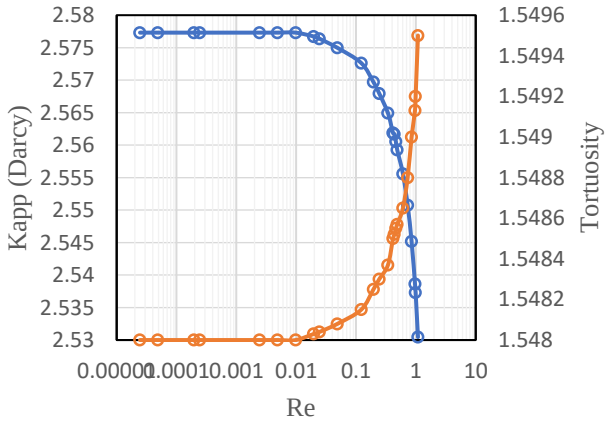

Sample 10 ($\emptyset = 0.10$)

Figure 4-11: Tortuosities and apparent permeabilities are plotted as functions of Re for virtual samples with different porosity and PSD.

4.5.3 Effect of average grain sphericity on non-Darcy flow

There has been a technical debate between researchers looking to find a generic empirical correlation to estimate the inertial factors of various porous media. Some of them related the non-Darcy coefficient to just absolute permeability and porosity (Janicek and Katz, 1955; Geertsma,1974; Coles and Hartman,1998), while others believed that tortuosity as a parameter should be considered in their correlation (Liu et al.,1995; Thauvin and Mohanty,1998; Cooper et al.,1999). To investigate whether or not the tortuosity should get involved as a parameter in an empirical correlation, two virtual porous media (Sample 2 and Sample 4) were generated with similar porosity ($\Phi = 0.22$) and the same particle size distribution but different average grains sphericities (Sample 2 average grain sphericity is 0.82 while Sample 4 average grain sphericity is 0.75) (Figure 4-12.a and Figure 4-12.b). Numerical simulations were run on the pore space in different pressure gradients to determine the onset of non-Darcy flow as well as Forchheimer coefficient for the two samples. (Figure 4-12.c and Figure 4-12.d) shows the flow streamlines for two generated porous media at the similar applied pressure gradient.

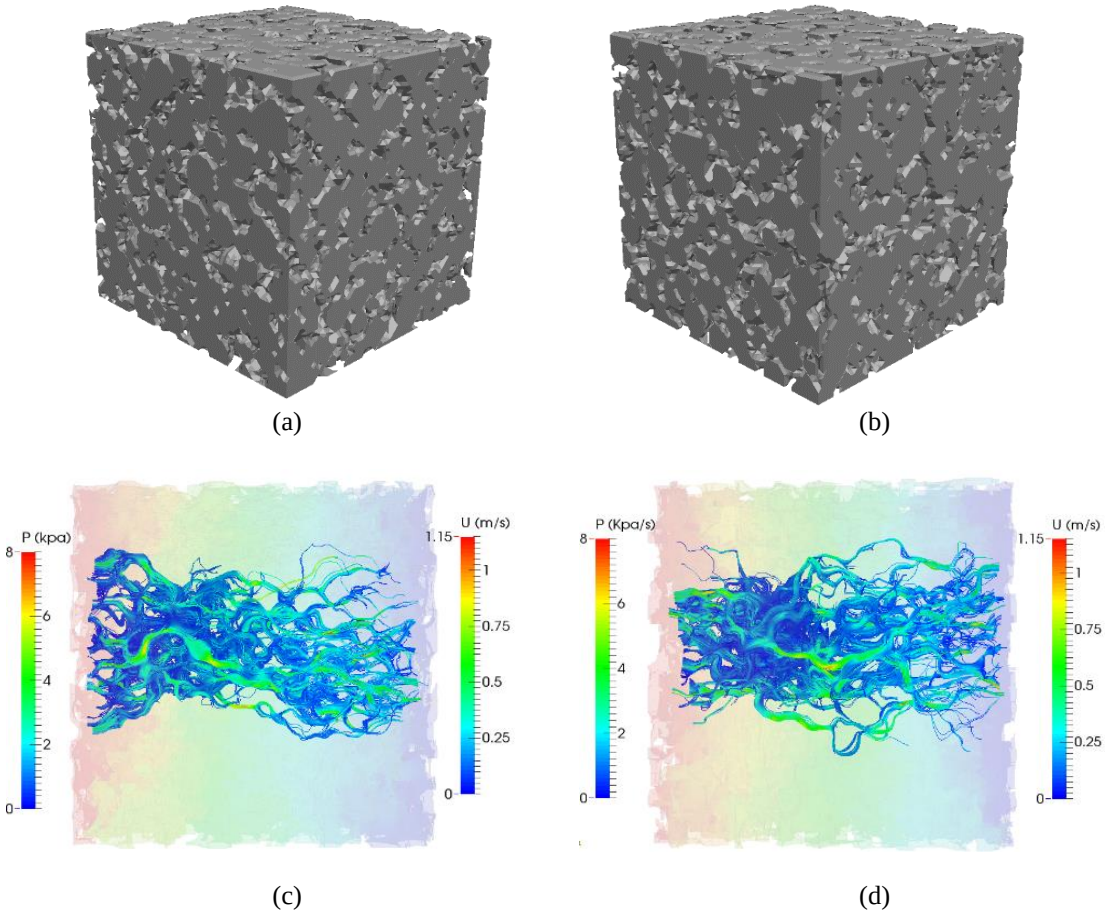

Figure 4-12: Two porous media constructed with similar particle size distribution and porosity but different average grains irregularity (a) 3D virtual porous medium of Sample 2 with 0.22 porosity and 0.82 average grain sphericity. (b) 3D virtual porous medium of Sample 4 with 0.22 porosity and 0.75 average grain sphericity. Plots of flow streamlines within pores of two generated porous media (c) Flow streamline within pore structure of sample 2 (d) Flow streamline within pore structure of sample 4 by applying similar pressure gradient (8000 Pa) at the opposite cross sections perpendicular to the flow direction. The streamlines are colored according to the magnitude of velocity.

In Figure 4-13, pressure gradient versus velocity for sample 2 and sample 4 is plotted. It shows that critical velocity decreases by reducing the average grain sphericity of the porous medium.

Table 4-6: Critical velocity for different samples with different average grain sphericity

Sample #	Average Grain Sphericity	Critical Velocity, m/s
2	0.82	0.00412
4	0.75	0.00328

Simulation results demonstrate that grains irregularity leads to pore-scale heterogeneity which can affect the Forchheimer coefficient and the onset of non-Darcy flow. It can be observed that

departure from Darcy to non-Darcy flow is more extreme in high flow rate for the sand containing more irregular grains while both virtual sandstones have almost similar porosity and particle size distribution (Figure 4-13). It can be concluded the effect of grain irregularity is more tangible in higher velocities which can affect non-Darcy coefficient. Therefore, tortuosity as a key parameter can affect the estimation of the non-Darcy coefficient and it should be considered in the proposed empirical correlations.

Table 4-7, shows the computed Darcy permeability and also the critical Reynolds number for the two generated sandstones. Although the effect of average grain sphericity on Darcy permeability of two generated sandstones is not noticeable, it affects the transition of Darcy flow to non-Darcy flow regime.

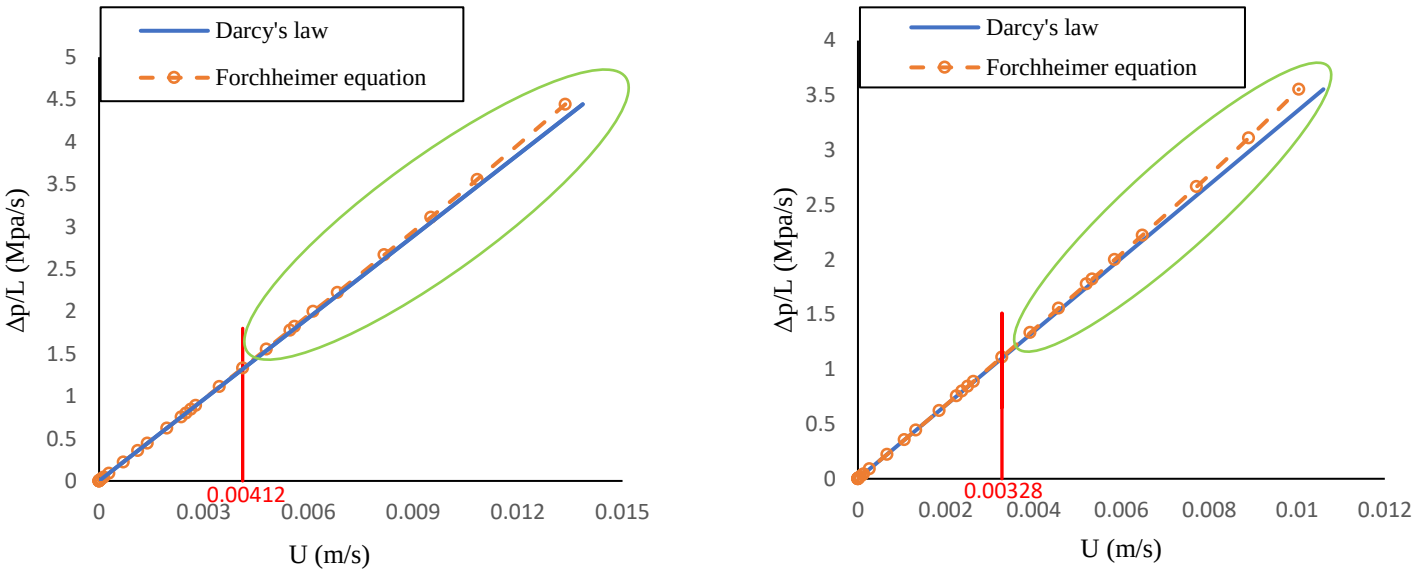

Sample 2 Sample 4

Figure 4-13: Departure from linear relationship between pressure gradient with velocity for two virtual Fontainebleau sandstones with similar porosities ($\Phi = 0.22$) but different average grain sphericity (Sample 2 contain grains with average grains sphericity 0.82 and Sample 4 with average grains sphericity 0.75) is indicated by red solid line.

Table 4-7: Critical Reynolds number and Darcy permeability for two samples with different average grains sphericity

Sample	Porosity	Average grain sphericity	Characteristic length (D): $(\frac{\pi}{S_v})$	Critical Reynolds number Re^*	K_D (mD)
Sample 2	0.22	0.82	1.934E-04	0.796	3159.8
Sample 4	0.22	0.75	2.03E-04	0.666	3021.2

In Figure 4-14, the dimensionless permeability K* is plotted against the Reynolds number (Re). It shows the transition from the Darcy to non-Darcy flow regimes for sample 2 and sample 4.

In Figure 4-15, tortuosity and apparent permeability for the two samples are plotted versus the Reynolds number. It indicates that the generated sample including more irregular grains (sample 4) has more tortuosity compared with sample 2.

The non-Darcy coefficients, β, for these two samples are estimated by plotting $\frac{1}{K_{app}}$ vs. $\frac{\rho U}{\mu}$ and obtaining the slope of line in the Forchheimer regime (Sample 2: average grain sphericity=0.82, β = 1.27E+6 (1/m). Sample 4: average grain sphericity =0.75, β =1.57E+6 (1/m) (Figure 4-16)).

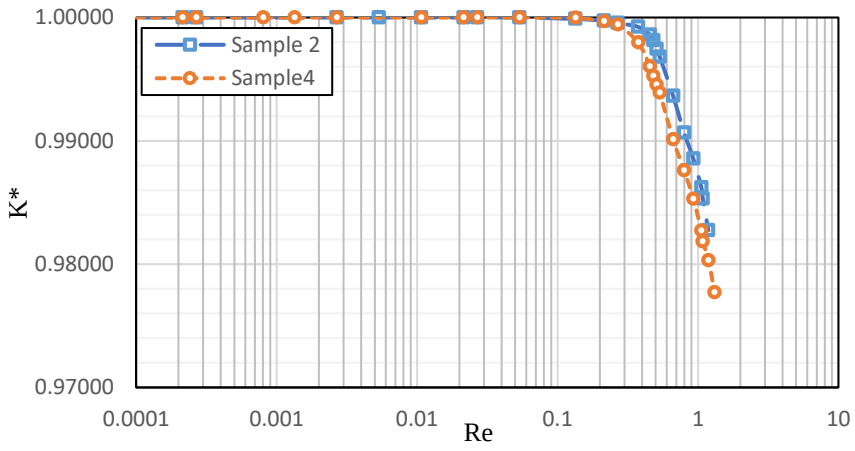

Figure 4-14: The dimensionless permeability K* as a function of Re shows the transition from the Darcy to non-Darcy flow regimes for sample 2 and sample 4.

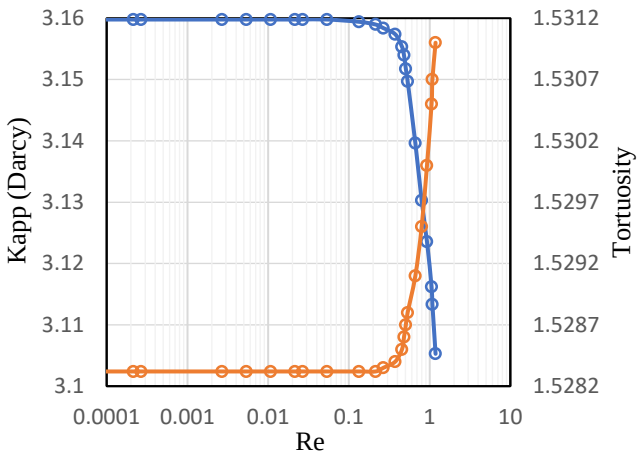

Sample 2

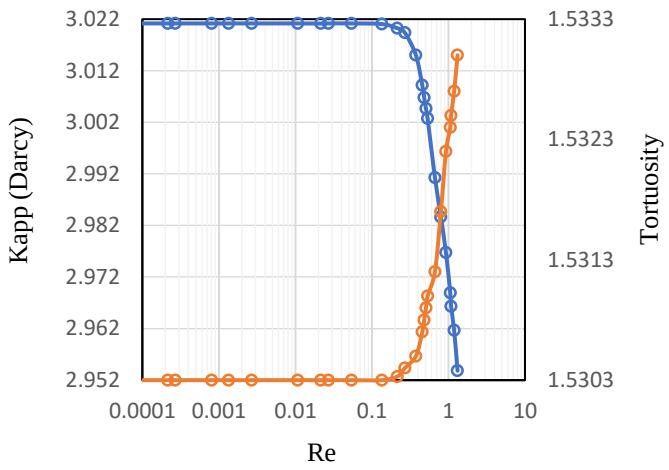

Sample 4

Figure 4-15: Tortuosities and apparent permeabilities are plotted as functions of Re for two virtual samples.

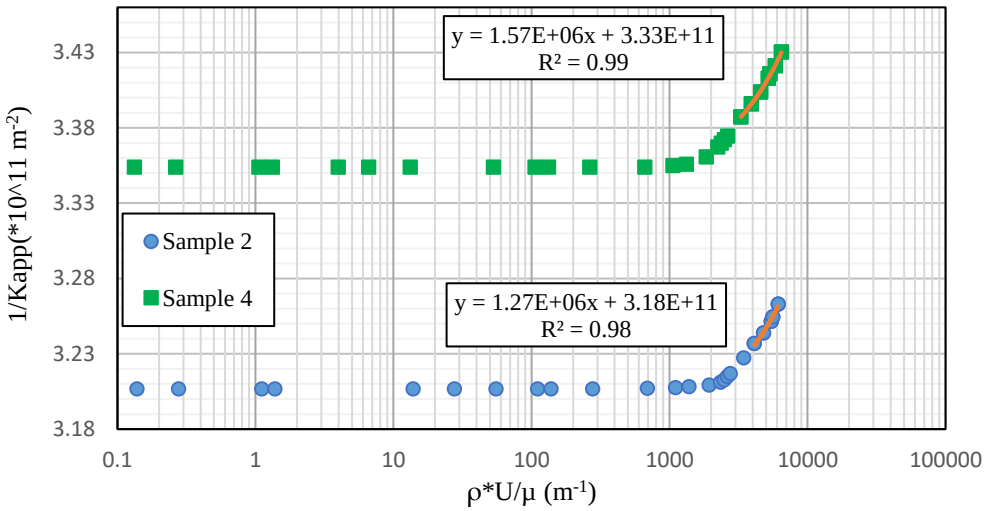

Figure 4-16: Obtaining β factors for sample 2 and sample 4 from the slops of the graphs in the Forchheimer regime.

4.5.4 Effect of connate water on non-Darcy flow

So far, the non-Darcy flow was studied in fully saturated porous media, however, geological formations are usually partially saturated with water. Basically, water fills the high-capillarity portions of the pore space. Since assessment of non-Darcy flow coefficient for the multiphase cases can be different from the estimation of single-phase non-Darcy flow coefficient, numerous researchers explored the effect of immobile water at various saturations on porous medium.

Gewers and Nichol (1969) presented an empirical correlation to estimate non-Darcy coefficient for carbonate rocks. They also attempted to determine the effect of an immobile liquid experimentally at different saturations on the non-Darcy flow coefficient. Glycerin was used in their research as the liquid phase at saturations of 10%, 20%, and 30%. They found that non-Darcy coefficient increases dramatically at higher saturations.

Geertsma (1974) not only proposed a β correlation in a single-phase system, but also, he offered a correlation to estimate β in a two-phase system. He actually modified the correlation which was developed to estimate non-Darcy coefficient at single-phase flow in porous medium. He assumed that single-phase permeability would be replaced by gas permeability in pore spaces which is not occupied with residual water saturation (Equation 4-29).

$$\beta = \frac{0.005}{K^{0.5}.\Phi^{5.5}} \frac{1}{(1-S_{wr})^{5.5}.\ {K_{rel}}^{0.5}} \qquad 4\text{-}29$$

Where K_{rel} is the gas relative permeability, S_{wr} is the residual water saturation, K is the absolute permeability (cm^2) and β is non-Darcy coefficient (cm^{-1}).

Kutasov (1993) proposed an empirical correlation for non-Darcy coefficient and claimed that the presented correlation (Equation 4-30) can estimate β for situations where mobile or immobile water saturation exist in system.

$$\beta = \frac{1432.6}{{K_g}^{0.5}[\Phi(1-S_{wr})]^{1.5}} \qquad 4\text{-}30$$

Where β is in 1/cm and k_g is in Darcy.

Frederick and Graves (1994) proposed two different proposed correlations (Equation 4-31 and Equation 4-32) tuning from two different regression methods on data sets which cover a wide span

of porous materials with various permeabilities. They found that these correlations are applicable in systems with mobile liquid saturation as well.

$$\beta = \frac{2.11\mathrm{E}+10}{{K_g}^{1.5}[\Phi(1-S_{wr})]} \qquad 4\text{-}31$$

$$\beta = \frac{1}{[\Phi(1-S_{wr})]^2}\, e^{45-\sqrt{407+81*\ln[\frac{K_g}{\Phi(1-S_{wr})}]}} \qquad 4\text{-}32$$

Where β is in ft^{-1} and K_g is gas effective permeability in md.

4.5.5 Multi-Phase fluid occupancies

The quasi-static pore morphological approach was utilized to reconstruct two-phase profiles through pore space domains, and simulates the fluid flow in porous media at low capillary numbers where the effect of gravity and viscous forces on the fluids propagation is negligible (Mohammadmoradi and Kantzas,2017). The fluid occupancy results describe the interfacial arrangements at capillary equilibria. To reach the irreducible water saturation, the primary drainage scenario is simulated within the reconstructed pore-level domains while the pixels of the images are treated as computational nodes. Hence, the reconstructed synthetic media are already discretized, and there is no need to mesh the domains. In this study, sample 4 was selected as a sample to investigate the effect of connate water on onset of non-Darcy flow and inertial coefficient for unconsolidated porous media. In summary, two-phase simulations are conducted applying the following step (Mohammadmoradi and Kantzas,2017):

- Enlarge an expanding sphere over each pixel of the pore space and extract its maximum allowable size where the sphere touches the grain surface.
- Replace the size of each pixel if there is a larger sphere covering it.
- Extract the pore size distribution of the whole domain.
- Saturate the pore space with water as the wetting phase.

- Select one boundary face as inlet and the rest as outlets.
- Increase the non-wetting phase pressure and at each step check the accessibility and pore size of each pixel and rearrange the interfaces accordingly.
- Continue pressure buildups until no more water is produced (the saturation of immobile water for sample 4 is 8.7 % of pore volume) (Figure 4-17.a).
- Extract the non-wetting phase profile by at the end of drainage (Figure 4-17.c).
- Apply a pressure difference between two opposite faces of the extracted profile (Figure 4-18).
- Calculate the porosity and average velocity in a cross-section perpendicular to the flow direction.
- Calculate the permeability of the non-wetting phase in the presence of connate water.

Figure 4-17.b illustrates the connate water occupancy profile through sample 4 as a packing of thousands of irregular gains. The water saturation profile through the medium with irregular grains appears amorphous and heterogeneous while the shape of residual water is analogous to pendular rings and lenses between solid grains.

To simulate fluid flow in porous medium, pressure gradient applied on two opposite faces perpendicular to fluid flow. The streamlines are colored according to the magnitude of velocity (Figure 4-18).

Figure 4-19 demonstrates the departure from Darcy flow to non-Darcy flow occurs in lower velocity at the unsaturated sandstone (sample 4, containing immobile water at 8.7% PV) compared to the fully saturate sandstone (sample 4, fully saturated).

In Figure 4-20, K^* as a function of Reynolds number is plotted for fully saturated and unsaturated of sample 4 (containing immobile water at 8.7% PV). It is concluded that critical Reynolds number as a criterion to identify the onset of non-Darcy flow is lower for unsaturated sample 4 in comparison with fully saturated-sample 4. Table 4-8 shows physical properties and

simulation results of saturated and unsaturated sandstone (sample 4).Figure 4-21 illustrates tortuosities and apparent permeabilities as functions of Reynolds number for the saturated and unsaturated sandstones (sample 4). It is found that the unsaturated sandstones (containing immobile water at 8.7% PV) appears less tortuous rather than totally saturated one.

It is observed that the non-Darcy flow coefficient dramatically increased when immobile water occupied some portions of the pore space (Figure 4-22). In this case study, where immobile water occupied just 8.7% of pore volume, β increases about 150% which means that the inertial term in Forchheimer equation is more dominant. Thus, the departure from Darcy flow occurs in the lower range of velocity for the unsaturated sandstone in comparison with the saturated one. Table shows the prediction of the proposed correlations in systems with mobile liquid saturation. As it can be observed, there is a good agreement between simulation result and the correlation presented by Frederick and Graves (1994) (Eq.33).

Table 4-8: Critical Reynolds number , darcy permeability and non-Darcy coefficient for fully saturated case of sample 4 compared to unsaturated one (Immobile water occupied 8.7% of PV in sample 4)

Sample	Porosity	K_D (mD)	Re_c (Eq.4-3)	Re_c (Eq.4-11)	β(1/m)
Sample4 fully saturated	0.22	3159.8	0.796	0.0163	1.35E+6
Sample4 containing immobile water	0.22	2363.3	0.669	0.0131	2.46E+6

Table 4-9: Estimation of available proposed empirical correlation to predict inertial coefficient

Proposed Correlation	Non-Darcy coefficient(1/m)
Geertsma (1974) (Eq.4-29)	1.506E+07
Kutasov (1993) (Eq.4-30)	9.296E+05
Frederick (1994) (Eq.4-31)	2.792E+06
Frederick (1994) (Eq.4-32)	8.699E+05

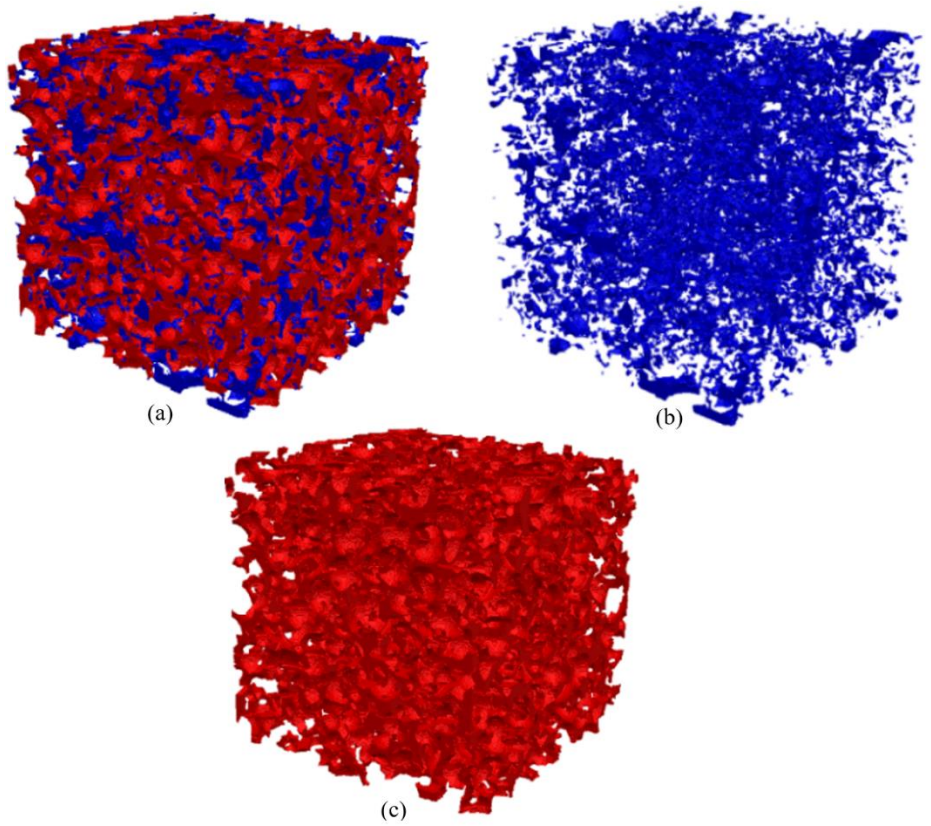

Figure 4-17: (a) Three-dimensional rendering of two-phase fluid occupancy at the end of drainage through Sample 4. (b) The connate water distribution profile at the end of drainage through Sample 4. (c) Pore structure after omitting connate water at the system.

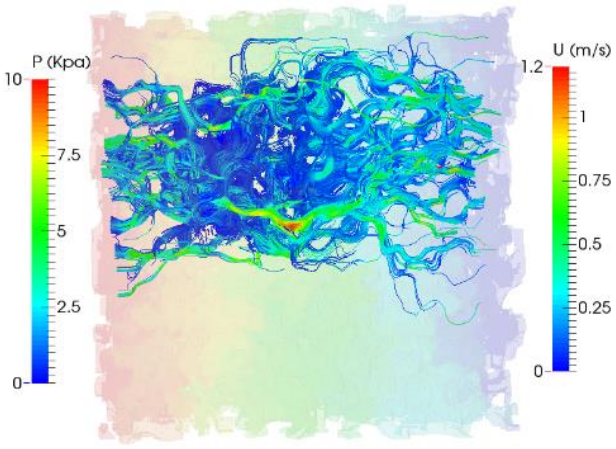

Figure 4-18: Pressure gradient applied on two opposite faces perpendicular to fluid flow. The streamlines are colored according to the magnitude of velocity.

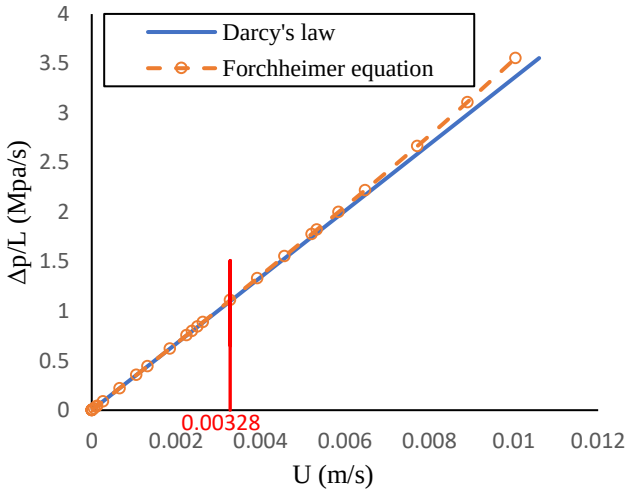

Sample 4 fully saturated

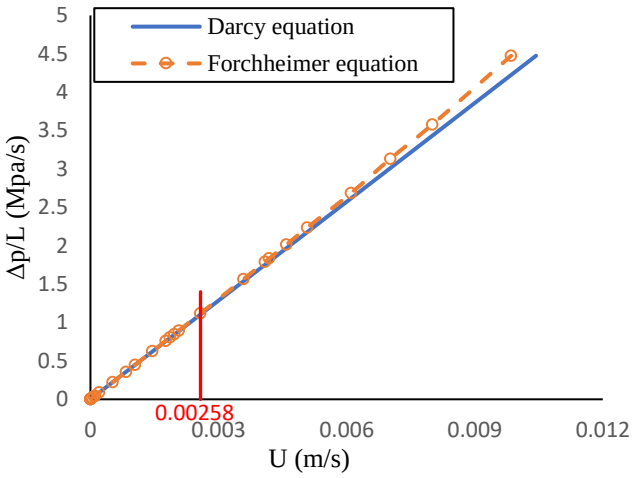

Sample 4 containing immobile water at saturations of 8.7% PV

Figure 4-19: Departure from Darcy to non-Darcy regime for fully saturated ($\Phi = 0.22$) and unsaturated (containing immobile water at saturation of 8.7% PV) Fontainebleau sandstone is indicated with solid line.

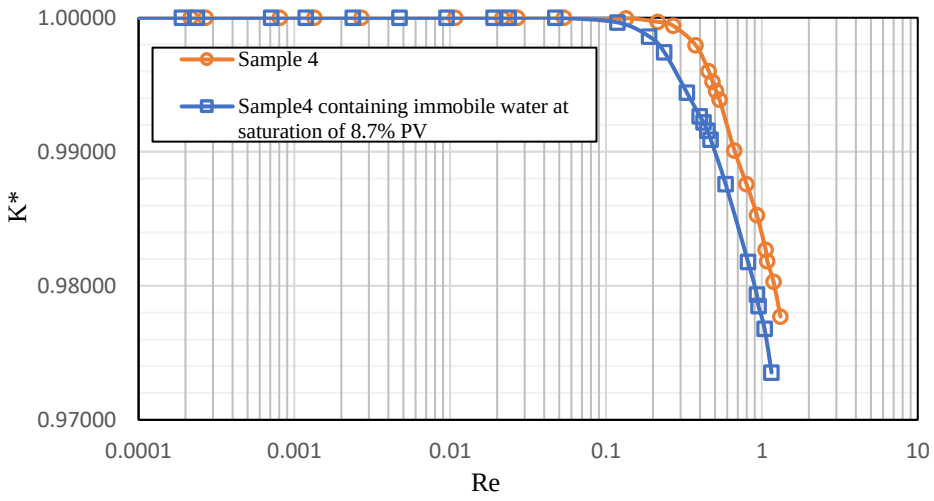

Figure 4-20: The dimensionless permeability K* as a function of Re shows the transition from the Darcy to non-Darcy flow regimes (occurs at K*= 0.99) for fully saturated and unsaturated sandstone.

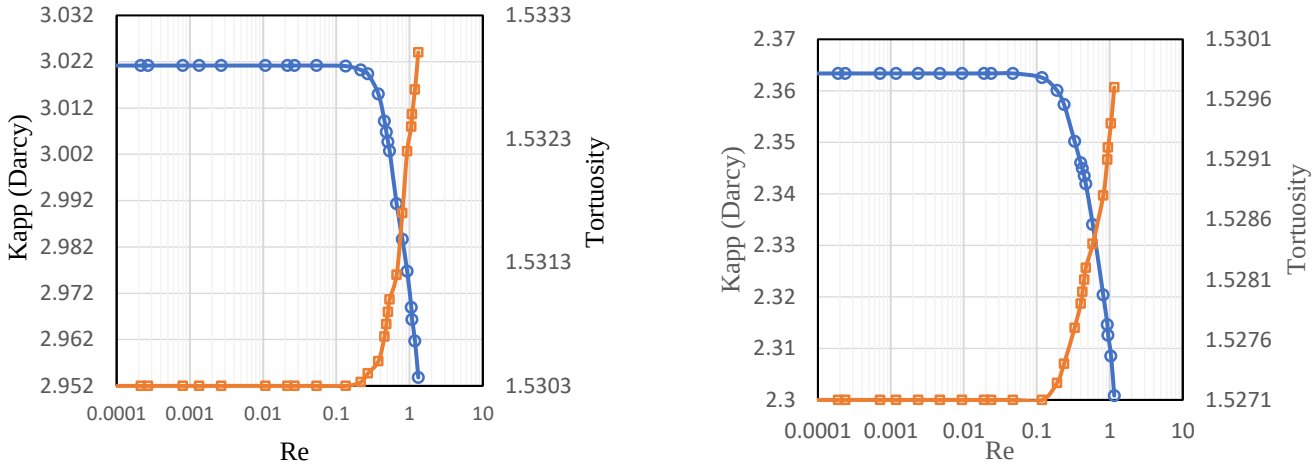

Sample 4, fully saturated

Sample 4, containing immobile water at saturations of 8.7% PV

Figure 4-21: Tortuosities and apparent permeabilities are plotted as functions of Re for saturated and unsaturated sandstone.

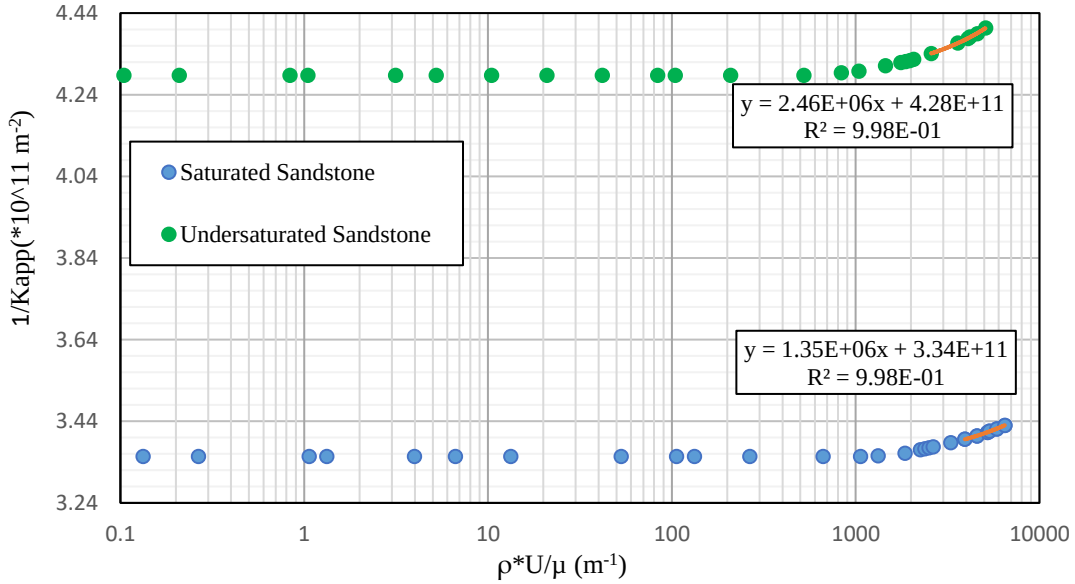

Figure 4-22: Obtaining of β factors for saturated and unsaturated of Sample 4 from the slops of the graphs in the Forchheimer flow regime.

5 CONCLUSIONS AND RECOMENATIONS

A new approach for numerical construction of virtual porous media inspired from the crystallization concept is proposed in chapter 2. This proposed approach is remarkably faster compared to previous models and produced more realistic virtual media compared to the other approaches. There is no limitation to generate synthetic porous media at low porosities, while the model accurately satisfies the target porosity and the given PSD. Moreover, grain irregularity can be controlled by user. In this methodology, as the target porosity of a virtual porous medium decreases, the grains inside the porous material tend to become more irregular while still honoring the provided PSD. This conforms to what happens at natural sandstones when overburden pressure compressed and deformed inside the formation. A virtual porous medium based on the given porosity and PSD of Fontainebleau sandstone generated and calculated single phase transport properties successfully matched with experimental result. Moreover, in this study, several virtual porous media at different ranges of porosities and variety of PSDs were constructed using the proposed approach. The simulation results on these media ended up with two correlations; one for estimation of permeability vs. porosity and the other one for estimation of formation factor as a function of porosity. These presented correlations were compared against the other available correlations. It was revealed that the presented correlations are practically more reliable and applicable to a wider range of data.

In chapter 4, several porous media with various porosities, PSD and average grain sphericities were generated. Afterward, the effects of porosity, average grain sphericities and presence of immobile water on the onset of non-Darcy flow by conducting the direct flow simulations (FVM method) through synthetic sandstones were investigated. The onset of non-Darcy flow was

defined as the point where pressure drop due to the linear term becomes less than 99% of the total (dimensionless apparent permeability K^*= 0.99). We find that the Forchheimer number is more physically consistent compared to standard Reynolds number as a criterion to determine the beginning of non-Darcy flow. Moreover, in our study, we find a good agreement between the calculated β factors for virtual sandstones and available experimental data sets. It is also concluded that the average grain sphericity can affect the estimation of β factors for sandstones. Although grain irregularity does not have a noticeable effect on Darcy flow where fluid flow velocity is slow (viscous term is dominant), the fluid flow through the porous medium can be affected by average grain sphericity where the inertial term is dominant. Furthermore, it is observed that the assessment of the non-Darcy flow coefficient for the multiphase cases can be dramatically different from the estimation of single-phase non-Darcy flow coefficient. In this work, we find that non-Darcy coefficient increases about 180% where 8.5% of pore volume occupied with immobile water.

RECOMMENDATION

Progress has been made in the developing of virtual porous media so that grain shape, porosity and PSD can be control by user, but many important research questions and technical support needs are still remaining. Investigation of grain irregularity effect on multi-phase flow, relative permeability and capillary pressure curves could be an interesting and valuable research topic for the future studies. Type and size of the applied mesh on the generated virtual media could have significant effects on the results and is recommended to be investigated in future research. Moreover, the run time of the developed program is high especially for generation of large media. The run time could be improved by applying parallel processing approaches providing us the ability to generate larger and more realistic virtual porous media.

REFRENCES

Adler, P. M. (1988). Fractal porous media III: Transversal Stokes flow through random and Sierpinski carpets. *Transport in Porous Media*, **3(2)**, 185-198.

Afshari, S., Beni, A. H., Taheri, S., Hejazi, H., and Kantzas, A. (2016, August). Longitudinal dispersion coefficient calculation during miscible flow in heterogeneous porous media using pore scale simulation. *In International Symposium of the Society of Core Analysts*. Colorado, USA.

Aharonov, E., and Rothman, D. H. (1993). Non-Newtonian flow (through porous media): A lattice-Boltzmann method. *Geophysical Research Letters*, **20(8)**, 679-682.

Almalowi, S. J., and Oztekin, A. (2012). Flow simulations using two-dimensional thermal Lattice Boltzmann method. *Journal of Applied Mathematics*, 2012.

Alreshedan, F., and Kantzas, A. (2016). Investigation of permeability, formation factor, and porosity relationships for Mesaverde tight gas sandstones using random network models. *Journal of Petroleum Exploration and Production Technology*, **6(3)**, 545-554.

Alreshedan, F., and Kantzas, A. (2016). Sensitivity Analysis of the Effect of Pore Structure and Geometry on Petrophysical and Electrical Properties of Tight Media: Random Network Modeling. *Journal of Petroleum Science and Technology*, **6(1)**, 28-45.

Andrade Jr, J. S., Costa, U. M. S., Almeida, M. P., Makse, H. A., and Stanley, H. E. (1999). Inertial effects on fluid flow through disordered porous media. *Physical Review Letters*, **82(26)**, 5249.

Archie, G. E. (1942). The electrical resistivity log as an aid in determining some reservoir characteristics. *Transactions of the AIME*, **146(01)**, 54-62.

Arns, C. H., Knackstedt, M. A., Pinczewski, M. V., and Lindquist, W. B. (2001). Accurate estimation of transport properties from microtomographic images. *Geophysical research letters*, **28(17)**, 3361-3364.

Auzerais, F. M., Dunsmuir, J., Ferreol, B. B., Martys, N., Olson, J., Ramakrishnan, T. S., ... and Schwartz, L. M. (1996). Transport in sandstone: a study based on three dimensional microtomography. *Geophysical Research Letters*, **23(7)**, 705-708.

Avila, C. E., and Evans, R. D. (1986, January). The effect of temperature and overburden pressure upon the non-Darcy flow coefficient in porous media. *In The 27th US Symposium on Rock Mechanics (USRMS)*. American Rock Mechanics Association.

Bashtani, F., Kryuchkov, S., Bryan, J., Maini, B., and Kantzas, A. (2016). Random network modelling approach to investigate the single-phase and quasi-static immiscible two-phase flow properties in the Mesaverde formation. *The Canadian Journal of Chemical Engineering*, **94(11)**, 2091-2106.

Bear, J.: Dynamics of Fluids in Porous Media, Dover Publications, Inc., New York (1972).

Békri, S., and Vizika, O. (2006, September). Pore-network modeling of rock transport properties: application to a carbonate. In International Symposium of the Society of Core Analysts, Trondheim, Norway, Sept (pp. 12-16).

Bekri, S., Laroche, C., and Vizika, O. (2002). Pore-network models to calculate transport properties in homogeneous and heterogeneous porous media. DEVELOPMENTS IN WATER SCIENCE, **47**, 1115-1122.

Berg, R. R. (1975). Capillary pressures in stratigraphic traps. *AAPG bulletin*, **59(6)**, 939-956.

Blunt, M. J., Jackson, M. D., Piri, M., and Valvatne, P. H. (2002). Detailed physics, predictive capabilities and macroscopic consequences for pore-network models of multiphase flow. *Advances in Water Resources*, **25(8)**, 1069-1089.

Bourbie, T., and Zinszner, B. (1985). Hydraulic and acoustic properties as a function of porosity in Fontainebleau sandstone. *Journal of Geophysical Research: Solid Earth*, **90(B13)**, 11524-11532.

Bourbié, T., Coussy, O., and Zinszner, B. (1987). Acoustics of porous media: Editions Technip.

Brown, R. L., and Hawksley, P. G. W. (1945). Packing of regular (spherical) and irregular particles. *Nature*, **156**(3962), 421-422.

Bryant, S. L., King, P. R., and Mellor, D. W. (1993). Network model evaluation of permeability and spatial correlation in a real random sphere packing. *Transport in porous media*, **11(1)**, 53-70.

Bryant, S., and Blunt, M. (1992). Prediction of relative permeability in simple porous media. *Physical Review A*, **46(4)**, 2004.

Carman, P. C. (1937). Fluid flow through granular beds. Transactions-Institution of Chemical Engineeres, **15**, 150-166.

Carman, P. C. (1956). Flow of gases through porous media. Academic press.

Carothers, J. E. (1968). A statistical study of the formation factor relation. *The Log Analyst*, ***9*(5)**, 13-20.

Caubit, C., Hamon, G., Sheppard, A. P., and Øren, P. E. (2009). Evaluation of the reliability of prediction of petrophysical data through imagery and pore network modelling. *Petrophysics*, **50(04)**.

Chilton, T. H., and Colburn, A. P. (1931). II—Pressure Drop in Packed Tubes1. *Industrial and Engineering Chemistry*, **23(8)**, 913-919.

Coelho, D., Thovert, J. F., and Adler, P. M. (1997). Geometrical and transport properties of random packings of spheres and aspherical particles. *Physical Review E*, **55(2)**, 1959.

Coles, M. E., and Hartman, K. J. (1998, January). Non-Darcy measurements in dry core and the effect of immobile liquid. *In SPE Gas Technology Symposium*. Society of Petroleum Engineers.

Comiti, J., and Renaud, M. (1989). A new model for determining mean structure parameters of fixed beds from pressure drop measurements: application to beds packed with parallelepipedal particles. *Chemical Engineering Science*, **44(7)**, 1539-1545.

Comiti, J., Sabiri, N. E., and Montillet, A. (2000). Experimental characterization of flow regimes in various porous media—III: limit of Darcy's or creeping flow regime for Newtonian and purely viscous non-Newtonian fluids. Chemical Engineering Science, **55(15)**, 3057-3061.

Cooper, J. W., Wang, X., and Mohanty, K. K. (1999). Non-Darcy -flow studies in anisotropic porous media. *SPE Journal*, **4(04)**, 334-341.

Cornell, D., and Katz, D. L. (1953). Flow of gases through consolidated porous media. *Industrial and Engineering Chemistry*, **45(10)**, 2145-2152.

Darcy, H. (1856). Les fontaines publiques de la ville de Dijon: exposition et application... Victor Dalmont.

Day, P. R. (1965). Particle fractionation and particle-size analysis. Methods of soil analysis. Part 1. Physical and mineralogical properties, including statistics of measurement and sampling, (methodsofsoilana), 545-567.

de Laat, D., de Oliveira Filho, F. M., and Vallentin, F. (2014, September). Upper bounds for packings of spheres of several radii. In Forum of Mathematics, Sigma (Vol. 2). Cambridge University Press.

Delfosse-Ribay, E., Djeran-Maigre, I., Cabrillac, R., and Gouvenot, D. (2004). Shear modulus and damping ratio of grouted sand. Soil Dynamics and Earthquake Engineering, **24(6)**, 461-471.

Dong, H., and Blunt, M. J. (2009). Pore-network extraction from micro-computerized-tomography images. *Physical review E*, **80(3)**, 036307.

Dullien, F. A. (2012). Porous media: fluid transport and pore structure. Academic press.

Durlofsky, L., and Brady, J. F. (1987). Analysis of the Brinkman equation as a model for flow in porous media. *The Physics of fluids*, **30(11)**, 3329-3341

Ergun, S. (1952). Fluid flow through packed columns. *Chem. Eng. Prog.*, **48**, 89-94.

Evans, E. V., and Evans, R. D. (1988). The Influence of an Immobile or Mobile Saturation Upon Non-Darcy Compressible Flow of Real Gases in Propped Fractures (includes associated papers 19901 and 21622). *Journal of petroleum technology*, **40(10)**, 1-343.

Fancher, G. H. and Lewis, J. A.: 1933, Flow of simple fluids through porous materials, Ind. Eng. Chem. **25(10)**, 1139–1147.

Fatt, I. (1956). The network model of porous media. 3. Dynamic properties of networks with tube radius distribution. *Transactions of the American institute of mining and metallurgical engineers*, **207(7)**, 164-181.

Feia, S., Dupla, J. C., Ghabezloo, S., Sulem, J., Canou, J., Onaisi, A., ... and Aubry, E. (2015). Experimental investigation of particle suspension injection and permeability impairment in porous media. *Geomechanics for Energy and the Environment*, **3**, 24-39.

Firoozabadi, A., and Katz, D. L. (1979). An analysis of high-velocity gas flow through porous media. *Journal of Petroleum Technology*, **31(02)**, 211-216.

Forchheimer P. Wasserbewegung durch boden. Zeit Ver Deutsch Ing 1901(45):1781–8.

Fourar, M., Radilla, G., Lenormand, R., and Moyne, C. (2004). On the non-linear behavior of a laminar single-phase flow through two and three-dimensional porous media. *Advances in Water resources*, **27(6)**, 669-677.

Frederick Jr, D. C., and Graves, R. M. (1994, January). New correlations to predict non-Darcy flow coefficients at immobile and mobile water saturation. In SPE Annual Technical Conference and Exhibition. *Society of Petroleum Engineers*.

Fredrich, J. T., Greaves, K. H., and Martin, J. W. (1993, December). Pore geometry and transport properties of Fontainebleau sandstone. *In International journal of rock mechanics and mining sciences and geomechanics abstracts* (**Vol. 30**, No. 7, pp. 691-697). Pergamon.

Garcia, X., Akanji, L. T., Blunt, M. J., Matthai, S. K., and Latham, J. P. (2009). Numerical study of the effects of particle shape and polydispersity on permeability. *Physical Review E*, **80(2)**, 021304.

Geertsma, J. (1974). Estimating the coefficient of inertial resistance in fluid flow through porous media. *Society of Petroleum Engineers Journal*, **14(05)**, 445-450.

Gewers, C. W. W., and Nichol, L. R. (1969). Gas turbulence factor in a microvugular carbonate. *Journal of Canadian Petroleum Technology*, **8(02)**, 51-36.

Ghomeshi, S., Kryuchkov, S., and Kantzas, A. (2018). An investigation into the effects of pore connectivity on T2 NMR relaxation. *Journal of Magnetic Resonance*, **289**, 79-91.

Ghomeshi, S., Taheri, S., Skripkin, E., Kryuchkov, S., and Kantzas, A. (2015). Determination of Physical Properties of Tight Porous Media Using Digital Core Physics/Analysis. *In Society of Core Analysis Symposium* (pp. 16-21).

Goldberg, M. (1971). On the densest packing of equal spheres in a cube. *Mathematics Magazine*, **44(4)**, 199-208.

Han, D. H., Nur, A., and Morgan, D. (1986). Effects of porosity and clay content on wave velocities in sandstones. *Geophysics*, **51(11)**, 2093-2107.

Hansen, D. (1992). The behaviour of flowthrough rockfill dams. *University of Ottawa* (Canada).

Hassanizadeh, S. M., and Gray, W. G. (1987). High velocity flow in porous media. *Transport in porous media*, **2(6)**, 521-531.

Hudson, D. R. (1949). Density and packing in an aggregate of mixed spheres. *Journal of Applied Physics*, **20(2)**, 154-162.

Ikeda, S., Nakano, T., Tsuchiyama, A., Uesugi, K., Suzuki, Y., Nakamura, K. (2001) Nondestructive three-dimensional element-concentration mapping of a Cs-doped partially molten granite by X-ray computed tomography using synchrotron radiation. *Am Mineral*. **89**: 1304-13.

Ioannidis, M. A., Kwiecien, M. J., and Chatzis, I. (1996). Statistical analysis of the porous microstructure as a method for estimating reservoir permeability. *Journal of petroleum science and engineering*, **16(4)**, 251-261.

Janicek, J. D., and Katz, D. L. V. (1955). Applications of unsteady state gas flow calculations.

Jin, G., Patzek, T. W., and Silin, D. B. (2003, January). Physics-based reconstruction of sedimentary rocks. *In SPE Western Regional/AAPG Pacific Section Joint Meeting*. Society of Petroleum Engineers.

Johnson, T. W., and Taliaferro, D. B. (1938). Flow of air and natural gas through porous media (No. BM-TP-592). *Bureau of Mines*, Bartlesville, Okla.(USA).

Jones, S. C. (1987, January). Using the inertial coefficient, b, to characterize heterogeneity in reservoir rock. In SPE Annual Technical Conference and Exhibition. *Society of Petroleum Engineers*.

Kalaydjian, F. M., Bourbiaux, B. J., and Lombard, J. M. (1996, January). Predicting gas-condensate reservoir performance: how flow parameters are altered when approaching production wells. In SPE Annual Technical Conference and Exhibition. *Society of Petroleum Engineers*.

Kameda, A. (2004). Permeability evolution in sandstone: Digital rock approach (*Doctoral dissertation, Stanford University*).

Keehm, Y. (2003). Computational rock physics: Transport properties in porous media and applications.

Khalifa, A., Garnier, J., Thomas, P., and Rault, G. (2000, May). Scaling laws of water flow in centrifuge models. *In International Symposium on Physical Modelling and Testing in Environmental Geotechnics* (**Vol. 56**, pp. 207-216).

Koponen, A., Kataja, M., and Timonen, J. (1996). Tortuous flow in porous media. *Physical Review E*, **54(1)**, 406.

Kutasov, I. M. (1993). Equation predicts non-Darcy flow coefficient. *Oil and Gas Journal*;(United States), **91(11)**.

Laroche, C., and Vizika, O. (2005). Two-phase flow properties prediction from small-scale data using pore-network modeling. *Transport in Porous Media*, **61(1)**, 77-91.

Li, D., and Engler, T. W. (2001, January). Literature review on correlations of the non-Darcy coefficient. In SPE Permian Basin Oil and Gas Recovery Conference. *Society of Petroleum Engineers*.

Lindquist, W. B., and Venkatarangan, A. (1999). Investigating 3D geometry of porous media from high resolution images. Physics and Chemistry of the Earth, Part A: *Solid Earth and Geodesy*, **24(7)**, 593-599.

Liu, X., Civan, F., and Evans, R. D. (1995). Correlation of the non-Darcy flow coefficient. *Journal of Canadian Petroleum Technology*, **34(10)**.

Ma, H., and Ruth, D. W. (1993). The microscopic analysis of high Forchheimer number flow in porous media. *Transport in Porous Media*, **13(2)**, 139-160.

Macdonald, I. F., El-Sayed, M. S., Mow, K., and Dullien, F. A. L. (1979). Flow through porous media-the Ergun equation revisited. *Industrial and Engineering Chemistry Fundamentals*, **18(3)**, 199-208.

Manwart, C., Aaltosalmi, U., Koponen, A., Hilfer, R., and Timonen, J. (2002). Lattice-Boltzmann and finite-difference simulations for the permeability for three-dimensional porous media. *Physical Review E*, **66(1)**, 016702.

Martins, R. (1990). Turbulent seepage flow through rockfill structures. *International Water Power and Dam Construction*, **42(3)**, 41-42.

Mohammadmoradi, P., and Kantzas, A. (2017). Toward Direct Pore-Scale Modeling of Three-Phase Displacements. *Advances in Water Resources*.

Mostaghimi, P., Bijeljic, B., and Blunt, M. (2012). Simulation of flow and dispersion on pore-space images. *SPE Journal*, **17(04)**, 1-131.

Muljadi, B. P., Blunt, M. J., Raeini, A. Q., and Bijeljic, B. (2016). The impact of porous media heterogeneity on non-Darcy flow behaviour from pore-scale simulation. *Advances in Water Resources*, **95**, 329-340.

Narayanaswamy, G., Sharma, M. M., and Pope, G. A. (1998, January). Effect of heterogeneity on the non-Darcy flow coefficient. *In SPE Gas Technology Symposium. Society of Petroleum Engineers*

Newman, M. S., and Yin, X. (2013). Lattice Boltzmann simulation of non-Darcy flow in stochastically generated 2D porous media geometries. *SPE Journal*, **18(01)**, 12-26.

Nolan, G. T., and Kavanagh, P. E. (1995). Random packing of nonspherical particles. *Powder technology*, **84(3)**, 199-205.

Noman, R., and Archer, J. S. (1987, January). The effect of pore structure on non-Darcy gas flow in some low-permeability reservoir rocks. In Low Permeability Reservoirs Symposium. Society of Petroleum Engineers.

O'Toole, P. I., and Hudson, T. S. (2011). New high-density packings of similarly sized binary spheres. *The Journal of Physical Chemistry* C, **115(39)**, 19037-19040.

Omidvar, M., Iskander, M., and Bless, S. (2014). Response of granular media to rapid penetration. *International Journal of Impact Engineering*, **66**, 60-82.

Ovaysi, S., and Piri, M. (2010). Direct pore-level modeling of incompressible fluid flow in porous media. *Journal of Computational Physics*, **229(19)**, 7456-7476.

Pape, H., Riepe, L., and Schopper, J. R. (1987). Interlayer conductivity of rocks—A fractal model of interface irregularities for calculating interlayer conductivity of natural porous mineral systems. *Colloids and Surfaces*, **27(1-3)**, 97-122.

Pascal, H., and Quillian, R. G. (1980, January). Analysis of vertical fracture length and non-Darcy flow coefficient using variable rate tests. *In SPE Annual Technical Conference and Exhibition. Society of Petroleum Engineers.*

Patil, V. A., and Liburdy, J. A. (2013). Flow characterization using PIV measurements in a low aspect ratio randomly packed porous bed. *Experiments in fluids*, **54(4)**, 1497.

Peng, S., Hu, Q., Dultz, S., and Zhang, M. (2012). Using X-ray computed tomography in pore structure characterization for a Berea sandstone: Resolution effect. *Journal of hydrology*, **472**, 254-261.

Pilotti, M. (1998). Generation of realistic porous media by grains sedimentation. *Transport in Porous Media*, **33(3)**, 257-278.

Powell, M. J. (1980). Computer-simulated random packing of spheres. *Powder Technology*, **25(1)**, 45-52.

Raeini, A. Q., Bijeljic, B., and Blunt, M. J. (2015). Modelling capillary trapping using finite-volume simulation of two-phase flow directly on micro-CT images. *Advances in Water Resources***, 83**, 102-110.

Raeini, A. Q., Blunt, M. J., and Bijeljic, B. (2014). Direct simulations of two-phase flow on micro-CT images of porous media and upscaling of pore-scale forces. *Advances in Water Resources*, **74**, 116-126.

Rahmanian, M., and Kantzas, A. (2018). Stochastic generation of virtual porous media using a pseudo-crystallization approach. *Journal of Natural Gas Science and Engineering*.

Ramstad, T., Idowu, N., Nardi, C., and Øren, P. E. (2012). Relative permeability calculations from two-phase flow simulations directly on digital images of porous rocks. *Transport in Porous Media*, **94(2)**, 487-504.

Revil, A., and Cathles, L. M. (1999). Permeability of shaly sands. *Water Resources Research*, **35(3)**, 651-662.

Rodriguez, J., Allibert, C. H., and Chaix, J. M. (1986). A computer method for random packing of spheres of unequal size. *Powder technology*, **47(1)**, 25-33.

Rose, H. E. (1945). An investigation into the laws of flow of fluids through beds of granular materials. *Proceedings of the Institution of Mechanical Engineers*, **153(1)**, 141-148.

Ruth, D., and Ma, H. (1992). On the derivation of the Forchheimer equation by means of the averaging theorem. *Transport in Porous Media*, **7(3)**, 255-264.

Saboorian-Jooybari, H., and Pourafshary, P. (2015, January). Non-Darcy Flow Effect in Fractured Tight Reservoirs: How Significant Is It at Low Flow Rates and away from Wellbores? In SPE Middle East Unconventional Resources Conference and Exhibition. *Society of Petroleum Engineers.*

Sahimi, M. (2011). Flow and transport in porous media and fractured rock: from classical methods to modern approaches. *John Wiley and Sons*.

Santiago, C., Ghomeshi, S., Kryuchkov, S., and Kantzas, A. (2016). Pore level modeling of imbibition in heavy oil saturated media. *Journal of Petroleum Science and Engineering*, **140**, 108-118.

Scheidegger, A. (1958). The physics of flow through porous media. *University of Toronto Press: London.*

Schwartz, L. M., and Banavar, J. R. (1989). Transport properties of disordered continuum systems. *Physical Review B*, **39(16)**, 11965.

Skripkin, E., Kryuchkov, S., Taheri, S., and Kantzas, A. Prediction of Thermal Conductivity of Oil Sands Based on Particle Size Distribution.

Sloane, N. J. A. (1977). Binary codes, lattices and sphere packings. Combinatorial Surveys'', *edited PJ Cameron, Academic Press*, NY, 117-164.

Spanne, P., Thovert, J. F., Jacquin, C. J., Lindquist, W. B., Jones, K. W., and Adler, P. M. (1994). Synchrotron computed microtomography of porous media: topology and transports. *Physical Review Letters*, **73(14)**, 2001.

Stewart, M. L., Ward, A. L., and Rector, D. R. (2006). A study of pore geometry effects on anisotropy in hydraulic permeability using the lattice-Boltzmann method. *Advances in water resources*, **29(9)**, 1328-1340.

Taheri, S., Ghomeshi, S., and Kantzas, A. (2017). Permeability calculations in unconsolidated homogeneous sands. *Powder Technology*, **321**, 380-389.

Taheri, S., Ghomeshi.S., Skripkin,E., Brayan.J., Hejazi.,H and Kantzas.,A, "Prediction of oil sand permeability", *GeoConvention Conference*, Calgary, Canada 2015.

Taheri, S., Kantzas, A., and Abedi, J. (2010, January). Mass Diffusion Into Bitumen: A Sub-Pore Scale Modeling Approach. *In Canadian Unconventional Resources and International Petroleum Conference. Society of Petroleum Engineers*.

Thauvin, F., and Mohanty, K. K. (1998). Network modeling of non-Darcy flow through porous media. *Transport in Porous Media*, **31(1)**, 19-37.

Timur, A., Hempkins, W. B., and Worthington, A. E. (1972). Porosity and pressure dependence of formation resistivity factor for sandstones. *Trans., Cdn. Well Logging Soc, 4*.

Torquato, S. (2013). Random heterogeneous materials: microstructure and macroscopic properties (**Vol. 16**). *Springer Science and Business Media*.

Tory, E. M., Cochrane, N. A., and Waddell, S. R. (1968). Anisotropy in simulated random packing of equal spheres.

Valvatne, P. H., and Blunt, M. J. (2004). Predictive pore-scale modeling of two-phase flow in mixed wet media. *Water Resources Research*, **40(7)**.

Varloteaux, C., Békri, S., and Adler, P. M. (2013). Pore network modelling to determine the transport properties in presence of a reactive fluid: From pore to reservoir scale. *Advances in Water Resources*, **53**, 87-100.

Visscher, W. M., and Bolsterli, M. (1972). Random packing of equal and unequal spheres in two and three dimensions. *Nature*, **239**(5374), 504-507.

Wadell, H. (1935). Volume, shape, and roundness of quartz particles. *The Journal of Geology*, **43(3)**, 250-280.

Wang, X., Thauvin, F., and Mohanty, K. K. (1999). Non-Darcy flow through anisotropic porous media. *Chemical Engineering Science*, **54(12)**, 1859-1869.

Wildenschild, D., and Sheppard, A. P. (2013). X-ray imaging and analysis techniques for quantifying pore-scale structure and processes in subsurface porous medium systems. *Advances in Water Resources*, **51**, 217-246.

Wildenschild, D., Hopmans, J. W., Rivers, M. L., and Kent, A. J. R. (2005). Quantitative analysis of flow processes in a sand using synchrotron-based X-ray microtomography. *Vadose Zone Journal*, **4(1)**, 112-126.

Wildenschild, D., Vaz, C. M. P., Rivers, M. L., Rikard, D., and Christensen, B. S. B. (2002). Using X-ray computed tomography in hydrology: systems, resolutions, and limitations. *Journal of Hydrology*, **267(3)**, 285-297.

Winsauer, W. O., Shearin Jr, H. M., Masson, P. H., and Williams, M. (1952). Resistivity of brine-saturated sands in relation to pore geometry. *AAPG bulletin*, ***36*(2)**, 253-277.

Youssef, S., Rosenberg, E., Gland, N. F., Kenter, J. A., Skalinski, M., and Vizika, O. (2007, January). High resolution CT and pore-network models to assess petrophysical properties of homogeneous and heterogeneous carbonates. *In SPE/EAGE Reservoir Characterization and Simulation Conference. Society of Petroleum Engineers*.

Zeng, Z., and Grigg, R. (2006). A criterion for non-Darcy flow in porous media. *Transport in porous media*, **63(1)**, 57-69.

APPENDIX A: COPYRIGHT PERMISSIONS

ELSEVIER LICENSE
TERMS AND CONDITIONS

Apr 02, 2018

This Agreement between Meysam Rahmanian Shahri ("You") and Elsevier ("Elsevier") consists of your license details and the terms and conditions provided by Elsevier and Copyright Clearance Center.

License Number	4320850509304
License date	Apr 02, 2018
Licensed Content Publisher	Elsevier
Licensed Content Publication	Powder Technology
Licensed Content Title	Permeability calculations in unconsolidated homogeneous sands
Licensed Content Author	Saeed Taheri,Shahin Ghomeshi,Apostolos Kantzas
Licensed Content Date	Nov 1, 2017
Licensed Content Volume	321
Licensed Content Issue	n/a
Licensed Content Pages	10
Start Page	380
End Page	389
Type of Use	reuse in a thesis/dissertation
Intended publisher of new work	other
Portion	figures/tables/illustrations
Number of figures/tables/illustrations	4
Format	both print and electronic
Are you the author of this Elsevier article?	No
Will you be translating?	No
Original figure numbers	Figures 1,3,4.a,12.b
Title of your thesis/dissertation	Effect of Grain Irregularity on Rock Petrophysical Properties: A Numerical Pore-level Study
Expected completion date	Apr 2018
Estimated size (number of pages)	130
Requestor Location	Meysam Rahmanian Shahri 909 4944 Dalton Drive Nw calgary, AB T3a2E6 Canada Attn: Meysam Rahmanian Shahri
Publisher Tax ID	GB 494 6272 12
Total	0.00 CAD
Terms and Conditions	

ELSEVIER LICENSE
TERMS AND CONDITIONS

Apr 02, 2018

This Agreement between Meysam Rahmanian Shahri ("You") and Elsevier ("Elsevier") consists of your license details and the terms and conditions provided by Elsevier and Copyright Clearance Center.

License Number	4320850085749
License date	Apr 02, 2018
Licensed Content Publisher	Elsevier
Licensed Content Publication	Advances in Water Resources
Licensed Content Title	Pore network modelling to determine the transport properties in presence of a reactive fluid: From pore to reservoir scale
Licensed Content Author	Clément Varloteaux,Samir Békri,Pierre M. Adler
Licensed Content Date	Mar 1, 2013
Licensed Content Volume	53
Licensed Content Issue	n/a
Licensed Content Pages	14
Start Page	87
End Page	100
Type of Use	reuse in a thesis/dissertation
Intended publisher of new work	other
Portion	figures/tables/illustrations
Number of figures/tables/illustrations	1
Format	both print and electronic
Are you the author of this Elsevier article?	No
Will you be translating?	No
Original figure numbers	Figure 1
Title of your thesis/dissertation	Effect of Grain Irregularity on Rock Petrophysical Properties: A Numerical Pore-level Study
Expected completion date	Apr 2018
Estimated size (number of pages)	130
Requestor Location	Meysam Rahmanian Shahri 909 4944 Dalton Drive Nw calgary, AB T3a2E6 Canada Attn: Meysam Rahmanian Shahri
Publisher Tax ID	GB 494 6272 12
Total	0.00 CAD
Terms and Conditions	

SPRINGER NATURE LICENSE
TERMS AND CONDITIONS

Apr 02, 2018

This Agreement between Meysam Rahmanian Shahri ("You") and Springer Nature ("Springer Nature") consists of your license details and the terms and conditions provided by Springer Nature and Copyright Clearance Center.

License Number	4320851108612
License date	Apr 02, 2018
Licensed Content Publisher	Springer Nature
Licensed Content Publication	Transport in Porous Media
Licensed Content Title	Generation of Realistic Porous Media by Grains Sedimentation
Licensed Content Author	Marco Pilotti
Licensed Content Date	Jan 1, 1998
Licensed Content Volume	33
Licensed Content Issue	3
Type of Use	Thesis/Dissertation
Requestor type	academic/university or research institute
Format	print and electronic
Portion	figures/tables/illustrations
Number of figures/tables/illustrations	1
Will you be translating?	no
Circulation/distribution	10,001 to 20,000
Author of this Springer Nature content	no
Title	Effect of Grain Irregularity on Rock Petrophysical Properties: A Numerical Pore-level Study
Instructor name	n/a
Institution name	n/a
Expected presentation date	Apr 2018
Portions	Figure 10.b
Requestor Location	Meysam Rahmanian Shahri 909 4944 Dalton Drive Nw calgary, AB T3a2E6 Canada Attn: Meysam Rahmanian Shahri
Billing Type	Invoice
Billing Address	Meysam Rahmanian Shahri 909 4944 Dalton Drive Nw calgary, AB T3a2E6 Canada Attn: Meysam Rahmanian Shahri
Total	0.00 CAD
Terms and Conditions	

American Physical Society
Reuse and Permissions License

11-Apr-2018

This license agreement between the American Physical Society ("APS") and Meysam Shahri ("You") consists of your license details and the terms and conditions provided by the American Physical Society and SciPris.

Licensed Content Information

License Number:	**RNP/18/APR/003252**
License date:	11-Apr-2018
DOI:	10.1103/PhysRevE.55.1959
Title:	Geometrical and transport properties of random packings of spheres and aspherical particles
Author:	D. Coelho, J.-F. Thovert, and P. M. Adler
Publication:	Physical Review E
Publisher:	American Physical Society
Cost:	USD $ 0.00

Request Details

Does your reuse require significant modifications: No

Specify intended distribution locations:	United States,Canada

Does your reuse require significant modifications: No

Specify intended distribution locations:	Canada
Reuse Category:	Reuse in a thesis/dissertation
Requestor Type:	Academic Institution
Items for Reuse:	Figures/Tables
Number of Figure/Tables:	1
Figure/Tables Details:	Figure 3.a
Format for Reuse:	Print and Electronic
Total number of print copies:	More Than 10000

Information about New Publication:

University/Publisher:	University Of Calgary
Title of dissertation/thesis:	Effect of Grain Irregularity on Rock Petrophysical Properties: A Numerical Pore-level Study
Author(s):	Meysam Rahmanian Shahri
Expected completion date:	Apr. 2018

License Requestor Information

Name:	Meysam Shahri
Affiliation:	Individual
Email Id:	meysam655@Yahoo.com
Country:	Canada